New effective interaction for f_5pg_9-shell nuclei

M. Honma,[1] T. Otsuka,[2,3,4] T. Mizusaki,[5] and M. Hjorth-Jensen[6]

[1]*Center for Mathematical Sciences, University of Aizu, Tsuruga, Ikki-machi, Aizu-Wakamatsu, Fukushima 965-8580, Japan*
[2]*Department of Physics and Center for Nuclear Study, University of Tokyo, Hongo, Bunkyo-ku, Tokyo 113-0033, Japan*
[3]*RIKEN, Hirosawa, Wako-shi, Saitama 351-0198, Japan*
[4]*National Superconducting Cyclotron Laboratory, Michigan State University, East Lansing, Michigan 48824-1321, USA*
[5]*Institute of Natural Sciences, Senshu University, Higashimita, Tama, Kawasaki, Kanagawa 214-8580, Japan*
[6]*Department of Physics and Center of Mathematics for Applications, University of Oslo, N-0316 Oslo, Norway*

(Received 25 June 2009; published 30 December 2009)

We present a new effective interaction for shell-model calculations in the model space consisting of the single-particle orbits $1p_{3/2}$, $0f_{5/2}$, $1p_{1/2}$, and $0g_{9/2}$. Starting with a realistic interaction based on the Bonn-C potential, 133 two-body matrix elements and four single-particle energies are modified empirically so as to fit 400 experimental energy data out of 69 nuclei with mass numbers $A = 63 \sim 96$. The systematics of binding energies, electromagnetic moments and transitions, and low-lying energy levels are described. The soft $Z = 28$ closed core is observed, in contrast to the stable $N = 50$ shell closure. The new interaction is applied to systematic studies of three different chains of nuclei, Ge isotopes around $N = 40$, $N = Z$ nuclei with $A = 64 \sim 70$, and $N = 49$ odd-odd nuclei, focusing especially on the role of the $g_{9/2}$ orbit. The irregular behavior of the 0_2^+ state in Ge isotopes is understood as a result of detailed balance between the $N = 40$ single-particle energy gap and the collective effects. The development of the band structure in $N = Z$ nuclei is interpreted in terms of successive excitations of nucleons into the $g_{9/2}$ orbit. The triaxial/γ-soft structure in ^{64}Ge and the prolate/oblate shape coexistence in ^{68}Se are predicted, showing a good correspondence with the experimental data. The isomeric states in ^{66}As and ^{70}Br are obtained with the structure of an aligned proton-neutron pair in the $g_{9/2}$ orbit. Low-lying energy levels in $N = 49$ odd-odd nuclei can be classified as proton-neutron pair multiplets, implying that the obtained single-particle structure in this neutron-rich region appears to be appropriate. These results demonstrate that, in spite of the modest model space, the new interaction turns out to describe rather well properties related to the $g_{9/2}$ orbit in various cases, including moderately deformed nuclei.

DOI: 10.1103/PhysRevC.80.064323 PACS number(s): 21.60.Cs, 21.30.Fe, 27.50.+e, 27.60.+j

I. INTRODUCTION

In recent years, stimulating new data have been accumulated, due to rapid and wide developments of experiments, in the outer region of the nuclear chart around the pf shell. The nuclei in this region attract much attention and interest because of observed and expected phenomena, for instance, shape-coexistence, anomalously low-lying 0^+ excited states, various kinds of isomers, and double β decay. Among such topics, the evolution of the shell structure can be found in many nuclei. The measured mass systematics show the narrowing of the $N = 50$ shell gap toward $Z = 32$ [1], while the persistence of the $N = 50$ shell closure is suggested in ^{80}Ge based on the new $B(E2)$ data [2]. In Cu isotopes, the large energy gap above the $19/2^-$ state in ^{71}Cu [3] is interpreted as a support of the stability of the $N = 40$ shell gap. On the other hand, beyond $N = 40$, the low excitation energies of $1/2^-$ states and the measured large $B(E2)$ values among low-lying states in ^{71}Cu and ^{73}Cu indicate an onset of collective effects [4]. The recent measurements of $B(E2)$ values in Zn isotopes suggest the importance of the proton-core excitation across the $Z = 28$ shell gap as well as the stability of the $N = 50$ shell closure [5]. Thus, the shell structure really evolves in the region to be discussed.

Another interesting problem is the shape evolution around $N = Z$ nuclei. The oblate ground-state band coexisting with the prolate excited band has been observed for ^{68}Se. Such a shape coexistence is investigated also for ^{70}Se and ^{72}Se through the lifetime measurements [6]. Also, the structure of ^{76}Ge and ^{76}Se, which are relevant to the double β decay, has been studied focusing on the occupation of valence neutron orbits [7], which demands the improvements in theoretical predictions. Because of such a rich variety of phenomena in this mass region, it should be a challenging and intriguing task for nuclear theory to seek for a unified description of them from a single Hamiltonian.

A unified shell-model approach has contributed critically to detailed understandings and quantitative predictions in lighter-mass regions. As examples, the Cohen-Kurath [8] and the USD interactions [9,10] have been shown to be quite successful for the p shell and the sd shell, respectively, while in the combined $p + sd$ shell-model space, the SFO interaction [11] has been used. For the pf shell, we have proposed and developed the GXPF1 interaction [12,13] that provides us with a systematic and yet quite accurate description of nuclei in the pf shell. The KB3 interaction and its descendants [14] have been frequently used also for the pf shell. However, this kind of approach has been missing in the region mentioned in the previous paragraph. We present in this article an attempt along this line, that is, to provide an effective interaction for nuclei in the upper part of the pf shell. To achieve this, we construct an effective interaction in the model space consisting of four spherical orbits, namely the single-particle orbits $p_{3/2}$, $f_{5/2}$,

$p_{1/2}$, and $g_{9/2}$. The model space is called f_5pg_9 shell hereafter. Our purposes behind this choice are as follows: (i) To explore the possibility of systematic description for upper pf-shell nuclei within the shell-model framework. (ii) To fix cross-shell matrix elements between the upper pf shell and the $g_{9/2}$ shell, aiming at future extensions to a model space that includes the full pf shell and $g_{9/2}$ shell (and beyond). Especially, the monopole matrix elements between the $f_{5/2}$ and the $g_{9/2}$ orbit are of interest from the viewpoint of the relation between the change of the shell structure in neutron-rich nuclei and the contribution of the tensor force [15]. (iii) To investigate the "intruder" effects from the $f_{7/2}$ orbit, in other words, the core excitations across the $Z, N = 28$ shell gap. It has been shown in our previous study on nuclei in the lower part of the pf shell that the ^{56}Ni core is rather "soft" and that core excitations affect significantly the structure of Ni and neighboring isotopes. Thus, it is interesting to see to what extent the missing $f_{7/2}$ orbit affects the overall description of upper pf-shell nuclei.

Historically, the model space consisting of only the upper two orbits $p_{1/2}$ and $g_{9/2}$ has been frequently adopted [16–20] for the description of nuclei around $Z \sim 40$, $N \sim 50$. In this case, an inert ^{88}Sr ($Z = 38$, $N = 50$) core is assumed and neutrons are treated as holes. Effective interactions for this model space have been proposed where two-body matrix elements and single-particle energies are treated as parameters and are determined by a fit to the available body of experimental levels. Such an approach is feasible for this model space, because the number of parameters is relatively small [18 two-body matrix elements (TBME) and two single-particle energies (SPE), with the assumption of good isospin symmetry]. This model space with pertaining fitted interaction and single-particle energies was shown to give a systematic and precise description of several energy levels, including high-spin states. In fact, Johnstone and Skouras [20] obtained an rms deviation of 128 keV between their shell-model results and the experimental data for 477 energy levels from $38 \leqslant Z \leqslant 50$ and $47 \leqslant N \leqslant 50$ nuclei. There are, however, several exceptionally large discrepancies between their shell-model predictions and experimental data. These can be clear indications of the "intruder" effects and may provide us with important information on the relation between the upper ($p_{1/2}$, $g_{9/2}$) and the lower ($p_{3/2}$, $f_{5/2}$) orbits.

For larger shells, it becomes difficult to carry out such a direct fitting, chiefly because the number of parameters increases drastically and not all of them can be determined unambiguously by existing experimental levels. In the derivation of the effective interaction for the sd shell, Chung and Wildenthal [21] introduced the so-called linear combination method. In this method, a shell-model Hamiltonian is assumed first. This initial guess can be obtained from a microscopic calculation or from a phenomenological model. We modify the parameters of the Hamiltonian by a fit to experimental levels. The parameters are changed rather modestly in practice. One can find selected linear combinations of the parameters that are sensitive to the given set of experimental data. The remaining linear combinations are kept unchanged from that of the initial Hamiltonian. The fitted linear combinations are determined by diagonalizing the error matrix, and we can efficiently separate well-determined linear combinations from the rest according to the corresponding eigenvalues. We have applied this method to the derivation of the above-mentioned GXPF1 interaction for pf-shell nuclei, where 70 linear combinations of 195 parameters were varied.

The f_5pg_9 model space has been adopted in several investigations. For example, Xi and Wildenthal [22] developed an empirical effective interaction for the $N = 50$ isotones. Note that only the $T = 1$ part of the effective interaction was determined. They started with the empirical interaction of Schiffer and True type with a central force only and modified 35 linear combinations of 69 Hamiltonian parameters (two-body matrix elements and single-particle energies) by fitting them to 170 experimental energy data. They attained an rms deviation of 150 keV. Recently, Lisetskiy *et al.* have proposed effective interactions [23] for $Z = 28$ isotopes and $N = 50$ isotones separately in the f_5pg_9 shell, both of which were determined by similar but separate fitting calculations. They started with a realistic effective interaction derived form the Bonn-C nucleon-nucleon potential and varied only 20 linear combinations. For protons ($N = 50$ isotones), they adopted a similar data set for the fitting calculations as that of Ref. [22], and the resultant rms deviations was 124 keV for 132 energy data entries.

It should be noted that, contrary to the similarity in the quality of the overall fit, the two interactions of Ref. [22] and Ref. [23] differ quite a lot. For example, the SPE of the $g_{9/2}$ orbit relative to the $p_{3/2}$ orbit is 6.112 and 4.533 MeV, respectively. The two-body matrix elements (TBMEs) are rather different too. For example, the off-diagonal matrix element with the largest difference is $\langle p_{3/2}g_{9/2}|V|f_{5/2}g_{9/2}\rangle_{J=6,T=1}$, which is -0.8948 MeV and $+0.2833$ MeV in Ref. [22] and in Ref. [23], respectively. As for the diagonal ones, the most significant difference is seen in $\langle f_{5/2}g_{9/2}|V|f_{5/2}g_{9/2}\rangle_{J=7,T=1}$, which is -2.5513 MeV and -0.6009 MeV in Ref. [22] and in Ref. [23], respectively.

Such large differences are found mainly in the cross-shell matrix elements between the lower two orbits ($p_{3/2}$, $f_{5/2}$) and the upper two orbits ($p_{1/2}$, $g_{9/2}$). Thus there remain uncertainties in these matrix elements that cannot be determined well in the fitting calculations using the data from the $N = 50$ isotones. One possible reason for this uncertainty is that these matrix elements affect mainly the low-lying energy spectra of the $Z < 38$ nuclei, which are neutron-rich and unstable nuclei. There are few experimental data in this region. Such a limitation can be relaxed by considering data from the $N < 50$ nuclei. These nuclei are less neutron rich, but the price we pay is that we have to include the $T = 0$ TBME in the fitting calculations.

It has been a challenging problem to determine the $T = 0$ part of the effective interaction for the f_5pg_9 shell. Sinatkas *et al.* [24,25] have proposed such an interaction. They used the Sussex matrix elements as interaction to first order and calculated the effective interaction microscopically to second order in the interaction. An inert ^{100}Sn core was assumed, and protons and neutrons were treated as holes. The SPE were determined by a least-squares fit to the experimental energy spectra. The above authors showed that the $N = 50$ isotones with $34 \leqslant Z \leqslant 46$ can be reasonably described by their semimicroscopic approach. On the other

hand, for the application to $N = 49$ and $N = 48$ nuclei with $38 \leqslant Z \leqslant 44$, they needed to introduce phenomenological scaling parameters in several $T = 0$ TBME including the $g_{9/2}$ and the $p_{1/2,3/2}$ orbits. This fact seems to indicate the necessity of the modification of the interaction for cases with many valence particles. Because of computational limitations, they introduced the weak-coupling approximation for the shell-model calculations, which may give rise to additional uncertainty in the derived effective interaction.

In this article, we present the results of fitting calculations including both $T = 1$ and $T = 0$ TBME. We start with the same effective interaction interaction as in Ref. [23] and utilize the linear combination method. The advantage of the present model space, the f_5pg_9 shell, is that it is free from the spurious center-of-mass motion. Although this model space is huge enough to prevent us from carrying out the standard Lanczos diagonalization of the Hamiltonian matrix in the largest cases (maximum M-scheme dimension is 13 billions of states), many nuclei of interest in the present study are still within the tractable scope of such a conventional method by using the efficient shell-model code MSHELL [26]. In fact, in the final fit, all calculations were carried out using exact diagonalization techniques. Note that in the determination of the pf-shell effective interaction GXPF1 [12] we overcame this difficulty in the shell-model calculation by adopting an approximation [27] based on the Monte Carlo method [28].

We shall start with systematics of the masses, electromagnetic moments and levels. We then discuss in detail the stability of the $N = 40$ shell closure in Ge isotopes, the development of deformation and the band structure of $N = Z$ nuclei, and the appearance of the proton-neutron pair in neutron-rich nuclei.

For heavier pf-shell nuclei, the effects of intruder configurations outside the $0\hbar\omega$ space appear even in the low-lying states or near the yrast line. In addition, collective effects such as deformation become significant especially around the $N = Z$ line, which is difficult to describe within the restricted pf-shell model space. It is expected that a large part of such intruder effects can be taken into account by introducing only the $g_{9/2}$ orbit because of the existence of the $Z, N = 50$ shell closure.

This article is organized as follows: In Sec. II, we describe the derivation of the effective interaction and investigate its basic properties. The results of systematic properties obtained by using this interaction are presented in Sec. III. We summarize our results in Sec. IV.

II. DERIVATION OF EFFECTIVE INTERACTION

In the fitting calculations, the choice of the experimental data set is crucial. First, it is expected that in Ni isotopes the ^{56}Ni core can be rather "soft" [13,29] and that excitations from the $f_{7/2}$ to other orbits is significant. Therefore we exclude all data on Ni and Cu isotopes from the fit. In addition, for many nuclei in the middle of the present f_5pg_9 shell, very large $B(E2)$ values are observed experimentally for transitions among low-lying states, suggesting a significant deformation. We found that the present model space is insufficient to describe such a large quadrupole collectivity because of the lack of the $f_{7/2}$ orbit in the $N_{\rm osc} = 3$ shell and the $d_{5/2}$ orbit in the $N_{\rm osc} = 4$ shell, both important orbits needed to account for the development of such a collectivity [30]. Therefore, we also exclude data on nuclei with $N < 46$ and $Z > 33$. As a result, the target nuclei for which we can expect a reasonable description within the f_5pg_9 shell are mainly the $Z \sim 32$ nuclei and the $N \sim 50$ nuclei. In order to keep the number of data as low as possible, we exclude data on odd-odd nuclei except for the $N = 50$ isotones. In total, we take 400 experimental binding and excitation energy entries out of 69 nuclei with $A = 63$–96. Figure 1 shows a part of the nuclear chart that is covered by the present f_5pg_9 model space. The boxes in the chart indicate that the corresponding isotopes are included as data points in our fitting calculations.

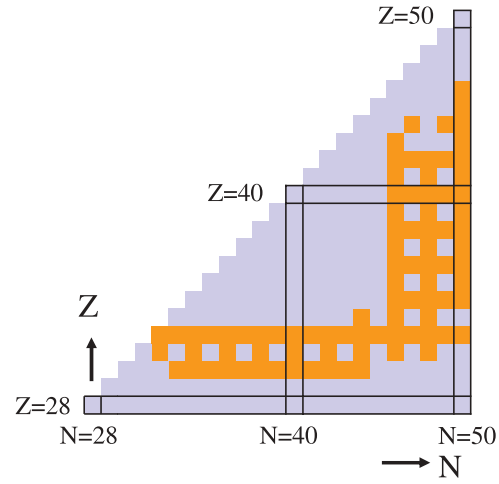

FIG. 1. (Color online) Isotopes used in the fitting calculation.

As a starting Hamiltonian, we take a microscopic interaction [31] derived from the Bonn-C potential, which we label G-f5pg9 hereafter. The same type of interaction [32] was used in the derivation of the GXPF1 interaction for the pf-shell nuclei. In the traditional shell-model approach, the single-particle energies (SPE) are taken from the experimental energy levels of one-particle or one-hole states relative to the assumed inert core. However, such a treatment is not justified because the present inert core, ^{56}Ni, can be rather soft and the low-lying states in ^{57}Ni cannot be regarded as the pure "single-particle" states. Instead, we treat the SPE as fitting parameters.

Assuming isospin symmetry, the shell-model Hamiltonian for the f_5pg_9 shell is specified by 133 TBME and four SPE. In the final step of the iteration, we have varied 45 well-determined linear combinations of these parameters. A common mass dependence factor $A^{-0.3}$ is assumed for all TBME, as in the cases of the USD and the GXPF1 interaction. We have attained an rms error of 185 keV with the resultant interaction, JUN45. In Table I, we present the TBME of the JUN45 interaction as well as the starting G-f5pg9 interaction.

In Fig. 2, we find a reasonable correlation of the TBME between the JUN45 interaction and the G-f5pg9 interaction. As in the case of the pf shell, a general trend is that the $T = 0$

TABLE I. Two-body matrix elements $\langle ab|V|cd\rangle_{J,T}$ (in MeV) of JUN45 interaction. An inert ^{56}Ni core is assumed. Single-particle energies are taken to be −9.8280, −8.7087, −7.8388, and −6.2617 MeV for the $p_{3/2}$, $f_{5/2}$, $p_{1/2}$, and $g_{9/2}$ orbit, respectively. For calculations of mass A nuclei, the two-body matrix elements should be multiplied by a factor $(A/58)^{-0.3}$. For comparison, TBME of the starting realistic interaction G-f5pg9 are also shown.

$2j_a$	$2j_b$	$2j_c$	$2j_d$	J	T	$V_{\rm JUN45}$	V_G	$2j_a$	$2j_b$	$2j_c$	$2j_d$	J	T	$V_{\rm JUN45}$	V_G	$2j_a$	$2j_b$	$2j_c$	$2j_d$	J	T	$V_{\rm JUN45}$	$V_{\rm G}$
3	3	3	3	1	0	−1.0684	−0.8184	5	5	9	9	1	0	−0.8714	−0.8814	3	1	3	1	1	1	0.5150	0.1459
3	3	3	3	3	0	−2.0445	−1.7455	5	5	9	9	3	0	−0.3035	−0.3041	3	1	3	1	2	1	−0.2137	−0.6902
3	3	3	5	1	0	0.0861	0.0385	5	5	9	9	5	0	−0.1580	−0.1574	3	1	5	5	2	1	−0.3992	−0.3620
3	3	3	5	3	0	0.4040	0.3920	5	1	5	1	2	0	−0.5993	−0.3669	3	1	5	1	2	1	−0.2440	−0.4820
3	3	3	1	1	0	1.6046	1.5645	5	1	5	1	3	0	−1.7471	−1.3962	3	1	9	9	2	1	0.2161	0.2559
3	3	5	5	1	0	0.1354	0.1708	5	1	9	9	3	0	−0.1898	−0.1837	3	9	3	9	3	1	−0.3907	−0.8340
3	3	5	5	3	0	0.0069	−0.0134	5	9	5	9	2	0	−3.4022	−3.4170	3	9	3	9	4	1	0.0278	−0.0564
3	3	5	1	3	0	0.0353	0.0293	5	9	5	9	3	0	−1.8885	−1.6384	3	9	3	9	5	1	−0.1312	−0.1621
3	3	1	1	1	0	0.5883	0.6636	5	9	5	9	4	0	−1.2615	−0.9664	3	9	3	9	6	1	0.7710	0.0186
3	3	9	9	1	0	0.5723	0.5768	5	9	5	9	5	0	−1.4200	−1.1302	3	9	5	9	3	1	0.4086	0.3964
3	3	9	9	3	0	0.4317	0.4404	5	9	5	9	6	0	−0.7879	−0.4261	3	9	5	9	4	1	0.2286	0.0922
3	5	3	5	1	0	−1.9118	−1.8396	5	9	5	9	7	0	−1.9539	−1.8837	3	9	5	9	5	1	0.1110	0.2393
3	5	3	5	2	0	−1.3183	−1.1537	5	9	1	9	4	0	−0.5829	−0.7882	3	9	5	9	6	1	−0.1824	0.0572
3	5	3	5	3	0	−0.6974	−0.4232	5	9	1	9	5	0	−0.6245	−0.8828	3	9	1	9	4	1	0.0506	−0.2213
3	5	3	5	4	0	−1.5765	−1.2638	1	1	1	1	1	0	−1.1597	−0.9246	3	9	1	9	5	1	−0.1161	0.4101
3	5	3	1	1	0	−0.6039	−0.6059	1	1	9	9	1	0	−0.2570	−0.2518	5	5	5	5	0	1	−1.1849	−1.6000
3	5	3	1	2	0	−0.4551	−0.4510	1	9	1	9	4	0	−1.2904	−1.4070	5	5	5	5	2	1	−0.0551	−0.1964
3	5	5	5	1	0	0.4494	0.5214	1	9	1	9	5	0	−0.6868	−0.8081	5	5	5	5	4	1	0.2520	0.3815
3	5	5	5	3	0	0.3725	0.4074	9	9	9	9	1	0	−1.1378	−0.9402	5	5	5	1	2	1	−0.3796	−0.5008
3	5	5	1	2	0	0.7192	0.8048	9	9	9	9	3	0	−0.5987	−0.3970	5	5	1	1	0	1	−0.5890	−0.7210
3	5	5	1	3	0	0.7098	0.7171	9	9	9	9	5	0	−0.3830	−0.3685	5	5	9	9	0	1	1.5628	1.8939
3	5	1	1	1	0	0.4903	0.5530	9	9	9	9	7	0	−0.5605	−0.6596	5	5	9	9	2	1	0.4302	0.3594
3	5	9	9	1	0	0.2610	0.2852	9	9	9	9	9	0	−2.2067	−1.7927	5	5	9	9	4	1	0.2260	0.1783
3	5	9	9	3	0	−0.0803	−0.0567	3	3	3	3	0	1	−0.6492	−1.0554	5	1	5	1	2	1	−0.4100	−0.4021
3	1	3	1	1	0	−2.2696	−2.3363	3	3	3	3	2	1	0.2459	−0.3098	5	1	5	1	3	1	0.4051	0.2304
3	1	3	1	2	0	−1.9496	−1.9404	3	3	3	5	2	1	−0.3536	−0.1472	5	1	9	9	2	1	0.6536	0.4821
3	1	5	5	1	0	−0.1361	−0.1129	3	3	3	1	2	1	−0.5932	−0.5358	5	9	5	9	2	1	−0.4912	−0.6468
3	1	5	1	2	0	0.5858	0.6340	3	3	5	5	0	1	−0.8404	−0.8959	5	9	5	9	3	1	−0.1689	−0.2718
3	1	1	1	1	0	0.3466	0.3581	3	3	5	5	2	1	−0.3949	−0.1738	5	9	5	9	4	1	0.3020	0.0654
3	1	9	9	1	0	−0.6070	−0.5544	3	3	5	1	2	1	−0.2312	−0.2053	5	9	5	9	5	1	0.2901	−0.1726
3	9	3	9	3	0	−0.7602	−0.8334	3	3	1	1	0	1	−1.2153	−1.2903	5	9	5	9	6	1	0.4587	0.1383
3	9	3	9	4	0	−0.6201	−0.6600	3	3	9	9	0	1	1.1553	0.9800	5	9	5	9	7	1	−0.8117	−1.1289
3	9	3	9	5	0	−0.1087	−0.1499	3	3	9	9	2	1	0.5269	0.3715	5	9	1	9	4	1	−0.0559	−0.1510
3	9	3	9	6	0	−1.6766	−1.8878	3	5	3	5	1	1	0.3994	−0.1330	5	9	1	9	5	1	−0.1922	−0.4556
3	9	5	9	3	0	0.6525	0.7944	3	5	3	5	2	1	0.2848	0.0509	1	1	1	1	0	1	0.0309	−0.2500
3	9	5	9	4	0	−0.4157	−0.5424	3	5	3	5	3	1	0.3447	0.2108	1	1	9	9	0	1	0.6420	0.6771
3	9	5	9	5	0	0.0521	0.1719	3	5	3	5	4	1	−0.2842	−0.5282	1	9	1	9	4	1	0.2673	−0.0222
3	9	5	9	6	0	−0.6235	−0.7274	3	5	3	1	1	1	−0.0276	−0.0253	1	9	1	9	5	1	0.0128	−0.4597
3	9	1	9	4	0	−0.8237	−0.9745	3	5	3	1	2	1	−0.3659	−0.2212	9	9	9	9	0	1	−1.6907	−1.2762
3	9	1	9	5	0	0.1758	0.3079	3	5	5	5	2	1	−0.6209	−0.0882	9	9	9	9	2	1	−0.9594	−0.7383
5	5	5	5	1	0	−0.7273	−0.7330	3	5	5	5	4	1	−0.3904	−0.3603	9	9	9	9	4	1	−0.0871	−0.2925
5	5	5	5	3	0	−0.2237	−0.3180	3	5	5	1	2	1	−0.2977	−0.4322	9	9	9	9	6	1	0.1515	−0.0869
5	5	5	5	5	0	−1.7087	−1.6931	3	5	5	1	3	1	0.2066	−0.0865	9	9	9	9	8	1	0.2689	0.0159
5	5	5	1	3	0	−0.6877	−0.6609	3	5	9	9	2	1	0.4910	0.3718								
5	5	1	1	1	0	−0.2295	−0.2372	3	5	9	9	4	1	0.3972	0.3886								

matrix elements tend to be more attractive, while the $T = 1$ matrix elements tend to be more repulsive. Large changes appear mainly in the monopole-related diagonal matrix elements with large values of the total angular momentum J.

In our discussions below, we introduce the shorthand notation $V(abcd; JT)$ for the TBME $\langle ab|V|cd\rangle_{J,T}$, where a, b, ... stand for the single-particle orbits. We note that large modifications are found also in the monopole pairing matrix elements among like nucleons. These matrix elements are given by the shorthand notation $V(aabb; 01)$.

It has been pointed out that the realistic interaction can be improved for practical descriptions of experimental data by modifying its "monopole" part [33]. The monopole part of the interaction is important for the description of bulk properties of nuclei such as binding energies and shell gaps. It is difficult to derive this part quantitatively in a microscopic way from

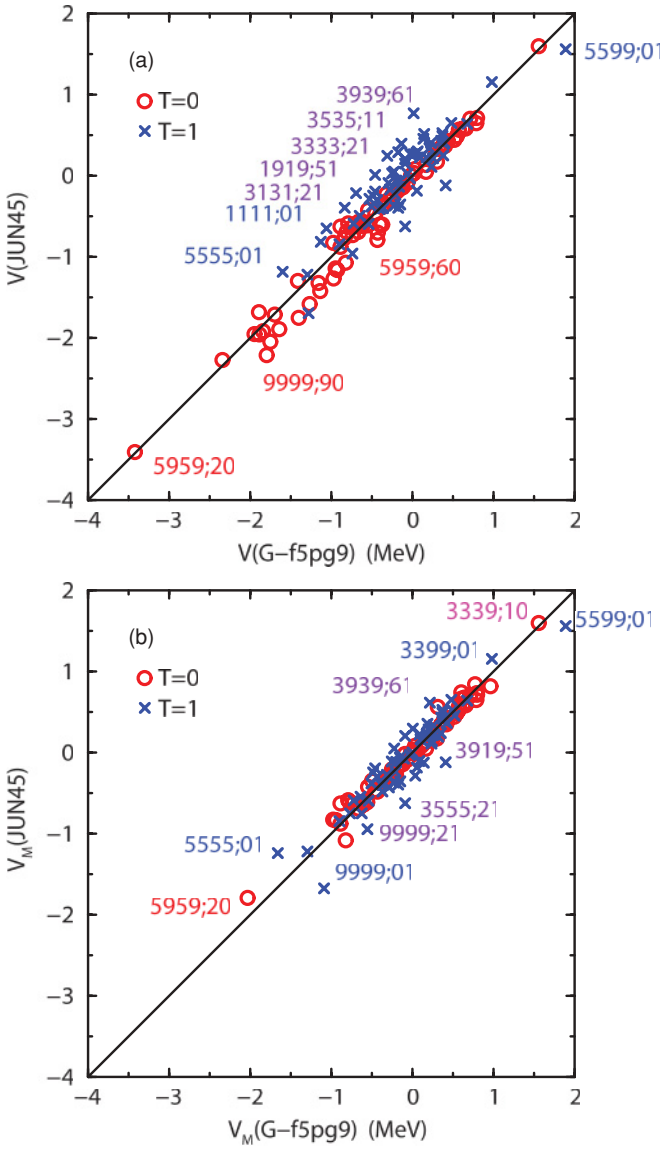

FIG. 2. (Color online) (a) Correlations in the TBME $V(abcd;JT)$ between the G-f5pg9 and the JUN45. The $T=0$ and $T=1$ matrix elements are shown by open circles and crosses, respectively. The quantum numbers are shown for several matrix elements by using the notation $2j_a2j_b2j_c2j_d;JT$. (b) Correlations in the monopole-subtracted TBME V_M between the G-f5pg9 and the JUN45.

realistic two-body interaction models. Therefore, it is argued that such monopole corrections come from three-body forces. We do not consider here such three-body forces explicitly but investigate the possibility to renormalize their effects empirically via effective two-body interactions. The matrix elements (centroids) of the monopole Hamiltonian are defined as the angular-momentum-averaged diagonal matrix elements: $V(ab;T)=\sum_J(2J+1)V(abab;JT)/\sum_J(2J+1)$. Thus, the modifications of the diagonal TBME affect the monopole properties of the interaction.

The lower panel of Fig. 2 shows similar correlations for the monopole-subtracted TBME. These elements are defined as

TABLE II. Comparison of the monopole-subtracted two-body matrix elements $V_M(abcd;JT)$ (MeV) for which the difference between G-f5pg9 and JUN45 is larger than 300 keV.

$2j_a$	$2j_b$	$2j_c$	$2j_d$	J	T	G	JUN45	Difference
9	9	9	9	0	1	−1.0882	−1.6745	−0.5863
3	5	5	5	2	1	−0.0882	−0.6209	−0.5327
3	9	1	9	5	1	0.4101	−0.1161	−0.5262
9	9	9	9	2	1	−0.5503	−0.9432	−0.3929
5	5	9	9	0	1	1.8939	1.5628	−0.3311
3	9	3	9	5	1	0.0351	−0.2836	−0.3187
3	9	3	9	6	1	0.2158	0.6186	+0.4028
5	5	5	5	0	1	−1.6568	−1.2387	+0.4181

$V_M(abcd;JT)=V(abcd;JT)-V(ab;T)\delta_{ac}\delta_{bd}$. The similarity of the TBME between the G-f5pg9 and the JUN45 are more significant after the subtraction of the monopole part, indicating that the modifications by the empirical fitting calculations were made mainly in the monopole part.

Table II lists several monopole-subtracted TBME for which the difference between the G-f5pg9 and the JUN45 is large. Note that all of them are $T=1$ ones, suggesting that the $T=0$ TBME of the starting G-f5pg9 interaction is already good and thus almost unaffected by the fit except for the monopole part. Most of the large modifications are related to the $g_{9/2}$ orbit, including both monopole pairing and quadrupole pairing. It can be seen that the monopole paring matrix elements including the $f_{5/2}$ orbit are also largely modified. Furthermore, the diagonal matrix elements with large J between the $p_{3/2}$ and the $g_{9/2}$ orbits are largely modified to be more attractive (repulsive) for $J=6$ ($J=5$).

The monopole centroids are shown in Fig. 3 for several effective interactions. From the comparison between the

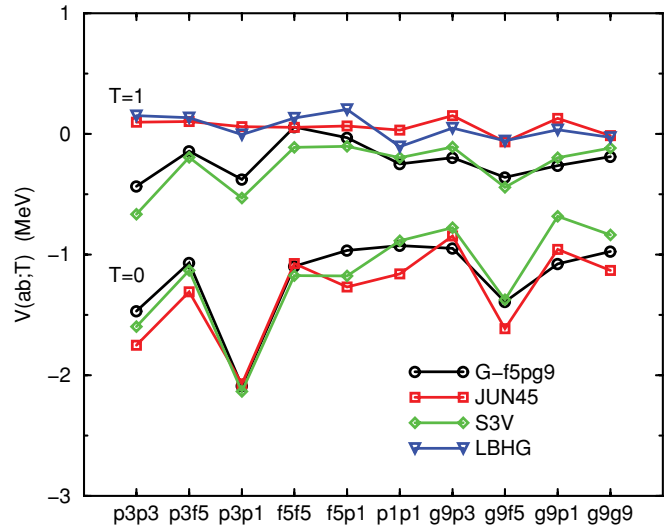

FIG. 3. (Color online) Comparison of the monopole matrix elements $V(ab;T)$ among the effective interactions G-f5pg9, JUN45, and S3V [24,25], which are shown by circles, squares, and diamonds, respectively. For $T=1$, the centroids for the LBHG interaction [23] are also shown by triangles. Lines are drawn to guide the eyes. The orbit-pair label "p3f5" stands for $a=p_{3/2}$ and $b=f_{5/2}$, for example.

JUN45 interaction and the G-f5pg9 interaction, we note that the modification to the realistic interaction is relatively large and repulsive for the $T = 1$ matrix elements, while it is small and attractive in most cases for the $T = 0$ matrix elements.

As for the $T = 0$ centroids, modifications to the f5-p1 and the p1-p1 matrix elements are relatively large. However, these modifications should not be taken seriously, because these centroids are related to only three TBME that may suffer from large uncertainties in the fit. Note also that these f5-p1 and p1-p1 TBME mainly affect the energy levels of $N \sim Z \sim 34$ to 38 nuclei, which are excluded from the input data for the fit. On the other hand, the modifications to the p1-g9, p3-g9, and f5-g9 centroids can be of significant importance for the shell evolution, i.e., the change of the shell structure due to the filling of specific single-particle orbits.

The fitting calculations have enlarged the differences among the p1-g9, p3-g9 centroids, and the f5-g9 centroid. The latter centroid is about 0.4 MeV in the original G-f5pg9 and is modified to be about 0.8 MeV in the JUN45. Because of this large difference, the effective single-particle energy (ESPE) of the proton $f_{5/2}$ orbit comes down rapidly relative to the $p_{3/2}$ orbit as the neutron $g_{9/2}$ orbit is occupied for $N > 40$, and it becomes lower than the $p_{3/2}$ for $N > 48$, as shown in the upper panel of Fig. 4. Such a change of the shell structure is needed to reproduce the low-lying energy levels of Cu isotopes as shown in the lower panel of Fig. 4. The original G-f5pg9 interaction does show such a shell-evolution effect, but it is not enough quantitatively. The S3V interaction gives almost the same differences in these centroids as those of the JUN45. The centroids of the Sussex matrix elements, on which the S3V interaction is based, are similar to those of the G-f5pg9 interaction, indicating strong similarities between various realistic interactions. In the derivation of the S3V interaction, in order to improve the description of $N = 49$ and 48 nuclei, Sinatkas *et al.* modified these centroids by multiplying the p1-g9 and p3-g9 diagonal part of the original Sussex matrix elements by a factor 0.68 and 0.88, respectively. This resulted in reasonable monopole corrections. This fact highlights the needs for empirical modifications of the microscopic effective interaction.

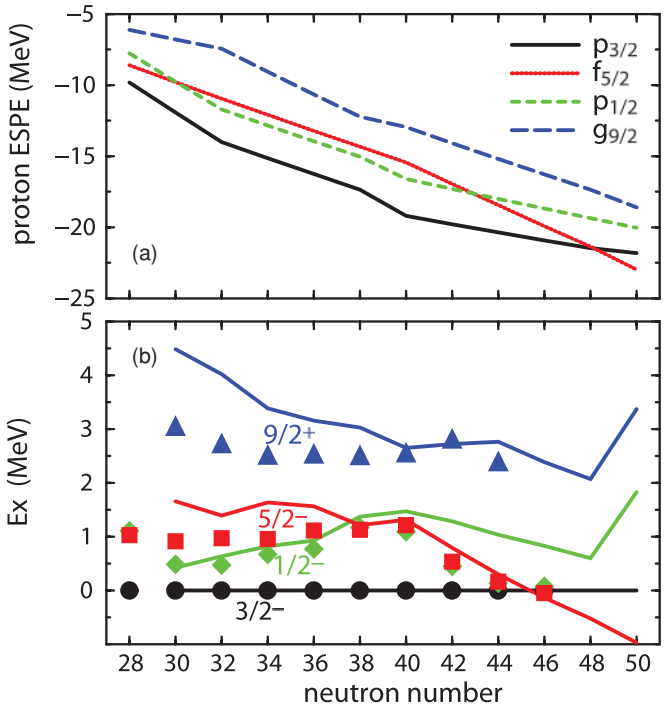

FIG. 4. (Color online) (a) Effective single-particle energies of proton orbits for Cu isotopes. (b) Comparison of the excitation energies of the lowest $1/2^-$, $5/2^-$, and $9/2^+$ states relative to the lowest $3/2^-$ state for odd-A Cu ($Z = 29$) isotopes between the experimental data (filled symbols) and the shell-model results (lines). Data are taken from Refs. [4,34,35].

As for the $T = 1$ part, the realistic interactions G-f5pg9 and S3V look, as expected, quite similar to each other. The fitted interactions JUN45 and LBHG of Ref. [23] are also similar, except for the f5-p1 and the p1-p1 centroids that is attributed to the uncertainty in the $T = 0$ part mentioned above.

The $T = 1$ monopole property can, in principle, affect the development of the shell structure as the $T = 0$ part does. For example, in the case of the pf shell, the effective interaction GXPF1 predicts a possible development of the $N = 34$ shell gap in neutron-rich Ca isotope mainly due to the $T = 1$ monopole effect [36], although it has not yet been confirmed experimentally. In the GXPF1, the p3-f5 centroid is more repulsive than the p3-p3 or p3-p1 centroid by about 0.35 MeV. These differences in the centroids enlarge the energy gap between the neutron $p_{1/2}$ orbit and the $f_{5/2}$ orbit as neutrons occupy the $p_{3/2}$ and $p_{1/2}$ orbits, giving rise to the $N = 34$ shell closure.

However, in the present f_5pg_9 model space, such a dramatic effect cannot be expected because the $T = 1$ monopole centroids of the JUN45 interaction show rather weak orbit dependence (see Fig. 3). In fact, in the JUN45 interaction, the value of the $T = 1$, f5-p3 centroid is almost the same as that of the GXPF1, while the p3-p3 and p3-p1 centroids are more repulsive than those of the GXPF1 by about 0.35 MeV. As a result, the values of these centroids become similar with each other, and the differences in the resultant neutron ESPE among the $p_{3/2}$, $f_{5/2}$, and $p_{1/2}$ orbits become almost constant for $28 < N < 40$, which is typically seen in Fig. 14 for the case of Ni isotopes.

It should be noted that the same centroid takes different value between the pf shell and the f_5pg_9 shell. Such a difference is already seen between the starting microscopic effective interactions, the G-pf and the G-f5pg9, both of which have been derived from the Bonn-C potential. In other words, the difference originates partly in the renormalization of the $f_{7/2}$ orbit. In fact, the values of the p3-p3, p3-f5, and p3-p1 centroids in the G-pf interaction are -0.588, -0.034, and -0.471 MeV, respectively, while the corresponding values are -0.434, -0.143, and -0.377 MeV in the G-f5pg9 interaction. Thus, the renormalization of the $f_{7/2}$ orbit gives the corrections of these centroids by $+0.154$, -0.109, and $+0.094$ MeV, respectively, which reduces the difference among these centroids. This explains partly the weaker orbit dependence of the $T = 1$ centroids in the JUN45 interaction.

III. RESULTS AND DISCUSSIONS

A. Binding energy

Binding energies are evaluated by taking into account the Coulomb energies according to the empirical formula given by Cole [37]

$$E_C(\pi,\nu) = \pi\varepsilon_C + \tfrac{1}{2}\pi(\pi-1)V_C + \left[\tfrac{1}{2}\pi\right]b_C + \pi\nu\Delta_{np}, \quad (1)$$

where π (ν) stands for the number of valence protons (neutrons). We use the parameter set 2 in Table I of Ref. [37] for values of ε_C, V_C, b_C, and Δ_{np}, which were determined by fitting to the measured Coulomb displacement energies of $28 \leqslant Z \leqslant 42$ and $32 \leqslant N \leqslant 50$ nuclei. The difference between experimental binding energies and the shell-model results are shown in Fig. 5. As for the isotope chains, it can be seen that the agreement is reasonable for $Z \geqslant 32$. The largest discrepancy is found in the Ni isotopes, partly because no data on Ni isotopes were included in the fit. The shell-model predictions result in underbinding for $N < 40$ and overbinding for $N > 40$, which can be understood by considering the effects of the missing $f_{7/2}$ orbit in the present model space. Because the $T = 0$ monopole attraction between the $\pi f_{7/2}$ and $\nu f_{5/2}$ [39] is much stronger than that of the $\pi f_{7/2}$ and $\nu g_{9/2}$ due to the tensor interaction [15], if the $f_{7/2}$ orbit were included, it should have relatively enhanced the binding for $N < 40$ and reduced for $N > 40$. The similar but somewhat weaker effect is found also among the Cu isotopes. Among the Zn and the Ga isotopes, the discrepancy is significant for $N > 40$, and the odd-even staggering is large. This result suggests a possible problem in the description of pairing correlations related to the $g_{9/2}$ orbit. Because there is only one positive parity orbit in the present model space, the blocking effect may be somewhat overestimated.

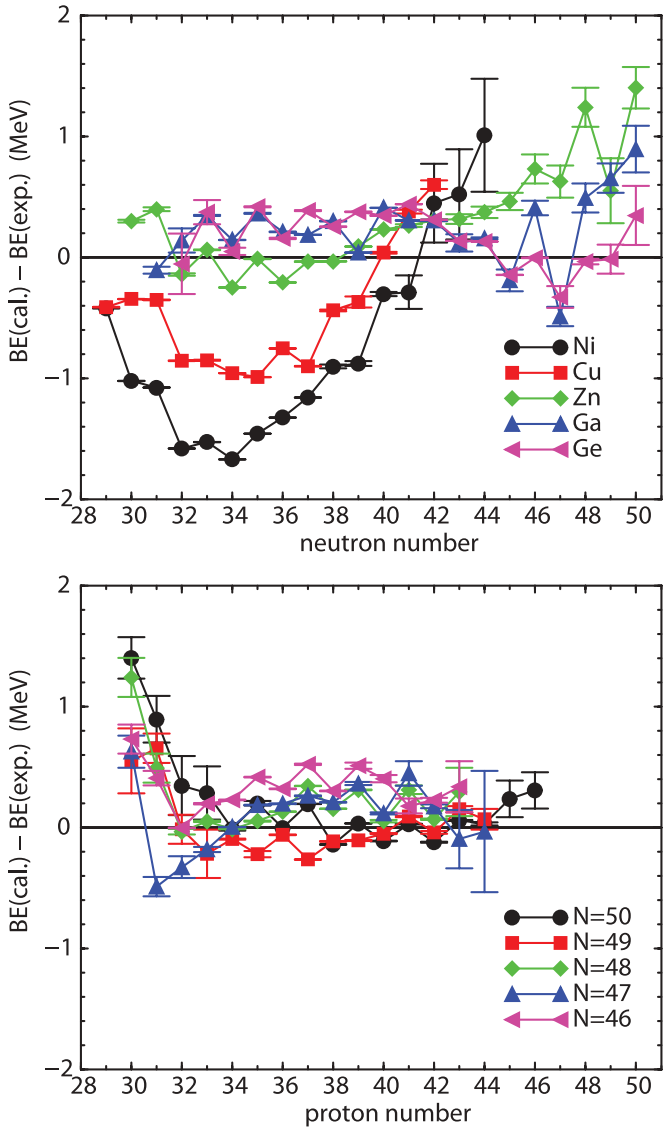

FIG. 5. (Color online) Differences between the experimental and the calculated binding energies for (a) $28 \leqslant Z \leqslant 32$ isotopes as a function of the neutron number and for (b) $46 \leqslant N \leqslant 50$ isotones as a function of the proton number. Experimental data are taken from Ref. [38].

The agreement between the experimental data and the shell-model results looks reasonable for the isotone chains with $N = 46 \sim 50$ and $Z \geqslant 32$. This result contrasts the case of the valence mirror counterparts, isotope chains with $Z = 28 \sim 32$. Such a difference can naturally be understood if we assume that the $N = 50$ shell closure is more stable than the $Z = 28$ closure, although the choice of the data for the fitting calculations is not symmetric.

B. Magnetic dipole moments

The magnetic dipole moments are calculated and compared with experimental data in Table III. The magnetic moment operator used in the present calculation is

$$\boldsymbol{\mu} = g_s\boldsymbol{s} + g_l\boldsymbol{l}, \quad (2)$$

where g_s and g_l are the spin and the orbital g factors, respectively.

By using the free-nucleon g factors $g_s = 5.586$, $g_l = 1$, for protons and $g_s = -3.826$, $g_l = 0$ for neutrons, the agreement between calculations ($\mu_{\rm th}^{\rm free}$) and experiment ($\mu_{\rm exp}$) appears to be reasonable. However, in Fig. 6, one can find small but systematic deviations from the diagonal line in several data points. Such deviations disappear almost when we introduce effective spin g factors, $g_s^{(\rm eff.)} = 0.7 g_s^{(\rm free)}$. Here, the "quenching" factor $q_s = 0.7$ is determined via a least squares fit to the experimental data. If we introduce also the effective orbital g factors in the form as $g_l^{(\rm eff.)} = g_l^{(\rm free)} \pm \delta g_l$ (+ for protons and − for neutrons) in order to take into account the effect of exchange currents, the least-squares fit gives $q_s = 0.65$ and $\delta g_l = 0.3$, but the improvement is almost negligible. Thus in Table III we show the results of $q_s = 0.7$ and $\delta g_l = 0$.

It has been discussed that in the case of $0\hbar\omega$ calculations for shells like the sd shell [45] and the pf shell [13], the free-nucleon g factors give a very good description of experimental data. The introduction of effective g factors gives only slight improvements due to the cancellation between configuration mixing effects and exchange currents. In contrast, in the present f_5pg_9 shell, the calculated magnetic moment definitely demands the quenching factor q_s. Note that the present value

TABLE III. Comparisons of experimental magnetic dipole moments $\mu_{\rm exp}$ (in unit μ_N) with theoretical values $\mu_{\rm th}^{\rm free}$ and $\mu_{\rm th}^{\rm eff}$, which are calculated by using the free and the effective g factors, respectively. The excitation energies (E_x) are also shown. Most of the data are taken from Refs. [34,40].

Nucl.	J^π	E_x (MeV)		Magnetic moment (μ_N)		
		Exp.	Cal.	$\mu_{\rm exp}$	$\mu_{\rm th}^{\rm free}$	$\mu_{\rm th}^{\rm eff}$
^{57}Ni	$3/2^-$	0.000	0.000	−0.7975(14)	−1.913	−1.339
^{58}Ni	2^+	1.454	1.298	+0.076(18)	−0.703	−0.492
^{59}Ni	$5/2^-$	0.339	0.542	+0.35(15)	1.132	0.792
^{60}Ni	2^+	1.333	1.635	+0.32(6)	−0.270	−0.189
^{61}Ni	$3/2^-$	0.000	0.080	−0.75002(4)	−1.308	−0.916
	$5/2^-$	0.067	0.000	+0.480(6)	1.055	0.739
^{62}Ni	2^+	1.173	1.820	+0.33(5)	0.108	0.076
^{63}Ni	$5/2^-$	0.087	0.000	+0.752(3)	1.197	0.838
^{64}Ni	2^+	1.346	1.637	+0.37(6)	0.109	0.077
^{65}Ni	$5/2^-$	0.000	0.008	0.69(6)	1.226	0.858
	$9/2^+$	1.017	0.667	−1.332(14)[a]	−1.876	−1.313
^{67}Ni	$(1/2)^-$	0.000	0.000	+0.601(5)	0.646	0.452
	$(9/2^+)$	1.007	0.510	0.56(3)	−1.894	−1.326
^{57}Cu	$3/2^-$	0.000	0.000	+2.582(7)[b]	3.793	2.955
^{59}Cu	$3/2^-$	0.000	0.000	+1.891(9)	3.010	2.263
^{60}Cu	2^+	0.000	0.000	+1.219(3)	2.785	2.057
^{61}Cu	$3/2^-$	0.000	0.000	+2.14(4)	3.179	2.422
^{62}Cu	1^+	0.000	0.159	−0.380(4)	−1.110	−0.841
	2^+	0.041	0.000	+1.32(3)	2.324	1.724
	4^+	0.390	0.239	+2.67(16)	4.392	3.338
^{63}Cu	$3/2^-$	0.000	0.000	+2.22329(18)	3.247	2.490
	$17/2^+$	4.498	4.144	+1.56(10)	2.561	2.057
^{64}Cu	1^+	0.000	0.031	−0.217(2)	−0.763	−0.592
	6^-	1.594	1.409	+1.06(3)	1.358	1.158
^{65}Cu	$3/2^-$	0.000	0.000	+2.38167(25)	3.292	2.535
	$5/2^-$	1.116	1.569	+4.4(9)	1.787	1.491
^{66}Cu	1^+	0.000	0.067	−0.282(2)	2.854	2.179
	$(6)^-$	1.154	0.661	+1.038(3)	1.460	1.262
^{67}Cu	$3/2^-$	0.000	0.000	2.54(2)[c]	3.346	2.598
^{68}Cu	1^+	0.000	0.090	+2.48(8)	3.069	2.363
	(6^-)	0.722	0.451	+1.24(8)	1.576	1.385
^{69}Cu	$3/2^-$	0.000	0.000	+2.84(1)	3.541	2.758
	$13/2^+$	2.714	2.731	+1.46(16)	1.697	1.472
^{70}Cu	(6^-)	0.000	0.092	(+)1.50(11)	1.762	1.536
	(3^-)	0.101	0.000	(−)3.50(13)	−4.326	−3.233
	1^+	0.243	0.297	+1.86(4)	2.941	2.261
^{71}Cu	$3/2^-$	0.000	0.000	+2.2747(8)[c,d]	3.395	2.645
^{73}Cu	$3/2^-$	0.000	0.000	+1.7426(8)[d]	3.255	2.536
^{75}Cu	$5/2^-$	0.000	0.000	+1.0062(13)[d]	0.563	1.129
^{62}Zn	2^+	0.954	0.939	+0.7(2)	0.869	0.840
^{63}Zn	$3/2^-$	0.000	0.000	−0.28164(5)	−0.441	−0.256
^{64}Zn	2^+	0.992	0.942	+0.89(6)	0.842	0.804
	4^+	2.307	2.188	+2.1(6)	1.390	1.298
	3^-	2.999	3.717	+1.5(9)	−1.341	−0.953
	7^-	4.635	4.172	1.6(3)	0.006	0.145
^{65}Zn	$5/2^-$	0.000	0.000	+0.7690(2)	1.263	0.938
	$3/2^-$	0.115	0.174	−0.78(20)	−0.242	−0.126
	$3/2^-$	0.207	0.377	+0.73(25)	0.028	0.072
	$9/2^+$	1.065	1.066	−1.73(49)	−1.648	−1.125
^{66}Zn	2^+	1.039	1.059	+0.80(8)	1.135	1.030
^{67}Zn	$5/2^-$	0.000	0.011	+0.875479(9)	1.388	1.008
	$1/2^-$	0.093	0.000	+0.587(11)	0.674	0.482
	$3/2^-$	0.185	0.374	+0.50(6)	0.768	0.588
	$9/2^+$	0.605	0.458	−1.097(9)	−1.685	−1.154
^{68}Zn	2^+	1.077	1.104	+0.87(10)	1.229	1.078
^{69}Zn	$9/2^+$	0.439	0.257	1.157(2)	−1.691	−1.156
^{70}Zn	2^+	0.884	1.108	0.76(8)	1.143	1.061
^{71}Zn	$9/2^+$	0.158	0.000	(−)1.035(18)	−1.700	−1.159
^{66}Ga	$(2)^+$	0.066	0.041	1.011(18)	1.186	0.967
	(7)[e]	1.464	1.420	+0.903(21)	−1.323	−0.263
	(9^+)	3.043	4.444	4.2(9)	4.497	4.256
^{67}Ga	$3/2^-$	0.000	0.000	+1.8507(3)	1.865	1.588
	$5/2^-$	0.359	0.479	1.40(65)	0.663	1.093
	$15/2^+$	3.578	3.342	−1.69(47)	−0.543	0.224
^{68}Ga	1^+	0.000	0.000	0.01175(5)	0.168	0.137
	7^-	1.230	0.997	+0.74(2)	−1.096	−0.061
^{69}Ga	$3/2^-$	0.000	0.000	+2.01659(4)	2.019	1.715
^{70}Ga	4^-	0.879	0.169	−0.26(10)	−0.135	−0.213
^{71}Ga	$3/2^-$	0.000	0.000	+2.56227(2)	2.645	2.188
^{72}Ga	3^-	0.000	0.200	0.13224(2)	−1.342	−1.048
^{67}Ge	$9/2^+$	0.752	0.867	−0.849(18)	−1.378	−0.870
^{68}Ge	2^+	1.016	0.960	+1.10(28)[f]	0.953	0.926
	6^+	3.696	3.801	+2.4()	1.889	2.069
	6^-	3.883	3.345	0.53(11)	−0.407	−0.100
	7^-	4.054	3.634	0.78(12)	0.309	0.473
	8^+	4.837	4.805	+0.8(3)	−2.259	−1.389
	8^+	5.050	5.390	−2.2(11)	−0.024	0.552
^{69}Ge	$5/2^-$	0.000	0.000	0.735(7)	1.397	1.051
	$9/2^+$	0.398	0.306	−1.0011(32)	−1.470	−0.952
^{70}Ge	2^+	1.040	0.905	+0.936(52)	0.684	0.711
^{71}Ge	$1/2^-$	0.000	0.000	+0.547(5)	0.607	0.438
	$5/2^-$	0.175	0.075	+1.018(10)	1.431	1.060
	$9/2^+$	0.198	0.107	−1.0413(7)	−1.540	−1.014
^{72}Ge	2^+	0.834	0.811	+0.798(66)	0.542	0.608
^{73}Ge	$9/2^+$	0.000	0.058	−0.8794677(2)	−1.480	−0.963
	$5/2^+$	0.013	0.625	−1.08(3)	−1.789	−1.377
^{74}Ge	2^+	0.596	0.717	+0.87(4)	0.495	0.578
	2^+	1.204	1.350	+0.82(24)	1.136	1.148
^{75}Ge	$1/2^-$	0.000	0.151	+0.510(5)	0.607	0.425
^{76}Ge	2^+	0.563	0.744	+0.838(46)	0.608	0.694
^{68}As	$9(^+)$	2.158	2.305	2.07(18)	4.767	4.527
^{69}As	$5/2^-$	0.000	0.000	+1.58(16)	0.884	1.305
	$9/2^+$	1.307	1.335	+4.72(58)	5.308	4.672
^{70}As	4^+	0.000	0.002	+2.1061(2)	1.770	1.940
	7^-	0.888	0.497	0.75(5)	−0.569	0.411
^{71}As	$5/2^-$	0.000	0.006	(+)1.6735(18)	0.826	1.278
	$9/2^+$	1.000	0.921	+5.15(9)	5.685	5.024
^{72}As	2^-	0.000	0.050	−2.1566(3)	−1.651	−1.608
	3^+	0.214	0.255	+1.580(18)	1.078	1.122
	$7(^-)$	0.563	0.513	+0.696(12)	−0.464	0.516
^{73}As	$5/2^-$	0.067	0.261	+1.63(10)	0.777	1.246
	$9/2^+$	0.428	0.920	+5.234(14)	5.686	5.024
^{74}As	2^-	0.000	0.560	−1.597(3)	−1.132	−1.057
	$(4)^+$	0.259	0.917	+3.24(4)	3.065	2.548
^{75}As	$3/2^-$	0.000	0.000	+1.439475(65)	1.506	1.333
	$3/2^-$	0.265	0.528	+0.98(19)	0.652	0.780
	$5/2^-$	0.280	0.442	+0.918(18)	0.792	1.183
^{76}As	2^-	0.000	0.100	−0.906(5)	−0.554	−0.555

TABLE III. (*Continued.*)

Nucl.	J^π	E_x (MeV)		Magnetic moment (μ_N)		
		Exp.	Cal.	$\mu_{\rm exp}$	$\mu_{\rm th}^{\rm free}$	$\mu_{\rm th}^{\rm eff}$
	$(1)^+$	0.044	0.286	+0.559(5)	−0.136	−0.165
^{77}As	$5/2^-$	0.264	0.212	+0.736(22)	0.473	0.982
	$9/2^+$	0.475	1.060	+5.525(9)	5.953	5.285
	$5/2^+$	0.632	1.742	+2.53(40)	4.389	3.754
^{79}Se	$7/2^+$	0.000	0.000	−1.018(15)	−1.288	−0.869
^{80}Se	2^+	0.666	0.726	0.87(5)	0.780	0.859
	2^+	1.449	1.716	0.70(20)	0.673	0.732
	4^+	1.702	1.784	2.7(10)	1.023	1.234
^{82}Se	2^+	0.655	0.728	+0.99(6)	0.866	0.955
	4^+	1.735	1.848	2.3(15)	1.579	1.787
^{80}Br	1^+	0.000	0.212	0.5140(6)	−0.331	−0.285
	2^-	0.037	0.000	−1.67(12)	−2.027	−1.703
	5^-	0.086	0.069	+1.3177(6)	0.652	0.766
^{81}Br	$3/2^-$	0.000	0.000	+2.270562(4)	2.101	1.793
	$5/2^-$	0.276	0.222	1.6(5)	1.139	1.481
	$9/2^+$	0.536	0.766	5.694(45)	6.194	5.475
	$(5/2)^-$	0.767	0.692	1.0(4)	1.262	1.409
	$7/2^-$	0.837	0.946	1.4(4)	1.764	1.904
^{82}Br	5^-	0.000	0.068	+1.6270(5)	1.077	1.144
^{84}Br	2^-	0.000	0.000	1.9(7)	−1.655	−1.661
^{81}Kr	$7/2^+$	0.000	0.041	−0.909(4)	−1.245	−0.831
	$1/2^-$	0.191	0.232	+0.586(2)	0.590	0.411
^{82}Kr	2^+	0.776	0.882	+0.80(4)	0.480	0.589
	4^+	1.821	2.001	+1.2(8)	0.395	0.665
^{83}Kr	$9/2^+$	0.000	0.000	−0.970669(3)	−1.458	−0.938
	$7/2^+$	0.009	0.077	−0.943(2)	−1.185	−0.779
	$1/2^-$	0.042	0.134	0.591(2)	0.626	0.447
^{84}Kr	2^+	0.882	0.990	+0.53(3)	0.560	0.667
	8^+	3.236	3.319	−1.968(16)	−2.624	−1.712
	12^+	5.373	5.027	+2.04(12)	1.063	2.006
^{85}Kr	$9/2^+$	0.000	0.000	−1.0025(25)	−1.433	−0.929
	$1/2^-$	0.305	0.031	+0.633(2)	0.694	0.505
^{86}Kr	2^+	1.565	1.255	+2.24(28)	2.640	2.406
^{82}Rb	1^+	0.000	0.472	+0.5545083(11)	−0.217	−0.062
	5^-	0.069	0.130	+1.5100082(2)	0.511	0.656
	6^+	0.192	0.277	+4.02(5)	3.911	3.625
^{83}Rb	$5/2^-$	0.000	0.000	+1.42(5)	0.901	1.328
^{84}Rb	2^-	0.000	0.000	−1.324116(2)	−1.557	−1.454
	6^-	0.464	0.400	+0.2129331(10)	0.063	0.638
^{85}Rb	$5/2^-$	0.000	0.146	+1.3570(10)	0.943	1.409
	$9/2^+$	0.514	0.712	+6.046(10)	6.520	5.736
	$19/2^-$	2.827	3.047	+1.3(4)	0.406	0.818
^{86}Rb	2^-	0.000	0.000	−1.6920(14)	−1.960	−1.896
	6^-	0.556	0.231	+1.8150(10)	1.607	1.557
^{87}Rb	$3/2^-$	0.000	0.000	+2.75131(12)	2.937	2.412
^{83}Sr	$7/2^+$	0.000	0.078	−0.829(2)	−1.114	−0.717
	$1/2^-$	0.259	0.264	+0.581(4)	0.539	0.364
^{84}Sr	2^+	0.793	0.850	+0.84(10)	0.705	0.760
	5^-	2.769	2.723	+8.0(10)	4.751	4.509
	8^+	3.332	3.271	−1.2(6)	−2.265	−1.384
	7^-	3.488	3.287	+4.2(14)	0.532	0.698
	8^+	3.680	3.748	+7.2(8)	10.839	9.576
	10^+	4.448	4.205	+2.0(10)	−1.533	−0.612
	10^+	4.534	4.671	+8.0(20)	11.240	10.115
	9^-	4.636	4.241	+0.00(36)	0.528	0.847

TABLE III. (*Continued.*)

Nucl.	J^π	E_x (MeV)		Magnetic moment (μ_N)		
		Exp.	Cal.	$\mu_{\rm exp}$	$\mu_{\rm th}^{\rm free}$	$\mu_{\rm th}^{\rm eff}$
^{85}Sr	$9/2^+$	0.000	0.000	−0.9994(7)	−1.456	−0.941
	$1/2^-$	0.239	0.333	+0.599(2)	0.605	0.432
^{86}Sr	2^+	1.077	1.177	+0.55(10)	0.574	0.659
	8^+	2.956	3.134	−1.920(24)	−2.479	−1.589
^{87}Sr	$9/2^+$	0.000	0.000	−1.0928(7)	−1.471	−0.967
	$1/2^-$	0.389	0.216	+0.624(4)	0.711	0.532
^{88}Sr	2^+	1.836	1.830	+2.3(3)	2.305	2.194
^{85}Y	$9/2^+$	0.020	0.000	6.2(5)	6.379	5.614
	$5/2^-$	0.266	0.328	+1.33(8)	1.219	1.534
^{86}Y	4^-	0.000	0.000	<0.6	−0.014	0.032
	(8^+)	0.218	0.181	4.8(3)	4.577	4.318
	2^-	0.243	0.377	−1.06(6)	−1.229	−1.156
	(7^-)	0.302	0.929	−0.581(21)	−0.477	0.464
^{87}Y	$9/2^+$	0.381	0.403	6.05(7)	6.598	5.792
^{88}Y	$(8)^+$	0.674	0.823	+4.87(5)	4.758	4.452
^{89}Y	$1/2^-$	0.000	0.000	−0.1374154(3)	−0.269	0.012
	$9/2^+$	0.909	0.967	+6.23(7)	6.811	5.966
^{86}Zr	8^+	3.298	3.122	+2.2(37)	10.795	9.526
	8^+	3.533	3.154	+15(12)	−1.066	−0.377
	10^+	4.326	3.879	−5(10)	−0.181	0.497
	10^+	4.419	4.315	−7(11)	9.929	8.938
	(12^+)	5.396	4.863	−20(10)	2.342	2.745
	(12^+)	5.524	5.188	+6.6(16)	8.557	7.894
	(14^+)	6.321	5.938	+31(7)	6.212	6.100
^{87}Zr	$9/2^+$	0.000	0.000	−0.895(5)	−1.342	−0.841
	$(1/2)^-$	0.336	0.362	+0.642(16)	0.622	0.451
^{88}Zr	(8^+)	2.888	2.937	−1.811(16)	−2.448	−1.537
^{89}Zr	$9/2^+$	0.000	0.000	−1.076(20)	−1.482	−0.954
	$1/2^-$	0.588	0.515	+0.795(18)	0.786	0.602
	$(21/2)^+$	2.995	2.838	9.3(4)	9.283	8.380
^{90}Zr	2^+	2.186	2.226	+2.5(4)	2.968	2.614
	5^-	2.319	2.260	6.25(13)	6.389	5.881
	3^-	2.748	2.816	3.0(2)	3.411	3.261
	8^+	3.589	3.468	+10.85(6)	12.133	10.623
^{87}Nb	$(17/2^-)$	2.412	2.410	+7.0(9)	4.677	4.331
	$(21/2^+)$	2.491	2.608	+4.3(14)	3.786	3.829
	$(21/2^+)$	2.861	2.841	−6(11)	6.542	6.120
	$(23/2^+)$	3.220	3.112	+16(9)	3.351	3.514
	$(25/2^+)$	3.446	3.381	+3(2)	4.378	4.447
	$(25/2^+)$	3.742	3.757	+1(3)	5.465	5.327
	$(25/2^-)$	4.131	3.823	+6(5)	5.834	5.534
	$(29/2^-)$	5.010	4.814	+7(2)	6.048	5.852
^{89}Nb	$(9/2^+)$	0.000	0.067	6.216(5)	6.586	5.783
	$(21/2^+)$	2.193	2.353	+3.40(7)	3.249	3.404
^{90}Nb	8^+	0.000	0.000	4.961(4)	4.689	4.433
	6^+	0.122	0.142	+3.720(24)	3.493	3.307
	(11^-)	1.880	1.923	+8.778(33)	9.301	8.630
^{91}Nb	$(13/2^-)$	1.984	2.065	+8.14(13)	8.660	7.871
	$(17/2^-)$	2.034	2.146	+10.82(10)	11.682	10.519
	$(21/2)^+$	3.467	3.491	+12.4(19)	15.962	13.966
^{89}Mo	$(21/2^+)$	2.584	2.342	+8.3(4)	8.289	7.584
^{90}Mo	5^-	2.549	2.501	5.5(14)	5.898	5.437
	8^+	2.875	2.845	−1.391(14)	11.052	9.733
	12^+	4.556	4.427	6.0(7)	6.884	6.552
	11^-	4.842	4.634	4.6(14)	5.102	5.029

TABLE III. (*Continued.*)

Nucl.	J^π	E_x (MeV)		Magnetic moment (μ_N)		
		Exp.	Cal.	$\mu_{\rm exp}$	$\mu_{\rm th}^{\rm free}$	$\mu_{\rm th}^{\rm eff}$
^{91}Mo	$21/2(^+)$	2.267	2.066	+8.88(8)	9.075	8.266
	$(17/2^-)$	2.280	2.107	+4.51(6)	4.967	4.834
^{92}Mo	2^+	1.509	1.334	+2.3(3)	3.020	2.647
	8^+	2.760	2.571	+11.30(5)	12.058	10.575
	(11^-)	4.486	4.554	+13.88(28)	15.519	13.868
^{92}Tc	(11^-)	2.003	2.016	8.87(22)	9.179	8.501
^{93}Tc	$9/2^+$	0.000	0.000	6.32(6)	6.788	5.952
	$(17/2)^-$	2.185	2.282	+10.46(5)	11.723	10.545
^{93}Ru	$(21/2)^+$	2.083	1.931	+8.970(21)	8.760	7.999
	$(17/2^-)$	2.280	2.075	+4.36(17)	5.089	4.908
^{94}Ru	6^+	2.498	2.433	+8.12(5)	9.053	7.937
	8^+	2.643	2.503	+11.10(4)	12.064	10.579
	11^-	4.489	4.604	+14.1(1.7)	15.608	13.924
	12^+	4.716	4.772	+12.4(1.7)	18.072	15.853
^{95}Rh	$(17/2^-)$	2.236	2.311	+10.88(34)	11.867	10.637
^{96}Pd	8^+	2.531	2.461	+10.97(6)	12.068	10.582

[a]Data from Ref. [41].
[b]Data from Ref. [42].
[c]Data from Ref. [43].
[d]Data from Ref. [35].
[e]$J^\pi = 7^-$ is assumed for the calculation.
[f]Data from Ref. [44].

$q_s = 0.7$ is much smaller than that we obtained by similar calculations in the pf shell, $q_s = 0.9$ [13]. Because the present model space is incomplete with respect to the spin-orbit partners, in other words, the ^{56}Ni core is not LS closed, the first-order configuration mixing (e.g., Ref. [46]) affects the magnetic moment significantly.

As expected, the description of Ni isotopes is poor for both the magnetic moments and the excitation energies, especially for the even-N cases. It is true also for the Cu isotopes with $N < 36$. For all these nuclei, the shell model in the pf-shell space [13,43] successfully reproduces the data, and the discrepancy can be understood as the effect of the missing $f_{7/2}$ orbit in the present model space. On the other hand, for heavier Cu, the agreement between experimental data and the shell-model results is reasonable except for the $5/2^-$ state of ^{65}Cu and the 1^+ state of ^{66}Cu. As for the latter, the shell model predicts the 1_2^+ state at 94 keV with $\mu = -0.272\mu_N$, which may correspond to the experimental 1_1^+ state.

For the Zn isotopes, the shell-model description is reasonable in most cases except for the 3^- and the 7^- states of ^{64}Zn and the $3/2_1^-$ and the $3/2_2^-$ states of ^{65}Zn. In the case of ^{64}Zn, the calculated excitation energies deviate largely from the experimental data, suggesting that the calculated states do not correspond to the experimental ones. The $3/2^-$ doublets in ^{65}Zn are reasonably described in the pf-shell calculations, Ref. [13], a fact that hints at the importance of the $f_{7/2}$ orbit for these states. On the other hand, in the pf-shell results [13] for 2^+ states, the magnetic moments are predicted to be systematically too large by about $0.3\mu_N$. This problem has been remedied to some extent in the present calculation. In fact, the deviations are reduced almost by a factor of 1/2.

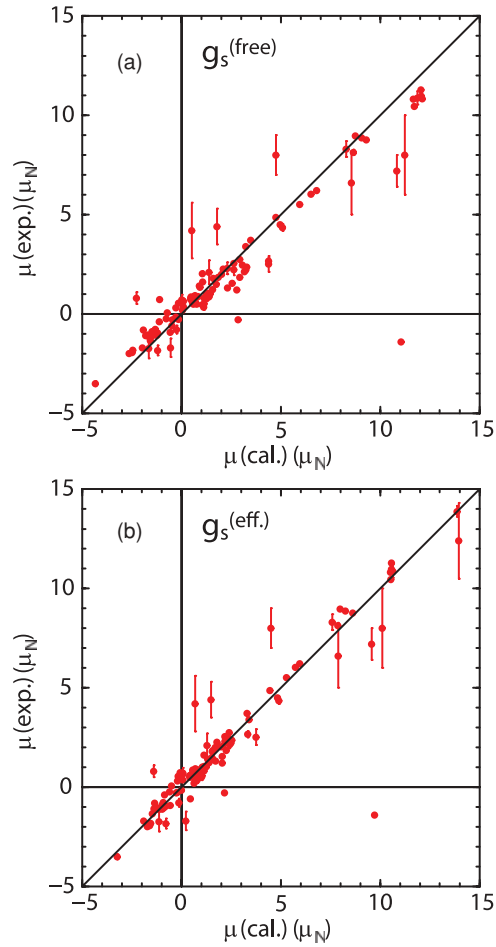

FIG. 6. (Color online) Comparisons of experimental magnetic dipole moments with the shell-model results. The latter are obtained by using (a) free and (b) effective nucleon g factors.

The calculated values for the 7^- states in ^{66}Ga and ^{68}Ga deviate largely from the experimental data. These values are very sensitive to the choice of the effective g factors. In order to improve the agreement, we need to take into account the orbital dependence. The difficulty in the 3^- state of ^{72}Ga is puzzling considering the reasonable agreement between the shell-model results and the experimental data in the neighboring nuclei.

In the calculated results for the Ge isotopes, relatively large deviations from the data can be seen for ^{68}Ge. As for the 6^- state, the 6_2^- state is predicted at 4.001 MeV with $\mu_{\rm th}^{\rm eff} = -0.409\mu_N$. The problem for the 8^+ doublet can be interpreted as a result of the incorrect prediction of their order. For the other Ge isotopes, the shell-model prediction is basically successful, and in most cases, the introduction of the effective spin g factors improves the description. Nevertheless, there remain small deviations from data by about 0.1–0.2μ_N.

As for the As isotopes, the shell-model description looks reasonable, except for the cases of the $9^{(+)}$ state in ^{68}As, the $(1)^+$ state in ^{76}As, and the $5/2^+$ state in ^{77}As. The $9^{(+)}$ state in ^{68}As is assigned to be $(7, 8)^-$ in Ref. [40]. Even considering such uncertainties in the spin-parity, there is no possible shell-model counterpart for this state. In ^{76}As, the 1_2^+ state is predicted at 461 keV with $\mu_{\rm th}^{\rm eff} = 0.384\mu_N$, which

may correspond to the experimental $(1)^+$ state. The problem in ^{77}As should be due to the missing $d_{5/2}$ orbit in the present model space, which is suggested also by the discrepancy in the excitation energy. In most other cases, by introducing the effective g factors, the calculated values are considerably improved, although the corrections are not necessarily enough to obtain a perfect agreement with the experimental data.

For nuclei with $Z \geqslant 34$, we present shell-model results for $N > 45$, keeping in mind the scope of the present model space as described in Sec. II. It should be noted that, for most of these nuclei, the shell-model predictions agrees reasonably well with the experiment. This observation suggests the validity of the shell-model framework in the vicinity of the $N = 50$ shell closure, even for neutron-rich cases.

There are few cases where the shell-model results disagree with the experimental data, taking into account a small experimental uncertainty: the 5^-, 7^-, and 9^- state in ^{84}Sr, the 8_1^+ and 8_2^+ state in ^{86}Zr, the 8^+ state in ^{90}Mo. In the shell-model results of ^{84}Sr, the 7_2^- state appears at 3.542 MeV with $\mu_{\rm th}^{\rm eff} = 6.458\mu_N$, which looks in better correspondence with the experimental 7^- state. Similarly, in ^{90}Mo, the 8_2^+ state is predicted at 2.874 MeV with $\mu_{\rm th}^{\rm eff} = -0.752\mu_N$ ($\mu_{\rm th}^{\rm free} = -1.516\mu_N$), which should correspond to the experimental 8^+ state. In the case of ^{86}Zr, the problem in the two 8^+ states can be interpreted as a result of the incorrect level order in the shell-model prediction, although the experimental uncertainty is large.

C. Electric quadrupole moments

The electric quadrupole moments are shown in Table IV. In the shell-model results, $Q_{\rm th1}$ and $Q_{\rm th2}$ correspond to two different choices of the effective charges: $(e_p,e_n) = (1.5,0.5)$ and $(1.5,1.1)$, respectively. The former set is the one we adopted in the pf-shell calculations [13], while the latter is determined by a least-squares fit to the experimental data. The correlation between the calculated electric quadrupole moments and the experimental data is shown in Fig. 7. It is clear that the latter choice gives a better description for most of the data points. In general we find that the deviation between theory and experiment is large for those cases where the experimental error bar is large.

The large neutron effective charge $e_n = 1.1$ may need more discussions. We have carried out the least-squares fit to the 49 known experimental values of the quadrupole moments for which the experimental errors are relatively small and we can expect reasonable description by the present shell model. According to the fit, the adopted data demand rather large isoscalar polarization charge $e^0 = 0.8$, while the dependence of the rms deviation on the isovector polarization charge (e^1) is very weak. We take a typical value $e^1 = 0.3$. These values lead to the above effective charges ($e_p = 1 + e^0 - e^1$, $e_n = e^0 + e^1$). Note that the experimental data demand a large e^0 but not a large e_n. There is no remarkable difference even if we take, for example, $e_p = 1.8$ and $e_n = 0.8$. According to the collective model by Bohr and Mottelson [47], the standard value of e^0 is estimated to be about $Z/A \sim 0.5$. The larger value is, qualitatively, expected for the present choice of the model space, because the active nucleons in the upper pf-shell

TABLE IV. Comparison of experimental electric quadrupole moments $Q_{\rm exp}$ with the theoretical values $Q_{\rm th1}$ and $Q_{\rm th2}$. The theoretical values are calculated using two different sets of effective charges, $(e_p,e_n) = (1.5,0.5)$ and $(1.5,1.1)$, respectively. The excitation energies (E_x) are also shown. Most of the data are taken from Refs. [34,40].

Nucl.	J^π	E_x (MeV)		Quadrupole moment (eb)		
		Exp.	Cal.	$Q_{\rm exp}$	$Q_{\rm th1}$	$Q_{\rm th2}$
^{58}Ni	2^+	1.454	1.298	−0.10(6)	−0.032	−0.070
^{60}Ni	2^+	1.333	1.635	+0.03(5)	−0.072	−0.158
^{61}Ni	$3/2^-$	0.000	0.080	+0.162(15)	0.046	0.101
	$5/2^-$	0.067	0.000	−0.20(3)	−0.037	−0.082
^{62}Ni	2^+	1.173	1.820	+0.05(12)	−0.030	−0.067
^{64}Ni	2^+	1.346	1.637	+0.35(20)	−0.023	−0.051
^{63}Cu	$3/2^-$	0.000	0.000	−0.211(4)	−0.131	−0.189
^{65}Cu	$3/2^-$	0.000	0.000	−0.195(4)	−0.133	−0.193
^{63}Zn	$3/2^-$	0.000	0.000	+0.29(3)	0.171	0.240
^{64}Zn	2^+	0.992	0.942	−0.32(6) or −0.26(6)	−0.233	−0.324
^{65}Zn	$5/2^-$	0.000	0.000	−0.023(2)	−0.036	−0.049
^{66}Zn	(6^-)	4.076	3.578	−0.081(13)	−0.276	−0.430
^{67}Zn	$5/2^-$	0.000	0.011	+0.150(15)	0.087	0.128
	$9/2^+$	0.605	0.458	0.60(6)	−0.293	−0.458
^{68}Zn	2^+	1.077	1.104	−0.11(2)	−0.010	0.032
^{69}Zn	$9/2^+$	0.439	0.257	−0.45(7)	−0.263	−0.410
^{70}Zn	2^+	0.884	1.108	−0.233(22)	−0.045	−0.015
^{66}Ga	$(7)^{\rm a}$	1.464	1.420	0.78(4)	−0.497	−0.714
^{67}Ga	$3/2^-$	0.000	0.000	0.195(5)	0.179	0.242
^{68}Ga	1^+	0.000	0.000	0.0277(14)	−0.005	−0.014
	7^-	1.230	0.997	0.72(2)	−0.493	−0.711
^{69}Ga	$3/2^-$	0.000	0.000	+0.168(5)	0.170	0.224
^{71}Ga	$3/2^-$	0.000	0.000	+0.106(3)	0.155	0.183
^{72}Ga	3^-	0.000	0.200	+0.52(1)	0.068	0.111
^{69}Ge	$5/2^-$	0.000	0.000	0.024(5)	0.102	0.140
^{70}Ge	2^+	1.040	0.905	+0.04(3)	0.095	0.161
	2^+	1.708	1.404	−0.07(4)	−0.126	−0.203
	4^+	2.153	2.025	+0.22(5)	0.014	0.079
	2^+	2.157	1.897	+0.26(10)	0.241	0.347
^{71}Ge	$9/2^+$	0.198	0.107	0.34(5)	−0.339	−0.484
^{72}Ge	2^+	0.834	0.811	−0.13(6)	0.122	0.205
^{73}Ge	$9/2^+$	0.000	0.058	−0.173(26)	−0.178	−0.247
	$5/2^+$	0.013	0.625	0.70(8)	0.108	0.164
^{74}Ge	2^+	0.596	0.717	−0.19(2)	0.114	0.189
	2^+	1.204	1.350	+0.26(6)	−0.109	−0.177
^{76}Ge	2^+	0.563	0.744	−0.19(6)	0.016	0.043
^{70}As	4^+	0.000	0.002	0.094(24)	−0.401	−0.544
^{71}As	$5/2^-$	0.000	0.006	−0.021(6)	−0.366	−0.491
^{72}As	2^-	0.000	0.000	−0.082(24)	−0.252	−0.350
^{73}As	$5/2^-$	0.067	0.261	0.356(12)	−0.370	−0.510
^{75}As	$3/2^-$	0.000	0.000	+0.314(6)	0.254	0.341
	$5/2^-$	0.280	0.442	0.30(10)	−0.006	−0.007
^{76}As	2^-	0.000	0.100	7(8)	−0.268	−0.382
^{78}Se	2^+	0.614	0.748	−0.26(9)	−0.125	−0.145
^{79}Se	$7/2^+$	0.000	0.000	+0.8(2)	0.362	0.472
^{80}Se	2^+	0.666	0.726	−0.31(7)	−0.297	−0.359
^{82}Se	2^+	0.655	0.728	−0.22(7)	−0.321	−0.378
^{80}Br	1^+	0.000	0.212	0.185(2)	0.116	0.156
	2^-	0.037	0.000	0.159(7)	0.093	0.126
	5^-	0.086	0.069	+0.69(2)	0.430	0.575

TABLE IV. (*Continued.*)

Nucl.	J^π	E_x (MeV)		Quadrupole moment (eb)		
		Exp.	Cal.	$Q_{\rm exp}$	$Q_{\rm th1}$	$Q_{\rm th2}$
^{81}Br	$3/2^-$	0.000	0.000	+0.276(4)	0.219	0.273
^{82}Br	5^-	0.000	0.068	+0.69(2)	0.550	0.704
^{81}Kr	$7/2^+$	0.000	0.041	0.629(13)	0.258	0.352
^{83}Kr	$9/2^+$	0.000	0.000	+0.26(3)	0.210	0.282
	$7/2^+$	0.009	0.077	+0.495(10)	0.377	0.501
^{85}Kr	$9/2^+$	0.000	0.000	+0.458(18)	0.389	0.482
^{82}Rb	1^+	0.000	0.472	+0.19(7)	0.026	0.033
	5^-	0.069	0.130	+1.01(12)	0.435	0.577
^{83}Rb	$5/2^-$	0.000	0.000	+0.196(22)	0.267	0.352
^{84}Rb	2^-	0.000	0.000	−0.015(35)	−0.000	−0.008
	6^-	0.464	0.400	0.57(27)	0.384	0.515
^{85}Rb	$5/2^-$	0.000	0.146	+0.23(4)	0.257	0.323
	$9/2^+$	0.514	0.566	−0.7(2)	−0.468	−0.536
^{86}Rb	2^-	0.000	0.000	+0.193(32)	0.163	0.216
	6^-	0.556	0.231	+0.369(95)	0.374	0.474
^{87}Rb	$3/2^-$	0.000	0.000	+0.132(1)	0.158	0.158
^{83}Sr	$7/2^+$	0.000	0.078	+0.781(67)	0.222	0.308
^{85}Sr	$9/2^+$	0.000	0.000	+0.282(15)	0.221	0.296
^{87}Sr	$9/2^+$	0.000	0.000	+0.34(2)	0.234	0.336
^{87}Zr	$9/2^+$	0.000	0.000	+0.42(5)	0.255	0.329
^{88}Zr	(8^+)	2.888	2.937	+0.51(3)	0.259	0.393
^{89}Zr	$9/2^+$	0.000	0.000	+0.28(10)	0.179	0.282
^{90}Zr	8^+	3.589	3.468	0.51(3)	−0.341	−0.341
^{90}Nb	8^+	0.000	0.000	+0.046(7)	−0.038	0.031
^{90}Mo	8^+	2.875	2.845	0.58(3)	−0.329	−0.396
^{92}Mo	8^+	2.760	2.571	−0.34()	−0.306	−0.306
^{93}Ru	$(21/2)^+$	2.083	1.931	+0.04(1)	0.222	0.286

[a] $J^\pi = 7^-$ is assumed for the calculation.

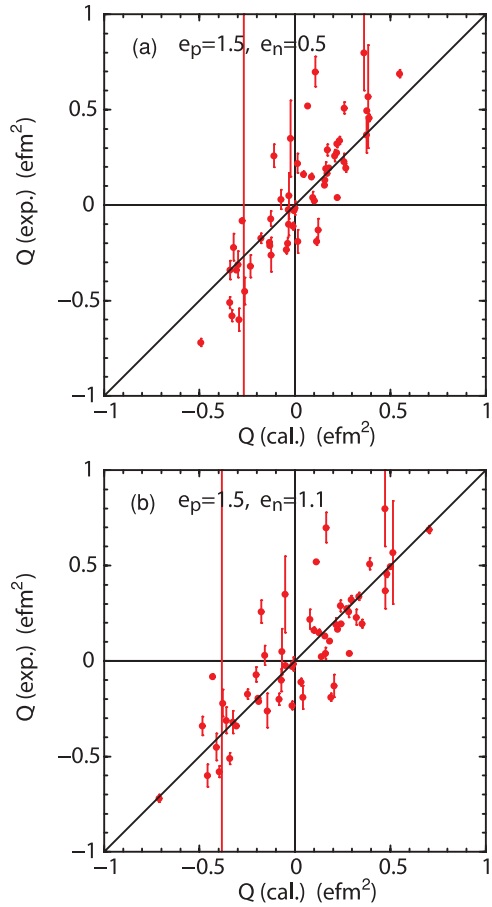

FIG. 7. (Color online) Comparison of experimental electric quadrupole moments with the shell-model results with two sets of effective charges: (e_p, e_n) = (a) (1.5,0.5) and (b) (1.5,1.1).

orbits can easily polarize the "core" including the $f_{7/2}$ orbit. Also, the isovector charge $e^1 \sim 0.3$ is almost consistent with the recent experimental result for nuclei around ^{56}Ni in the pf shell [48] and also with the theoretical prediction by Bohr and Mottelson.

As in the case of the magnetic moment, the shell-model description for the Ni isotopes exhibits a poor agreement with data, primarily due to the missing $f_{7/2}$ orbit. Nevertheless, for the odd-A Cu and Zn isotopes, the shell-model results agree fairly well with experiment. Also, the calculated values for Ga isotopes are in reasonable agreement with data, except for the 3^- state of ^{72}Ga, for which the description of the magnetic moment is poor. For ^{69}Ge and ^{70}Ge, the sign of the quadrupole moment is reproduced, but the quantitative agreement is not satisfactory. For the $5/2^+$ in ^{73}Ge, the calculated value largely deviates from the experimental excitation energy and quadrupole moment. Similar discrepancies are found in heavier Ge isotopes as well, as discussed in subsection III G. As for the As isotopes, the calculated absolute values are significantly larger than the experimental data for ^{70,71,72}As.

For $Z \geqslant 34$ isotopes, the results for $N > 45$ are shown, as in the case of the magnetic moments. The agreement between the shell-model predictions and the experimental data is reasonable in most cases. A relatively large discrepancy can be seen in the $7/2^+$ state of ^{81}Kr and ^{83}Sr, where the calculated values are somewhat too small. Moreover, the calculated values for high-spin isomer states, the 8^+ in ^{88,90}Zr, ^{90}Mo, and $21/2^+$ in ^{93}Ru are systematically larger than the experimental data, assuming the same sign for the experimental value as that of the calculation if it is unknown. These results suggest that the insufficiency in the collectivity becomes apparent toward the end of the model space.

D. Properties of 2_1^+ states

The first 2^+ state is a good test for the quality of systematic descriptions with the present theoretical framework. The reason for this is that there are relatively many experimental data, such as $B(E2)$ values and electromagnetic moments as well as excitation energies, to compare with. Figures 8 and 9 summarize the comparison between the calculation and experimental data for the $Z = 28$, 30, 32 isotopes and for the $N = 50$, 48, 46 isotones, respectively.

As for Ni isotopes, the excitation energy $E_x(2_1^+)$ takes the largest value at $N = 40$ and there the $B(E2)$ becomes smallest among the isotopes included in the figure, suggesting the presence of the neutron semimagic structure. The calculated E_x and $B(E2)$ values agree with the experimental data only at $N = 40$. The deviation between the calculation and the data is significant around $N = 32 \sim 34$, where the calculated E_x is

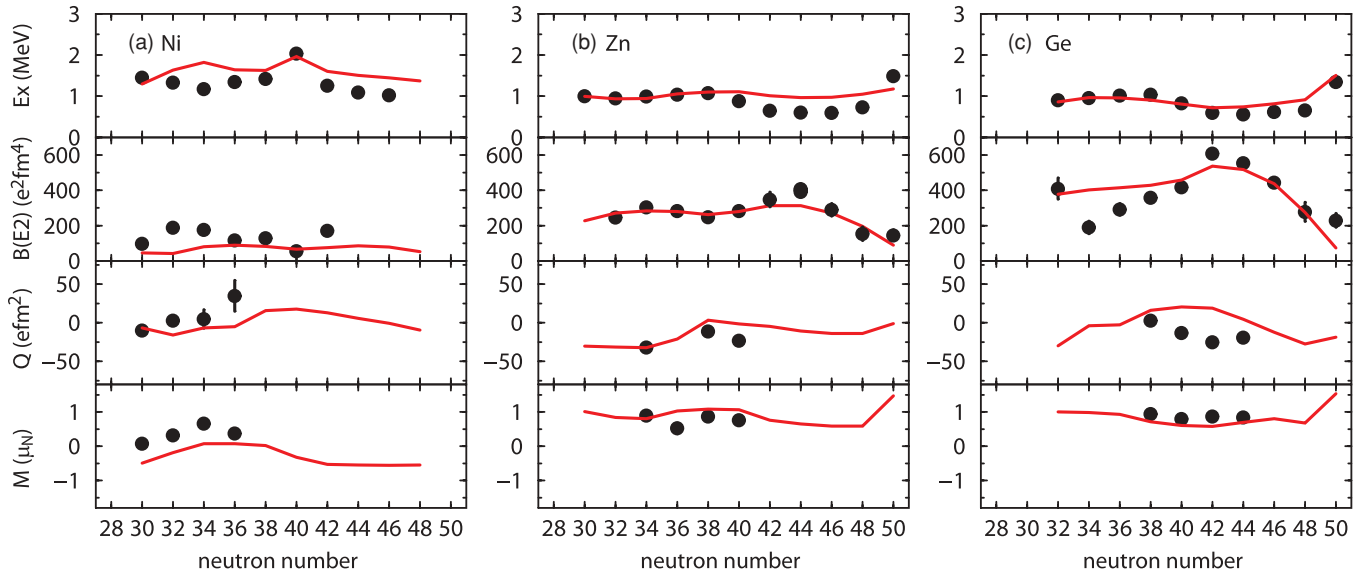

FIG. 8. (Color online) Systematics in the properties of the first 2^+ states for (a) Ni, (b) Zn, and (c) Ge isotopes. Excitation energies (E_x), $B(E2; 2_1^+ \rightarrow 0_1^+)$ values, electric quadrupole moments (Q), and magnetic moments (M) are compared between the shell-model calculations (solid lines) and the experimental data (filled circles). The effective charges $(e_p, e_n) = (1.5, 1.1)$ and the effective spin g factors $g_s^{(\mathrm{eff.})} = 0.7 g_s^{(\mathrm{free})}$ are used for the calculation. Data are taken from Refs. [34,40,49–52].

too large and $B(E2)$ is too small. Note that, the description of these isotopes is quite reasonable in our previous calculations in the pf-shell model space with the GXPF1 interaction [12]. Therefore, the problem in the present calculations in the f_5pg_9-shell space can be naturally understood as a result of the missing $f_{7/2}$ orbit. In fact, it has been shown in the pf-shell calculation that the ^{56}Ni core is most significantly broken at $N = 32 \sim 34$.

For $N > 40$, the experimental E_x goes down rapidly and the $B(E2)$ enhances significantly at $N = 42$. This feature suggests the development of the quadrupole collectivity, and the present calculation fails to reproduce it. Note that such lowering of the E_x can locally be reproduced by modifying some parts of the effective interaction, for example, the pairing TBME. In fact, the LBHG interaction [23] can successfully describe the E_x, but it also fails to reproduce the large $B(E2)$ at $N = 42$. The possible origin of this discrepancy is the insufficient quadrupole collectivity which cannot develop efficiently within the f_5pg_9-shell space due to the missing $d_{5/2}$ and $f_{7/2}$ single-particle orbits. If these orbits were included in the calculation, they would form the $\Delta l = 2$ orbit pairs with the $g_{9/2}$ and $f_{5/2}$ orbits, respectively (so-called

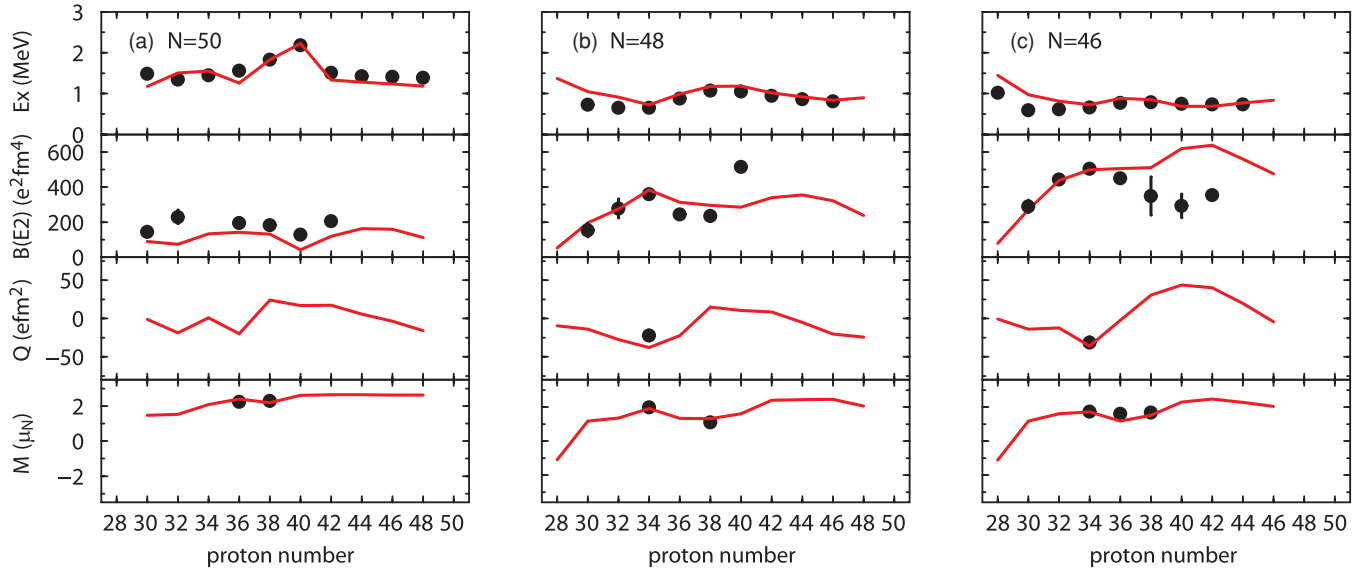

FIG. 9. (Color online) Systematics of the first 2^+ states for (a) $N = 50$, (b) $N = 48$, and (c) $N = 46$ isotones. Conventions are the same as those in Fig. 8.

quasi-SU(3) structure [30]), and the quadrupole collectivity would develop significantly through large off-diagonal matrix elements among them.

The calculated magnetic moments show systematic deviations from the available experimental data. Considering that there are no active protons in the present model space, this also indicates the importance of the breaking of the $Z = 28$ core in the Ni isotopes. In contrast, the magnetic moments of the $N = 50$ isotones are successfully described in the present calculations, suggesting the persistence of the inert $N = 50$ core.

The description of the Zn isotopes looks reasonable for $N < 40$. On the other hand, as in the case of the Ni isotopes, the present shell model fails to describe the lowering of E_x for $N > 40$ as well as the enhancement of the $B(E2)$. This fact suggests again the insufficient collectivity for $N > 40$ because of the small model space. It should be noted that, in contrast to the Ni isotopes, there is no prominent maximum in E_x at $N = 40$ among the isotope chain. Correspondingly, the $B(E2)$ value does not reach its minimum at $N = 40$, indicating that the $N = 40$ subshell effect almost disappears for Zn isotopes. The present shell-model calculation reasonably describes this feature.

For Ge isotopes, the overall description of E_x looks reasonable, although the decrease for $N > 40$ is not enough compared with experiment. However, the calculated $B(E2)$ values are too large for $N < 40$ except for ^{64}Ge. In the pf-shell results [12], the $B(E2)$ value is also predicted to be too large for $N = 34$, but it decreases toward $N = 40$ in contradiction with the experimental data. This is because of the limitation in the neutron model space. On the other hand, in the present results, the $B(E2)$ is almost constant (or increases gradually) from $N = 34$ to $N = 38$. The $B(E2)$ jumps up suddenly from $N = 40$ to $N = 42$, suggesting a dramatic change of the structure. The present shell-model calculation shows a qualitative agreement with experiment.

Note that, the small experimental $B(E2)$ around $N \sim 34$ in Ge isotopes breaks the systematics observed in Ni and Zn isotope chains. Because the structure of neutron-deficient nuclei in this mass region is considered to be rather complicated (see subsection III H), possible side-feedings from high-lying longer-lived states, which can be seen in the ^{68}Ge spectra [53], for example, may have lead to a longer lifetime [smaller $B(E2)$ values] than the reality. In fact, such a problem has been pointed out recently for Se [6] and Kr [54] isotopes. The good agreement between the shell-model prediction and the recent experimental data [52] for ^{64}Ge may be another suggestion for a possible problem in the experimental values for ^{68}Ge and ^{68}Ge. A direct Coulomb excitation measurement is desired to clarify this point.

The quadrupole moments have been measured for $N = 38 \sim 44$, suggesting a change in the quadrupole deformation as a function of N. It looks almost spherical or γ-soft ($Q \sim 0$) for $N \sim 38$–40, while it changes to prolate ($Q < 0$) for $N \sim 42$–44. The shell-model calculation predicts such a change in Q, but its onset is shifted to around $N = 46$. This result suggests the insufficiency of the quadrupole collectivity that favors the prolate deformation. The $f_{7/2}$ orbit is missing in the present model space, which is important to generate such prolate deformations. The excitations from the proton $f_{7/2}$ orbit become important especially when neutrons begin to occupy the $g_{9/2}$ orbit, because the strong repulsive force between the proton $f_{7/2}$ and the neutron $g_{9/2}$ orbit should lead to narrower $Z = 28$ shell gap [15]. Thus it is an interesting problem to extend the model space by including the $f_{7/2}$ orbit, which is definitely needed to investigate more neutron-rich cases.

As discussed above, if we look through the first 2^+ state along the isotopic chains (Fig. 8), we find several problems that are related to collective effects, even if we restrict ourselves to consider cases of a small number of valence protons (up to four). For smaller N, the problem should be due to the missing $f_{7/2}$ orbit (i.e., ^{56}Ni core excitation), while for larger N, the $d_{5/2}$ orbit may also become important in addition to the proton $Z = 28$ core excitation. Thus the problems are naturally understood as a result of the limitation in the model space. On the other hand, the overall description looks much better along the isotone chains with the corresponding number of valence neutron holes ($N \geqslant 46$), as shown in Fig. 9. In addition to the problems for $Z \leqslant 32$ cases described above, there are remarkable discrepancies between the experimental data and the shell-model results for the $B(E2)$ values of ^{86,88}Zr and ^{88}Mo. The very large $B(E2)$ for ^{88}Zr in the experimental data looks exceptional, considering the smooth behavior of the E_x along the isotone chain. The experimental data exhibit a clear minimum at $Z = 40$ (^{86}Zr) that suggests an almost spherical shape [55], while the shell-model result show a significant oblate deformation. This can be taken as a precursor of the failure of the present shell-model description toward ^{80}Zr.

E. Low-lying states of even-even nuclei

In addition to the 2_1^+ state, the energy levels of low-lying states in even-even nuclei reflect various basic properties of nuclei such as the shell structure and the collective excitations. Figures 10 and 11 display the comparison for the excitation energies of the low-lying states $2_1^+, 4_1^+, 2_2^+, 0_2^+$, and 5_1^- between the shell-model calculations and experiment. The former is for Ni, Zn, Ge isotopes as a function of neutron number, while the latter for the valence-mirror counterparts, the $N = 50, 48, 46$ isotones as a function of proton number. As in the case of the 2_1^+ states, the shell-model description is in general more successful for the isotones near the $N = 50$ shell closure than the isotopes near the $Z = 28$ core. The discrepancy between the shell-model results and the experimental data is more serious in the Ni isotopes, partly because we have excluded data for Ni and Cu isotopes from the fitting calculations. Nevertheless, even for Ni isotopes, the agreement between the shell-model results and the experimental data is quite good for $N \leqslant 40$ except for the 2_1^+ states around $N = 34$. Note that only the $T = 1$ TBME are relevant to the description of the Ni isotopes and the $N = 50$ isotones. Considering that the same TBME successfully describe the energy spectra of both the Ni isotopes and the $N = 50$ isotones, it is suggested that the $T = 1$ TBME are determined with a reasonable accuracy, and the problems around $N = 34$ in Ni isotopes should be ascribed to the $Z = 28$ core excitations.

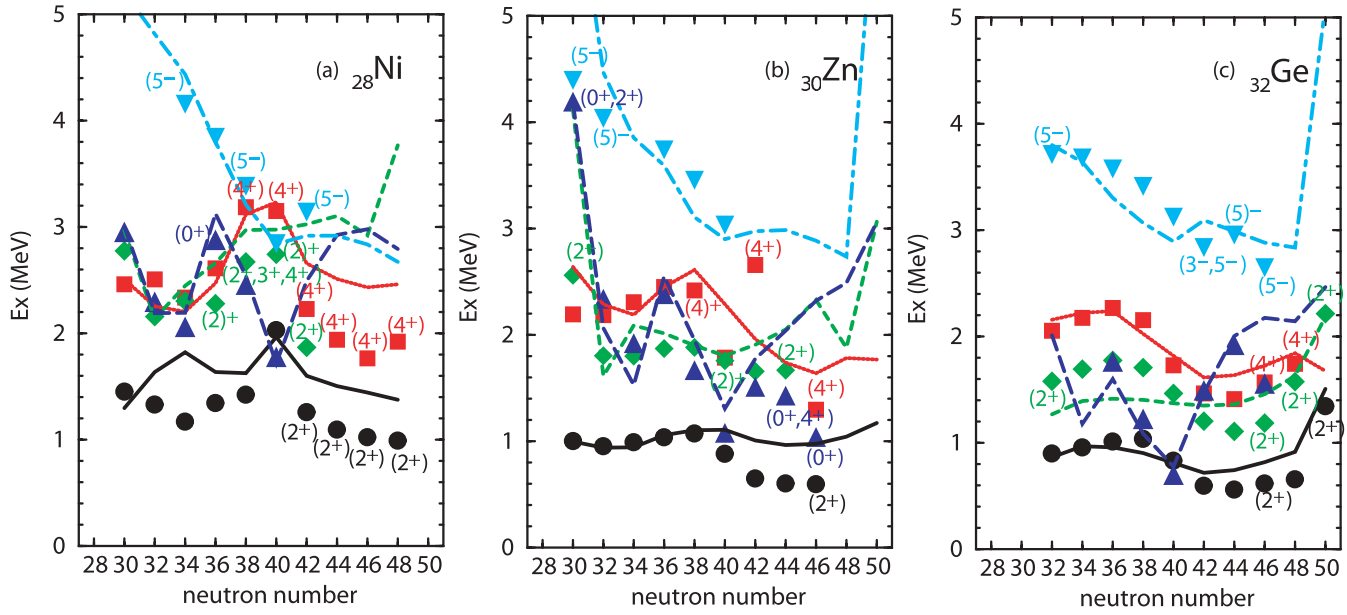

FIG. 10. (Color online) Energy levels of low-lying states for (a) Ni, (b) Zn, and (c) Ge isotopes with even number of neutrons. Calculated energy levels of the first 2^+, 4^+, 5^- states and the second 2^+, 0^+ states are shown with solid, dotted, dot-dashed, dashed, and long-dashed lines, respectively, which are compared with the experimental data denoted by circles, squares, down-triangles, diamonds, and up-triangles, respectively. Experimental spin assignments are explicitly shown for uncertain cases. Data are taken from Ref. [34].

The shell-model description is successful also for Zn isotopes with $N < 40$, while large discrepancies appear for $N > 40$. On the other hand, in the results of the valence-mirror counterparts, $N = 48$ isotones, there is no such difference in the quality of the description between the cases of $Z < 40$ and $Z > 40$. Note that the experimental data for Zn isotopes have been included in the present fitting calculations. This indicates that we cannot improve the fit for the $N > 40$ cases without destroying the quality of the description for the majority of the remaining data included in the fit. Therefore, such a local problem should be regarded as a result of intruder effects that cannot be renormalized sufficiently to the effective Hamiltonian within the present model space.

For the Ge isotopes, the 4_1^+ states as well as the 2_1^+ states are reasonably described by the shell model, although the lowering of the E_x for $N > 40$ is not enough in both states. As for

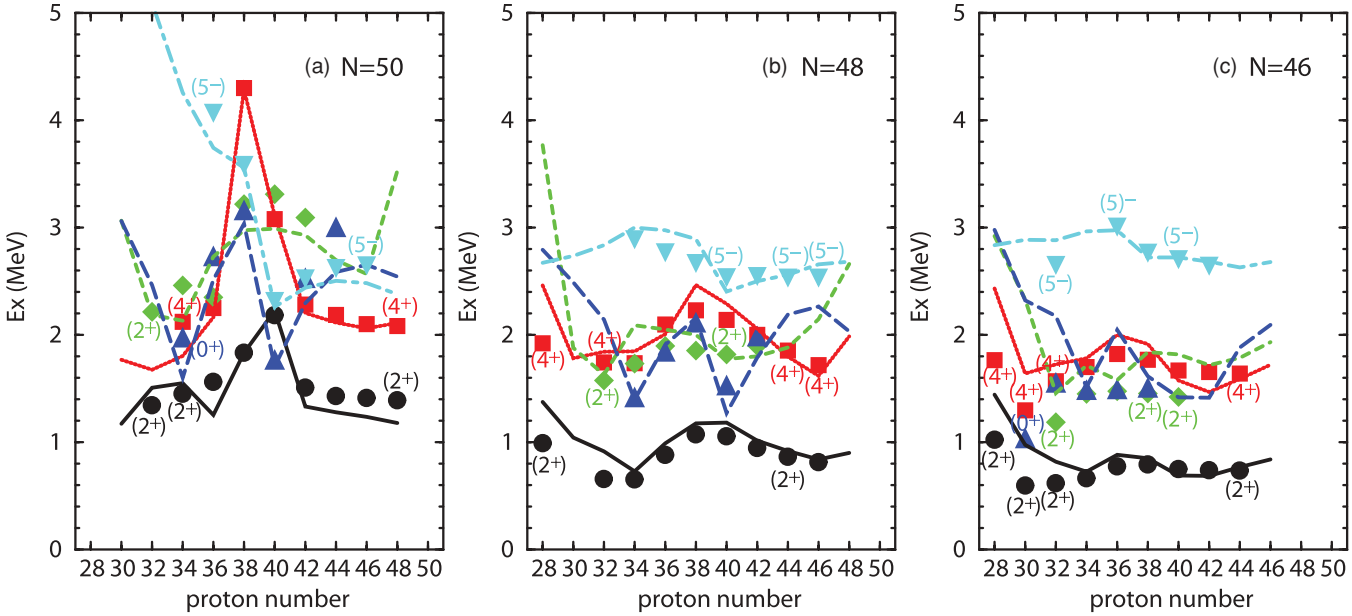

FIG. 11. (Color online) Systematics of the low-lying energy levels for (a) $N = 50$, (b) $N = 48$, and (c) $N = 46$ isotones with even number of protons. Conventions are the same as those in Fig. 10.

the 2_2^+ states, remarkable deviations from the experimental data can be seen on both sides of $N < 40$ and $N > 40$ with opposite directions. The overestimation of the E_x energies on the $N > 40$ side can be (basically the same problem as in the 2_1^+ and 4_1^+ states) traced back to the insufficiency of our model space in describing collective states. On the other hand, the problem on the $N < 40$ side should be considered as another difficulty inherent in the present model space without the $f_{7/2}$ orbit. The variation of the E_x energies in the Ge isotopes is more significant in comparison with that of the $N = 46$ isotones, in spite of the same numbers of valence nucleons. This feature suggests a more drastic change of the structure along the Ge isotope chain due to the contribution of $Z = 28$ core-excited configurations that develop the collectivity.

The overestimation of the E_x energies by the shell model can commonly be seen for Ni, Zn, and Ge isotopes with $N > 40$. It is interesting to note that in most cases, the amount of the overestimation looks similar within the same chain of isotopes. Thus the overall description can be drastically improved by modifying a small part of the TBME. For example, if we make the monopole pairing matrix elements for the $g_{9/2}$ orbit more repulsive by 0.5 MeV, the binding of the ground state is weakened, which remedies most of the problems for $N > 40$. However, in the present study, we stick to the use of common TBME for all nuclei.

In Figs. 10 and 11, the E_x energy of the second 0^+ state shows a systematic behavior with local minima at N or $Z = 34$ and 40, except for the case of the $N = 46$ isotones. The shell-model results successfully follow such a feature up to $N = 42$ for the Zn isotopes and up to $N = 44$ for the Ge isotopes. The property of the 0_2^+ states is discussed in subsection III G.

In order to check a typical energy difference between the positive- and the negative-parity states, we consider the lowest 5^- states. As shown in Figs. 10 and 11, one can find a reasonable agreement between the shell-model predictions and the experimental data for most of the isotopes and isotones shown in the figures.

F. Low-lying states of odd-*A* nuclei

The energy levels of low-lying states in odd-A nuclei provide us with useful information on the single-particle orbits, especially for the cases of nearly spherical nuclei. Here we consider nuclei with a small number (at most five) of valence protons (particle states) or neutrons (hole states) that are close to the semimagic nuclei, reducing thereby the significance of collective features.

1. Isotopes around $Z = 28$

First we discuss our results near the $Z = 28$ closure. Figure 12 shows the comparison between the shell-model results and the experimental data along various isotopic chains with an odd number of neutrons. The spin-parity of the ground states is expected to reflect the ordering of the neutron orbits occupied by the last neutron (Fermi levels). In fact it changes almost systematically and looks basically consistent with the naive filling configuration that assumes an ascending order of the ESPE for the single-particle orbits $p_{3/2}$, $f_{5/2}$, $p_{1/2}$, and $g_{9/2}$, as shown in the left panel of Fig. 14.

The shell-model results follow closely the behavior of the experimental level scheme within errors of the order 0.3 MeV. However, there are several exceptions for the cases of $N = 33 \sim 37$, where the negative-parity states $1/2^-$, $3/2^-$, and $5/2^-$ appear near the ground state within 0.3 MeV, and the

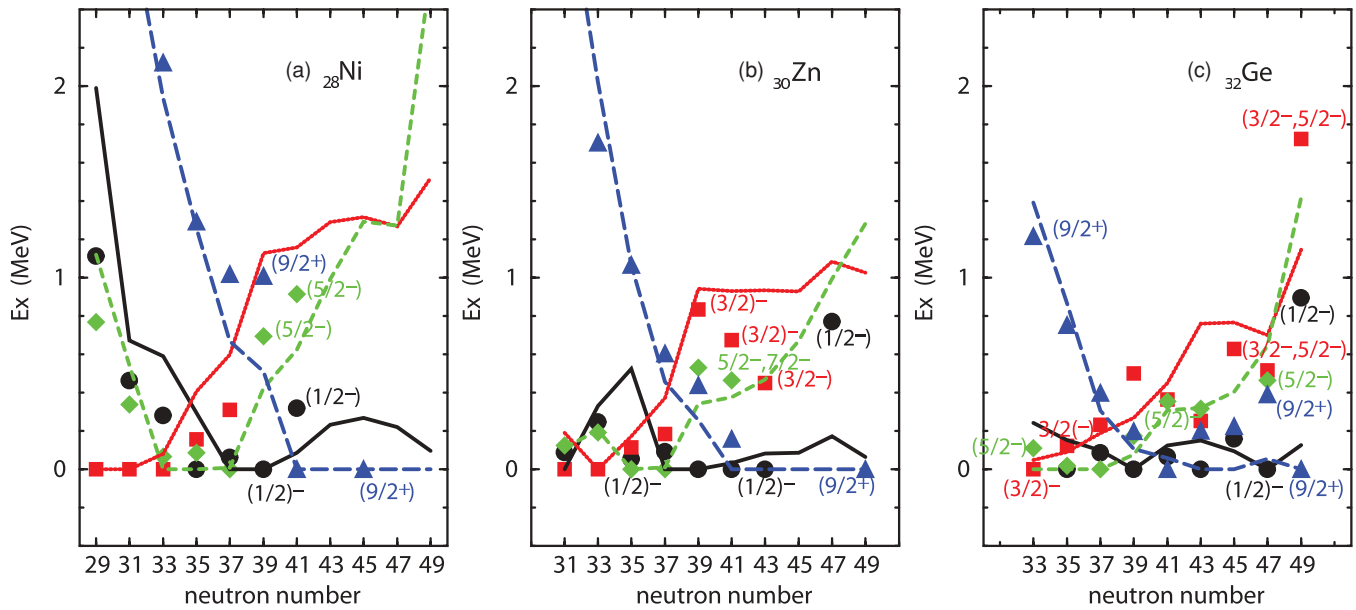

FIG. 12. (Color online) Energy levels of low-lying states for (a) Ni, (b) Zn, and (c) Ge isotopes with odd number of neutrons. Calculated energy levels of the yrast $1/2^-$, $3/2^-$, $5/2^-$, and $9/2^+$ states are shown with solid, dotted, dashed, and long-dashed lines, respectively, which are compared with the experimental data denoted by circles, squares, diamonds, and triangles, respectively. Experimental spin assignments are explicitly shown for uncertain cases. Data are taken from Ref. [34].

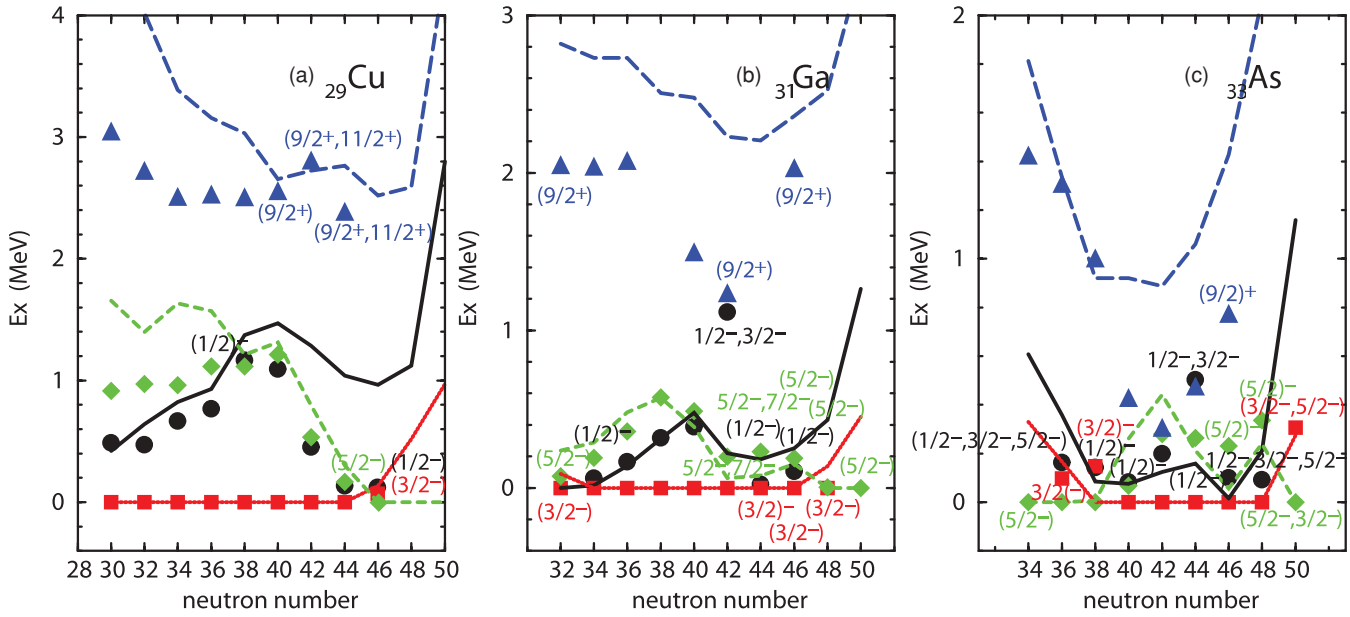

FIG. 13. (Color online) Systematics of the low-lying energy levels for (a) Cu, (b) Ga, and (c) As isotopes with even number of neutrons. Conventions are the same as those in Fig. 12. Data are taken from Refs. [4,34,35].

shell model sometimes fails to reproduce the experimental level ordering. As the number of protons increases, the level spacings become narrower due to collective effects.

It should be noted that, in all these isotopes, as the neutron $f_{5/2}$ orbit is occupied ($N = 33 \sim 37$), the $9/2^+$ state comes down rapidly. This can be interpreted as a result of the $T = 1$ monopole effect. In fact, in the case of the JUN45 interaction, the difference between the f5-f5 and f5-g9 monopole centroids is about 0.12 MeV, which gives 0.7 MeV ESPE gain for the $g_{9/2}$ orbit relative to the $f_{5/2}$ orbit on filling the $f_{5/2}$ orbit completely with six neutrons. The agreement between the shell-model results and the experimental data become worse for $N > 40$, although there remain some uncertainties in the experimental data.

Figure 13 shows the energy levels of odd-Z nuclei, Cu, Ga, and As isotopes as a function of neutron number. These results are useful in our analysis of the role played by the proton orbits near the $Z = 28$ shell closure. The results for Cu are the same as those in Fig. 4 except that the energy levels are now plotted relative to the ground state and relative not to the $3/2^-$ state. In this case, the number of active protons is constant within each panel and therefore the level order varies smoothly in comparison with that in Fig. 12. Assuming the correspondence between the low-lying energy levels and the single-particle orbits, one can infer that the $f_{5/2}$ orbit comes down as the number of neutrons are increased and crosses first the $p_{1/2}$ orbit at around $N = 40$ and then the $p_{3/2}$ orbit. As discussed before, the lowering of the $f_{5/2}$ orbit is remarkable especially for $N > 40$, which can be understood as a result of the large attractive f5-g9 monopole centroid [56] with $T = 0$ due to the tensor force.

It should be noted that the calculated excitation energies of the $9/2^+$ states largely deviate from the experimental data. As discussed in Ref. [57], according to the available experimental data of proton stripping reactions for Cu isotopes with $N <$ 36, the lowest $9/2^+$ states carry relatively large spectroscopic strengths. On the other hand, the lowest $9/2^+$ states obtained in the present shell-model calculations consist mainly of neutron excitations, especially for heavier isotopes, and they cannot be regarded as single-particle like states with a dominant $\pi(g_{9/2})^1$ configuration. Therefore, in the present fitting calculations, these $9/2^+$ states are excluded from the data that enter our fit. We have confirmed that if these states are included, we cannot attain a reasonable convergence of the fit.

The shell-model description is not successful also for the $5/2^-$ states of Cu isotopes with $N = 30 \sim 36$. This can be attributed to the $Z = 28$ core excitations that are missing in the present calculation. This interpretation is supported by the pf-shell calculations with the GXPF1 interaction [12]. For example, the probability of the closed $(f_{7/2})^{16}$ configuration is only 53% in the calculated wave function of the ^{65}Cu $5/2^-_1$ state.

As protons are added, the level spacing becomes narrower (note that the range of the E_x is different between panels in Fig. 13). In addition, the lowest $9/2^+$ state comes down drastically and takes the minimum excitation energy at around $N = 42$ in As isotopes. The minimum at $N = 42$ has been associated with the development of deformation, and the correlation with the excitation energy of the first 2^+ state in the neighboring even-even nuclei [58] has been pointed out. In the present shell-model calculation, such a feature is qualitatively described, although the calculated excitation energies are systematically too large by about 1 MeV for the $9/2^+$ states. It has been discussed [59], based on the Coriolis coupling model with a pairing-type residual interaction that the low-lying $9/2^+$ state appears in the case of prolate deformation as a member of the $(9/2^+, 5/2^+)$ doublet, and the energy splitting of these two states decreases with deformation. Such a feature cannot be described in the present shell-model calculations. For example, in the case of ^{75}As ($N = 42$), the

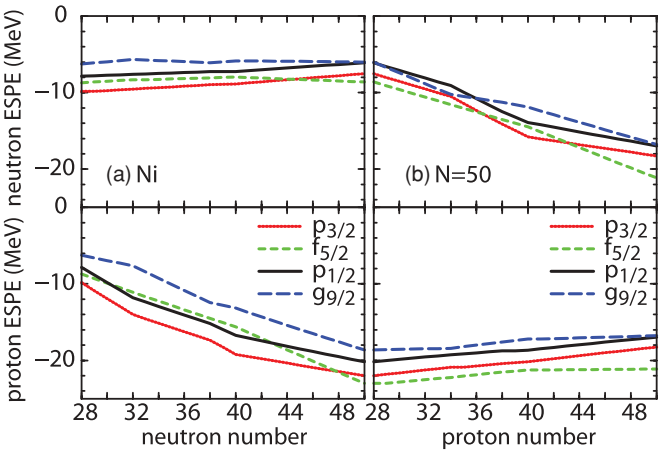

FIG. 14. (Color online) Effective single-particle energies obtained with the JUN45 interaction for (a) Ni isotopes and (b) $N = 50$ isotones as a function of the neutron number and the proton number, respectively.

lowest experimental $9/2^+$ and $5/2^+$ states appear at 304 and 401 keV, respectively, with a splitting of only 97 keV. On the other hand, the shell model predicts these states at 887 and 1628 keV, respectively. This result points again to the insufficiency of the present model space for the description of the prolate deformation.

2. *Isotones around $N = 50$*

Figure 15 shows the low-lying energy levels of odd-Z isotones as a function of proton number. These results correspond to the valence-mirror counterpart of Fig. 12. We expect that information on proton single-particle orbits around $N = 50$ core can be obtained from these results. The ground-state spin changes systematically, which can be naturally associated with the single-particle orbit occupied by the last proton. In this case, the ordering of the single-particle orbits seems consistent with the ascending order of $f_{5/2}$, $p_{3/2}$, $p_{1/2}$, and $g_{9/2}$, which is different from that of the neutron orbits around $Z = 28$ for the first two single-particle orbits. In fact, such a difference can be seen in the comparison of ESPE between the left and the right panels of Fig. 14. Because the bare single-particle energies are taken to be the same for proton and neutron orbits, this inversion occurs due to the attraction through the two-body interaction from the neutrons in the (closed) valence orbits. Thus, the difference in the calculated energy spectra between the valence mirror pair (Fig. 12 and Fig. 15) comes partly from the mass dependence factor ($A^{-0.3}$) of the TBME and partly from the ESPE. We find that the overall description by the shell model is much better in comparison with the cases in Fig. 12, suggesting that the $N = 50$ core is relatively inert in comparison with the $Z = 28$ core and that excitations across the core are less important.

The valence mirror counterpart of Fig. 13 is shown in Fig. 16, where energy levels of the low-lying states are shown for the $N = 49$, 47, and 45 isotones with even number of protons. From these states we can try to extract information about the neutron orbits around the $N = 50$ core. The above figure suggests that the single-particle energies of the three pf-shell orbits $p_{1/2}$, $p_{3/2}$, and $f_{5/2}$ vary smoothly and almost in parallel with each other for $Z = 34 \sim 42$. The shell model describes qualitatively such a trend. The energy difference between the $g_{9/2}$ and the $p_{1/2}$ orbits decreases gradually for smaller Z. The present shell-model calculation predicts almost degenerate $1/2^-$ and $9/2^+$ states for $Z < 32$. The experimental data for ^{81}Ge disagree with the shell-model results, although there are uncertainties in the spin assignments.

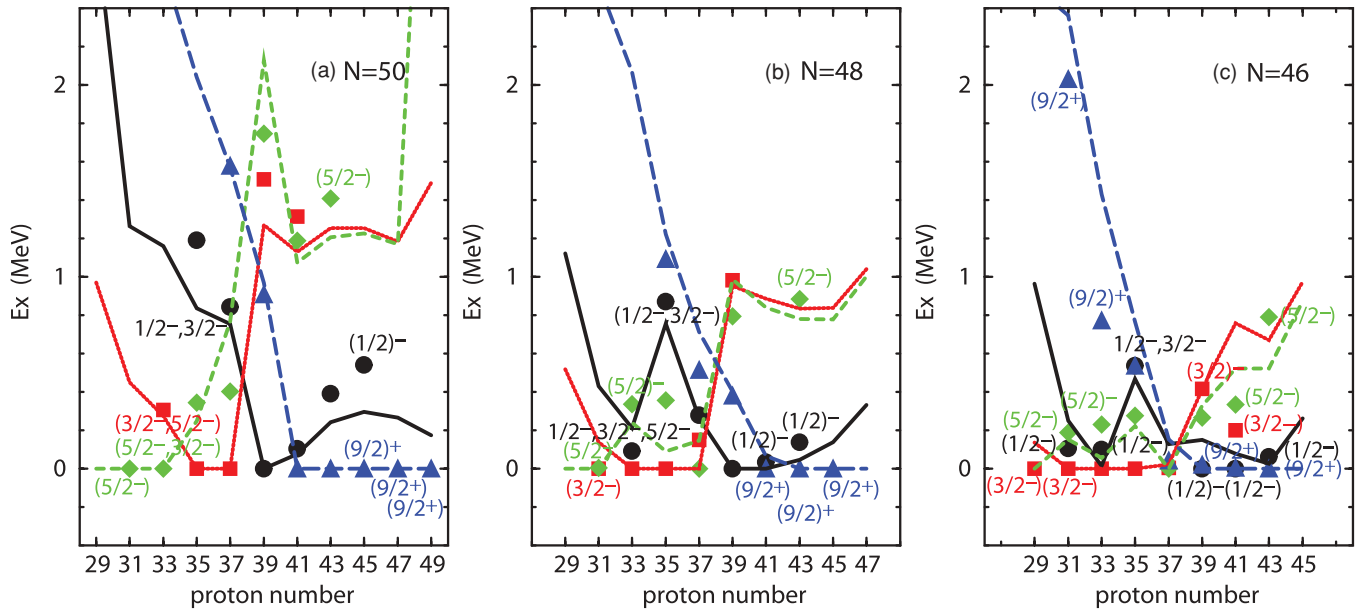

FIG. 15. (Color online) Systematics of the low-lying energy levels for (a) $N = 50$, (b) $N = 48$, and (c) $N = 46$ isotones with odd number of protons. Conventions are the same as those in Fig. 12.

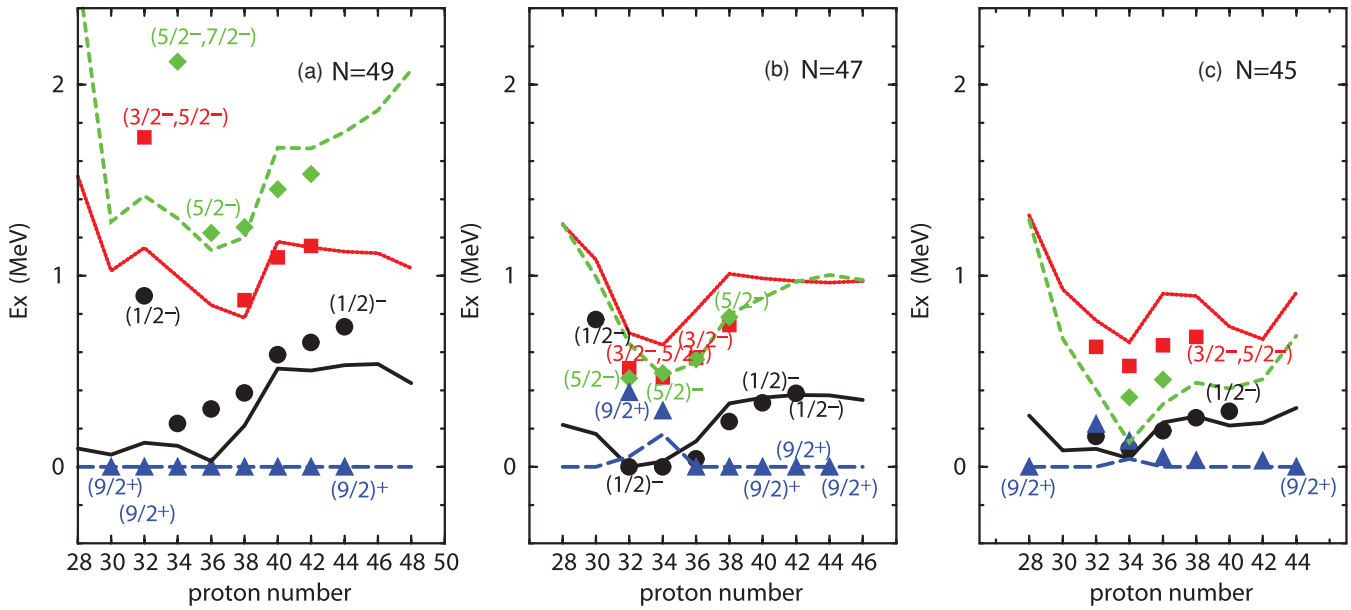

FIG. 16. (Color online) Systematics of the low-lying energy levels for (a) $N = 49$, (b) $N = 47$, and (c) $N = 45$ isotones with even number of protons. Conventions are the same as those in Fig. 12.

As neutrons are removed, that is going away from the $N = 50$ shell closure, the level spacing becomes narrower due to the collective effects discussed in connection with Fig. 13. The lowering of the excitation energies of the negative-parity hole states relative to the $9/2^+$ ground states corresponds to the lowering of the $g_{9/2}$ particle states in Fig. 13. In addition, the $5/2^-$ states come down rapidly, crossing the $3/2^-$ states at $N = 47$, and become even lower at $N = 45$. Such a change of the relative position of the negative-parity states can be understood as another consequence of the $T = 1$ f5-g9 monopole effect. In the JUN45 interaction, the $T = 1$ f5-g9 monopole centroid is more attractive than that of the p3-g9 and p1-g9 ones by about 0.2 MeV, which gives rise to the ESPE loss (that is a gain of the hole energy) for the $f_{5/2}$ orbit of 0.8 MeV relative to the $p_{3/2}$ and $p_{1/2}$ orbits by removing four neutrons from the $g_{9/2}$ orbit.

G. Structure of 0_2^+ states in Ge isotopes

It has been argued that there exists significant change of structure between the lighter ($N < 40$) and heavier ($N > 40$) Ge isotopes. This can be interpreted as a transition from the spherical (or oblate) to prolate shape [60]. It may also point a coexistence of these phases. Such a change can be seen in various experimental observables like nucleon transfer cross sections [61] and $B(E2)$ values and their ratios for low-lying states [62]. The behavior of the 0_2^+ state is especially interesting from a shell-model viewpoint that aims at including the "intruder" configuration. As a function of N, the excitation energy of the 0_2^+ state decreases rapidly and reaches its minimum at $N = 40$, which corresponds to the first excited state of ^{72}Ge. Experimental $B(E2)$ data suggest that there is no deformed band on top of this state, but it can be an "intruder" state with spherical shape [63]. There have been many theoretical approaches to this problem such as the boson expansion techniques [64], the interacting boson model [65], and the Hartree-Fock-Bogoliubov method with the quantum number projection [66]. These approaches are based on a mean-field picture or a collective model ansatz. Thus it is quite interesting to apply the microscopic shell model because it is suitable to describe detailed structure in such a transitional region, including the neighboring odd-mass nuclei, within a common framework.

As shown in Figs. 10 and 12, the shell-model calculations reasonably describe the experimental energy levels for both even-A and odd-A Ge isotopes at least around $N = 40$. Especially, the irregular behavior of the 0_2^+ states is successfully reproduced. In order to understand the structure of these states, in the following we examine first the validity of the shell-model description around ^{72}Ge in more detail. Both energy levels and transition properties are investigated along the isotope chain from $N = 37$ to 43 ($^{69-75}$Ge). This choice covers the cases of removal (addition) of at most three neutrons from (to) the ^{72}Ge ($N = 40$) core. The transition operators adopted in the present calculations are all one-body. Therefore, the $E1$ transition is not allowed in the present model space. The same effective g factors are used as those in subsection III B, and the adopted effective charges are the same as those for the calculation of $Q_{\rm th2}$ in subsection III C.

1. ^{69}Ge

Figure 17 shows the energy levels of ^{69}Ge. As for negative-parity states, one can find a reasonable one-to-one correspondence between the shell-model results and the experimental data. A relatively large difference is found in the second $9/2^-$ state, for which the calculation predicts lower excitation energy than the data by about 0.4 MeV. Considering that only the lowest three negative-parity states of this nuclei were taken as the data for the fitting calculations, the agreements in many

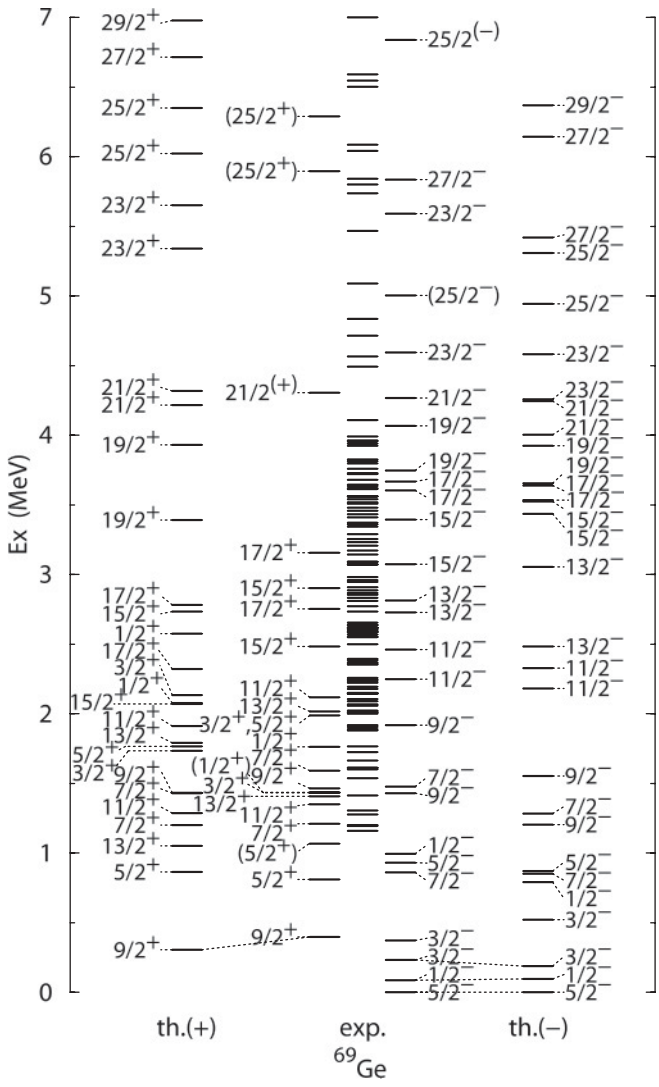

FIG. 17. Comparison of energy levels between the shell-model results and the experimental data for ^{69}Ge. Shell-model results are shown separately for positive- and negative-parity states [th.(+) and th.(−)], including at least two lowest states for each spin parity. For clarity, experimental data (exp.) that satisfy the same criterion are shown on the left and right sides with spin-parity labels, and the remaining data are shown in the center without spin-parity labels even if they are known experimentally. States connected by dotted lines are used as the data for the fitting calculation.

near-yrast states up to around 6 MeV are satisfactory. Thus, at the neutron number $N = 37$, single-particle excitations from the $f_{7/2}$ orbit are not apparent for low-lying states and near-yrast states currently considered. The shell-model description is reasonable also for the positive-parity states, for which only the lowest $9/2^+$ was taken as the data for the fitting. It should be noted that we can find several states for which there is no possible shell-model counterpart, such as the $(5/2^+)$ state at 933 keV, the $(1/2^+)$ state at 1438 keV, etc. This observation suggests a crucial contribution of the $d_{5/2}$ orbit for the description of these states. This single-particle orbit is missing in the present model space.

The electromagnetic transition properties are shown in Table V. For pure $M1$ and stretched $E2$ transitions, it can be seen that the calculated values agree with the data in many cases within a factor of 2, and the overall description is reasonable. The agreement becomes worse for transitions with where $M1/E2$ mixing is prevalent.

2. ^{70}Ge

The energy levels of ^{70}Ge from shell-model calculations and experiment are shown in Fig. 18. For the positive-parity states we note a reasonable correspondence between the shell-model results and the experimental data. The shell-model 3_1^+ state is predicted to be too low by about 0.5 MeV, giving rise to an incorrect level order. The transition property related to this state is reasonably described as shown in Table VI. As shown in Table IV, quadrupole moments have been measured for 2_1^+, 2_2^+, 2_3^+, and 4_1^+ states, and the shell model predicts the correct

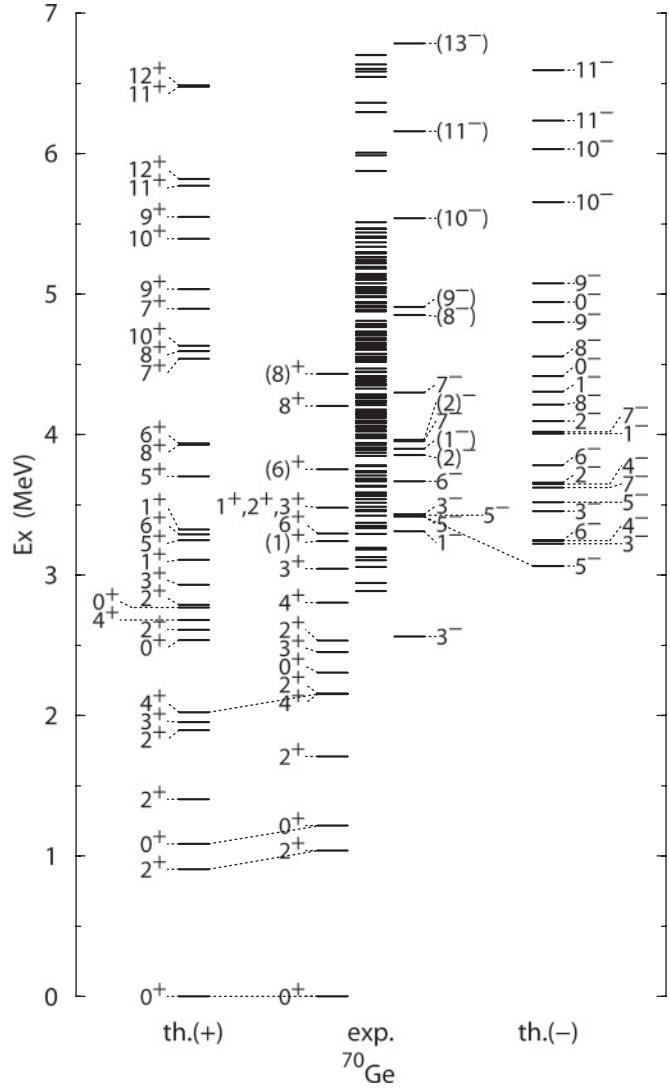

FIG. 18. Comparison of energy levels between the shell-model results and the experimental data for ^{70}Ge. Experimental data are taken from Ref. [34]. Conventions are the same as those in Fig. 17.

TABLE V. Transition matrix elements $B(E\lambda)$ and $B(M\lambda)$ for ^{69}Ge in Weisskopf units (W.u.). The excitation energies (E_x) are shown in keV. Experimental data are taken from Ref. [34].

Initial $J^\pi(E_x)$	Final $J^\pi(E_x)$	Multipole	Exp. (W.u.)	Th. (W.u.)
$1/2^-(87)$	$5/2^-(0)$	$E2$	0.583(25)	0.9
$3/2^-(233)$	$1/2^-(87)$	$M1$	0.0124(10)	0.0093
		$E2$	32(23)	4.5
	$5/2^-(0)$	$M1$	0.0042(8)	0.0001
		$E2$	65(19)	28.3
$9/2^+(398)$	$5/2^-(0)$	$M2$	0.0657(12)	0.206
$7/2^-(862)$	$9/2^+(398)$	$E1$	$2.0(6) \times 10^{-5}$	–
	$3/2^-(374)$	$E2$	4.0(14)	2.1
	$3/2^-(233)$	$E2$	12(5)	8.1
	$5/2^-(0)$	$M1$	0.0022(8)	0.0000
		$E2$	26(8)	19.7
$5/2^-(933)$	$3/2^-(374)$	$M1$	0.007(4)	0.0025
		$E2$	47(25)	6.9
	$3/2^-(233)$	$M1$	0.0019(9)	0.0002
		$E2$	0.7(4)	1.4
	$1/2^-(87)$	$E2$	8(5)	12.4
		$M3$	$2^{+8}_{-2} \times 10^5$	0.0291
	$5/2^-(0)$	$M1$	0.011(5)	0.0000
		$E2$	0.7(6)	8.8
$1/2^-(995)$	$3/2^-(374)$	$M1$	0.009(7)	0.0730
	$3/2^-(233)$	$M1$	0.015(10)	0.0024
		$E2$	19^{+20}_{-19}	1.3
	$5/2^-(0)$	$E2$	37(16)	0.6
$3/2^-(1160)$	$3/2^-(233)$	$M1$	0.0027(16)	0.0056
		$E2$	1.7(16)	10.6
	$1/2^-(87)$	$M1$	0.009(5)	0.0416
		$E2$	1.2(8)	1.2
	$5/2^-(0)$	$M1$	0.0016(9)	0.0001
$5/2^-(1196)$	$3/2^-(374)$	$M1$	0.016(9)	0.0256
		$E2$	18(18)	11.9
$1,3/2^-(1278)$[a]	$3/2^-(374)$	$M1$	0.006(5)	0.0092
$3/2^-(1307)$	$1/2^-(87)$	$M1$	0.009(4)	0.0088
		$E2$	0.8(6)	0.9
	$5/2^-(0)$	$M1$	0.007(3)	0.0017
$11/2^+(1351)$	$9/2^+(398)$	$M1$	0.029(4)	0.0436
		$E2$	27(4)	23.3
$13/2^+(1407)$	$9/2^+(398)$	$E2$	23(4)	19.8
$5/2^-(1415)$	$3/2^-(233)$	$M1$	0.0015(8)	0.0001
		$E2$	0.40(25)	0.6
	$5/2^-(0)$	$M1$	0.0035(17)	0.0039
		$E2$	1.1(6)	0.2
$9/2^-(1430)$	$5/2^-(0)$	$E2$	9.0(17)	17.0
$3/2^+(1433)$	$5/2^+(812)$	$M1$	0.04(3)	0.0120
		$E2$	$5^{+7}_{-5} \times 10^1$	6.0
$9/2^+(1466)$	$7/2^+(1210)$	$M1$	0.05(4)	0.0591
		$E2$	15(12)	19.2
	$7/2^-(862)$	$E1$	$2.5(18) \times 10^{-5}$	–
	$5/2^+(812)$	$E2$	14(10)	4.1
	$9/2^+(398)$	$M1$	0.0022(15)	0.0027
		$E2$	6(4)	4.3
$7/2^-(1479)$	$5/2^-(933)$	$M1$	0.026(9)	0.0000
		$E2$	4.8(19)	0.7
	$3/2^-(374)$	$E2$	12(8)	3.9
	$3/2^-(233)$	$E2$	1.7(6)	9.4
$3/2^-(1539)$	$3/2^-(374)$	$M1$	0.005^{+6}_{-5}	0.0063
		$E2$	1.1^{+13}_{-1}	0.6
	$1/2^-(87)$	$M1$	0.0038(22)	0.0090
		$E2$	0.6(6)	0.0
$7/2^+(1591)$	$5/2^+(812)$	$M1$	0.025(8)	0.2181
		$E2$	13(5)	30.0
	$9/2^+(398)$	$M1$	0.010(4)	0.0179
		$E2$	0.9(4)	2.9
$5/2^+(1601)$	$7/2^+(1210)$	$M1$	0.14(5)	0.0580
		$E2$	$8(6) \times 10^1$	6.2
	$5/2^+(812)$	$M1$	0.038(13)	0.0047
		$E2$	4(4)	1.6
	$3/2^-(374)$	$E1$	$4.3(15) \times 10^{-5}$	–
$7/2^-(1613)$	$5/2^-(933)$	$M1$	<0.0064	0.0196
		$E2$	<0.085	0.1
	$3/2^-(233)$	$E2$	<4.7	0.6
	$5/2^-(0)$	$M1$	<0.00064	0.0006
		$E2$	<1.4	0.0
$9/2^-(1920)$	$5/2^-(1196)$	$E2$	<11	17.7
	$7/2^-(862)$	$M1$	<0.0024	0.0025
		$E2$	<8.8	6.2
	$5/2^-(0)$	$E2$	<0.50	0.8
$13/2^+(2018)$	$13/2^+(1407)$	$M1$	0.00047(10)	0.0107
		$E2$	7.7(12)	4.0
	$11/2^+(1351)$	$M1$	0.028(5)	0.0795
		$E2$	22(6)	22.2
	$9/2^+(398)$	$E2$	0.34(9)	4.2
$11/2^-(2248)$	$9/2^-(1430)$	$M1$	0.0013(8)	0.0002
		$E2$	2.4(15)	10.1
	$7/2^-(862)$	$E2$	13(8)	6.6
$15/2^+(2483)$	$13/2^+(1407)$	$M1$	0.009(4)	0.0281
		$E2$	2.4(11)	17.1
	$11/2^+(1351)$	$E2$	10(4)	17.3
$17/2^+(2755)$	$13/2^+(1407)$	$E2$	12.4(21)	17.1
$15/2^-(3076)$	$13/2^-(2834)$	$M1$	0.40(9)	0.0023
		$E2$	$3^{+4}_{-3} \times 10^1$	0.3
	$13/2^+(1407)$	$E1$	0.00015(4)	–
		$M2$	0.9(7)	0.0001
$17/2^+(3157)$	$15/2^+(2483)$	$M1$	0.015(8)	0.0647
		$E2$	10(6)	18.2
	$13/2^+(2018)$	$E2$	11(4)	26.9
$17/2^-(3605)$	$13/2^-(2730)$	$E2$	20(11)	13.4
	$15/2^+(2483)$	$E1$	$2.5(14) \times 10^{-5}$	–
$19/2^-(3749)$	$17/2^+(3157)$	$E1$	$5.5(7) \times 10^{-5}$	–
		$M2$	0.1^{+3}_{-8}	0.0009
	$15/2^-(3076)$	$E2$	8.5(10)	18.8
	$17/2^+(2755)$	$E1$	$3.7(4) \times 10^{-5}$	–
		$M2$	0.15^{+21}_{-15}	0.0045
$21/2^-(4267)$	$19/2^-(3749)$	$M1$	0.033(4)	0.0173
		$E2$	1.2(4)	2.3
$23/2^-(4594)$	$21/2^-(4267)$	$M1$	0.0192(13)	0.0051
		$E2$	3.3(24)	0.5
	$19/2^-(4068)$	$E2$	14.2(12)	13.7
	$19/2^-(3749)$	$E2$	1.86(15)	0.7

[a] $J^\pi = 3/2^-$ is assumed for the calculation.

TABLE VI. Transition matrix elements for ^{70}Ge. Conventions are the same as those in Table V.

Initial $J^\pi(E_x)$	Final $J^\pi(E_x)$	Multipole	Exp. (W.u.)	Th. (W.u.)
$2^+(1039)$	$0^+(0)$	$E2$	21.0(4)	25.0
$0^+(1215)$	$2^+(1039)$	$E2$	48(3)	28.3
$2^+(1708)$	$0^+(1215)$	$E2$	25(14)	1.8
	$2^+(1039)$	$M1$	0.0025^{+31}_{-17}	0.0140
		$E2$	$1.11(60)\times10^2$	36.9
	$0^+(0)$	$E2$	1.0(5)	0.5
$4^+(2154)$	$2^+(1039)$	$E2$	24(6)	41.0
$0^+(2307)$	$2^+(1708)$	$E2$	>4.8(3)	3.7
	$2^+(1039)$	$E2$	>0.14(1)	0.9
$3^+(2452)$	$2^+(1708)$	$M1$	0.022(13)	0.0161
$3^-(2561)$	$2^+(1039)$	$E1$	0.00028(7)	–
		$M2$	<20	0.00119
$4^+(2807)$	$2^+(1708)$	$E2$	29(12)	12.8
$4^+(3059)$	$2^+(1039)$	$E2$	2.0(11)	0.7
$6^+(3297)$	$4^+(2154)$	$E2$	34(7)	48.6
$5^-(3417)$	$4^+(3059)$	$E1$	0.00013(3)	–
		$M2$	17^{+21}_{-13}	0.00005
	$3^-(2561)$	$E2$	2.0(3)	6.5
	$4^+(2154)$	$E1$	$6(1)\times10^{-6}$	–
		$M2$	<0.13	0.00012
$6^-(3667)$	$5^-(3417)$	$M1$	0.040(4)	0.0536
$6^+(3753)$	$4^+(2807)$	$E2$	27^{+12}_{-6}	17.7
$7^-(3955)$	$6^-(3667)$	$M1$	0.045(4)	0.0502
	$6^+(3297)$	$E1$	$1.3(3)\times10^{-5}$	–
$8^+(4204)$	$6^+(3297)$	$E2$	6.5(17)	7.7
$7^+(4299)$	$7^-(3955)$	$E1$	0.0015(5)	–
	$6^+(3296)$	$M1$	0.004^{+2}_{-1}	0.0158
		$E2$	0.08^{+8}_{-4}	0.02
$8^+(4432)$	$6^+(3297)$	$E2$	43(22)	31.9
$8^-(4852)$	$7^-(3955)$	$M1$	<0.0100	0.0072
		$E2$	<4.9	3.3
$10^-(5540)$	$8^+(4432)$	$M2$	0.22(9)	0.00014

sign of them. Although the reproduction of the experimental excitation energies is not necessarily perfect, the number of positive-parity states below 3 MeV is correctly described in the shell-model results. Above 3 MeV, the experimental level density becomes very high and there appear many states with no spin-parity assignment. The predicted position of the 6^+ and 8^+ states look consistent with the possible experimental candidates.

As for the negative-parity states, there is no 1^- single-particle excitation in the present model space. Thus the 1^- state is predicted to be too high in the shell-model results. Also, it is seen that the shell model fails to reproduce the lowest 3^- state probably due to the insufficient octupole collectivity in the present model space. This is the reason why the 3^- state was excluded from the fitting data. On the other hand, the predicted excitation energies of higher spin states such as the 10^- and 11^- states are in good agreement with the possible experimental counterparts. The leading neutron configuration in the calculated wave function of the 10^-_1 state is 1p-3h (62%) relative to the $N=40$ core, while it is 3p-5h (77%) in the 11^-_1 state. The good agreement with the experimental data suggests

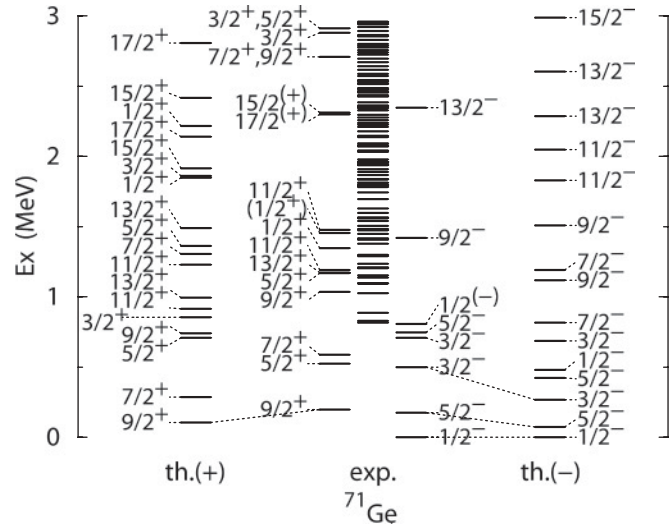

FIG. 19. Comparison of energy levels between the shell-model results and the experimental data for ^{71}Ge. Experimental data are taken from Ref. [34]. Conventions are the same as those in Fig. 17.

that the relative ESPE of the pf orbits and the $g_{9/2}$ orbit is reasonable in the present shell model.

3. ^{71}Ge

Energy levels of ^{71}Ge are shown in Fig. 19. As in the case of the ^{69}Ge, there is no shell-model counterpart for the experimental $5/2^+$ state at 525 keV. Also, the $1/2^+$ state is predicted to be too high in the shell model compared with data. It is difficult to examine the quality of the shell-model description because of many experimental low-lying states without any spin-parity assignment. The yrast states with relatively high spin such as the $17/2^+$ and $13/2^-$ states are predicted at reasonable excitation energies and compare well with the possible experimental candidate. The transition matrix elements are shown in Table VII. The agreement between the data and the shell-model results is typically within a factor of about 3.

TABLE VII. Transition matrix elements for ^{71}Ge. Conventions are the same as those in Table V.

Initial $J^\pi(E_x)$	Final $J^\pi(E_x)$	Multipole	Exp. (W.u.)	Th. (W.u.)
$5/2^-(175)$	$1/2^-(0)$	$E2$	2.29(6)	1.0
$9/2^+(198)$	$5/2^-(175)$	$M2$	0.0588(19)	0.274
$13/2^+(1172)$	$9/2^+(198)$	$E2$	42(8)	24.3
$11/2^+(1192)$	$9/2^+(198)$	$M1$	0.009(3)	0.0065
		$E2$	23(6)	6.3
$9/2^-(1422)$	$5/2^-(747)$	$E2$	44(11)	15.0
	$5/2^-(175)$	$E2$	8.7(18)	11.9
$11/2^+(1477)$	$7/2^+(590)$	$E2$	50(9)	2.0
	$9/2^+(198)$	$M1$	0.00045^{+31}_{-15}	0.0209
		$E2$	9.1(18)	19.2

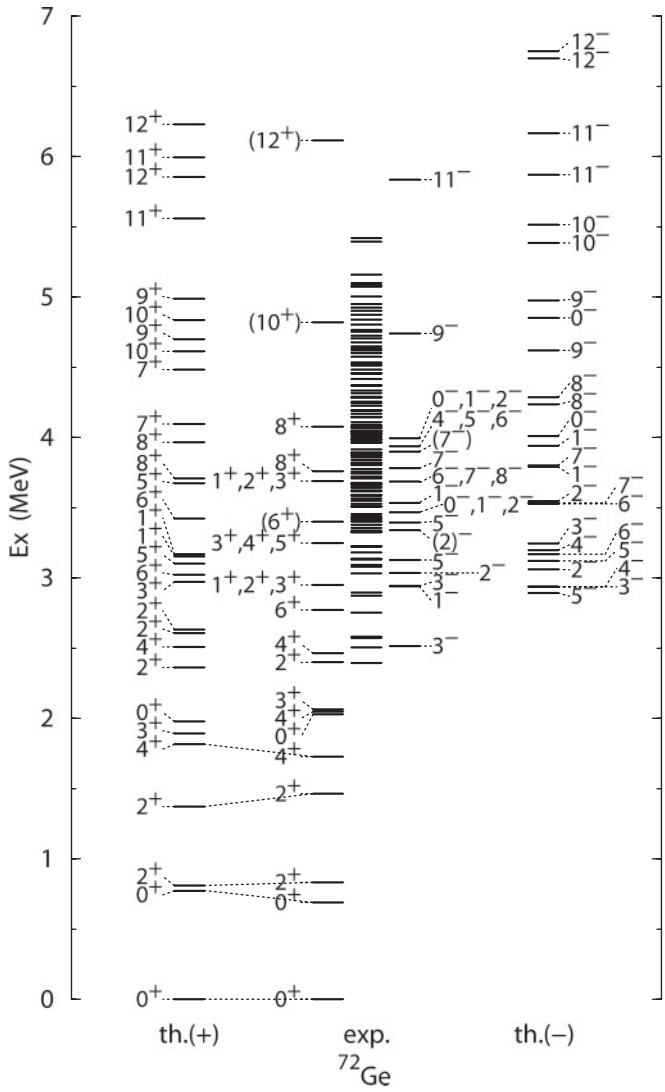

FIG. 20. Comparison of energy levels between the shell-model results and the experimental data for ^{72}Ge. Conventions are the same as those in Fig. 17.

4. ^{72}Ge

The energy levels of ^{72}Ge are expected to reflect most directly the property of the $N = 40$ subshell structure. In Fig. 20, one can find reasonable agreement between the calculated energy levels and the experimental data. There is a one-to-one correspondence for positive-parity states up to 3 MeV, although the level ordering is not necessarily reproduced correctly. The largest deviation from experiment is found for the 3_1^+ state, which is predicted to be too low by about 0.5 MeV in the shell-model result as in the case of the ^{70}Ge. For higher spin states, the experimental data are not necessarily certain, but the shell-model results for the yrast 10^+ and 12^+ states agree well with the experimental candidates within an error of 0.3 MeV. The shell-model description looks reasonable also for the negative-parity states. The agreement between the data and the shell-model results is good especially for the yrast states with relatively high spin, while the lowest 1^- and 3^- states are predicted to be too high by the shell model as in the case of ^{70}Ge.

TABLE VIII. Transition matrix elements for ^{72}Ge. Conventions are the same as those in Table V.

Initial $J^\pi(E_x)$	Final $J^\pi(E_x)$	Multipole	Exp. (W.u.)	Th. (W.u.)
$2^+(834)$	$0^+(691)$	$E2$	17.8(3)	6.8
	$0^+(0)$	$E2$	23.5(4)	25.8
$2^+(1464)$	$2^+(834)$	$M1$	0.00016(5)	0.0210
		$E2$	62(11)	38.6
	$0^+(691)$	$E2$	0.030(6)	0.1
	$0^+(0)$	$E2$	0.130(24)	1.0
$4^+(1728)$	$2^+(834)$	$E2$	37(5)	44.8
$3^+(2065)$	$2^+(1464)$	$M1$	<0.0023	0.0209
		$E2$	<150	51.0
$4^+(2464)$	$4^+(1728)$	$M1$	0.012^{+12}_{-9}	0.0240
	$2^+(1464)$	$E2$	15^{+15}_{-11}	4.0
	$2^+(834)$	$E2$	0.05^{+5}_{-4}	0.5
$3^-(2515)$	$4^+(2464)$	$E1$	0.00057(14)	–
	$2^+(2402)$	$E1$	0.00074(23)	–
	$4^+(1728)$	$E1$	$4.8(10)\times10^{-5}$	–
		$M2$	<0.8	0.00608
	$2^+(1464)$	$E1$	$3.9(8)\times10^{-5}$	–
		$M2$	16(6)	0.00000138
	$0^+(0)$	$E3$	29(6)	1.52
$6^+(2772)$	$4^+(1728)$	$E2$	36^{+49}_{-31}	48.4
$5^-(3129)$	$3^-(2515)$	$E2$	29()	5.0
$6^+(3402)$	$4^+(2464)$	$E2$	20()	17.6
$6^+(3667)$	$5^-(3129)$	$E1$	<0.0012	–
$8^+(3761)$	$6^+(2772)$	$E2$	$4(3) \times 10^1$	4.2
$7^-(3784)$	$5^-(3129)$	$E2$	<47	5.6
$8^+(4078)$	$8^+(3761)$	$M1$	0.12^{+23}_{-12}	0.0147
	$6^+(2772)$	$E2$	9^{+17}_{-9}	24.4
$9^-(4741)$	$7^-(3784)$	$E2$	35(6)	26.2
$10^+(4820)$	$8^+(3761)$	$E2$	47(7)	29.5
$11^-(5838)$	$9^-(4741)$	$E2$	22(10)	34.7
$12^+(6115)$	$10^+(4820)$	$E2$	26(6)	41.1

Transition properties are shown in Table VIII. The calculated $B(E2)$ values reproduce the experimental data within a factor of 2 for most cases. One of our principal interests is the structure of the 0_2^+ state. In the experimental data, there are two $E2$ transitions related to this state: 2_1^+ to 0_2^+ and 2_2^+ to 0_2^+. The former is much stronger than the latter, and the shell-model results qualitatively reproduce such a feature.

5. ^{73}Ge

Figure 21 and Table IX show the comparison of energy levels and transition matrix elements, respectively, between the shell-model results and the experimental data for ^{73}Ge. The shell model fails to reproduce the ground-state spin $9/2^+$ due to the inversion with the closely-lying $7/2^+$ state. One remarkable difference between the shell-model results and the experimental data is seen in the triplet near the ground state, where the $5/2^+$ state looks missing in the calculation. The shell model predicts too-high excitation energy by about 0.5 MeV for the lowest $5/2_1^+$ state, and it is also the case for the $1/2_1^+$ state. Such a feature has been seen systematically also in ^{69,71}Ge. In ^{73}Ge, because the neutron pf shell is closed

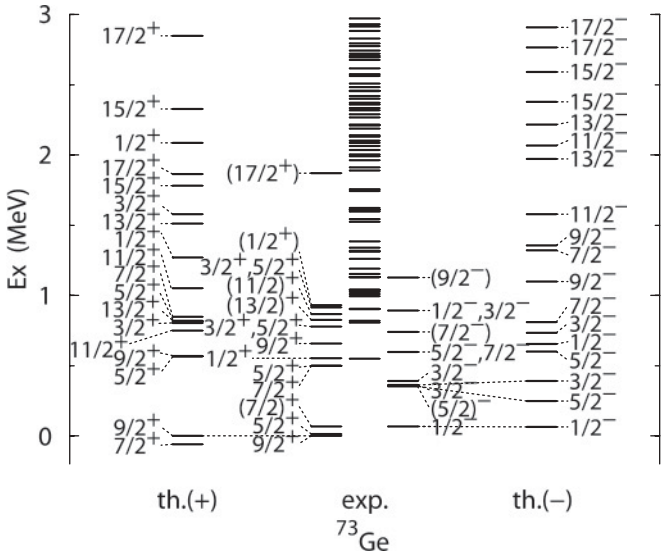

FIG. 21. Comparison of energy levels between the shell-model results and the experimental data for ^{69}Ge. Experimental data are taken from Ref. [34]. Conventions are the same as those in Fig. 17.

and the $N_{\rm osc} = 4$ shell is now an active valence shell, the influence of the missing $d_{5/2}$ orbit is expected to becomes more apparent in the low-lying states than the cases of the less-neutron Ge isotopes. As for the negative-parity states, there are two $3/2^-$ states around 0.8 MeV in the experimental data, while the shell model predicts only one state nearby. Thus, the quality of the shell-model description is not too good around the ground state. On the other hand, as for the higher spin states, the calculated yrast $11/2^+$, $13/2^+$, $17/2^+$, and $9/2^-$ states are in reasonable agreement with experiment. The experimental values of the $E2$ transition matrix elements are also successfully reproduced by the shell model, except for those related to the $5/2_1^+$ state. The reproduction of the $M1$ transition is in general not successful, probably because of the incomplete spin degrees of freedom in the present model space.

6. ^{74}Ge

Energy levels of ^{74}Ge are shown in Fig. 22. We observe a reasonable agreement between the shell-model results and the experimental data, except for the lowest 1^- and 3^- states as in the cases of ^{70,72}Ge. It is interesting to compare the energy levels between ^{70}Ge and ^{74}Ge. These levels correspond to neutron two-hole states and two-particle states, respectively, on top of the ^{72}Ge core. In the former, the calculated spectrum is slightly compressed compared with the experimental data, while it is expanded in the latter. This feature suggests that the low-lying states described by the shell model are too collective for $N < 40$, while the development of the collectivity is insufficient for $N > 40$. This interpretation is consistent with the variation of $B(E2)$ values shown in Fig. 8. Nevertheless, the overall description by the shell model is basically good not only for the energy levels but also for the transition properties, as shown in Table X.

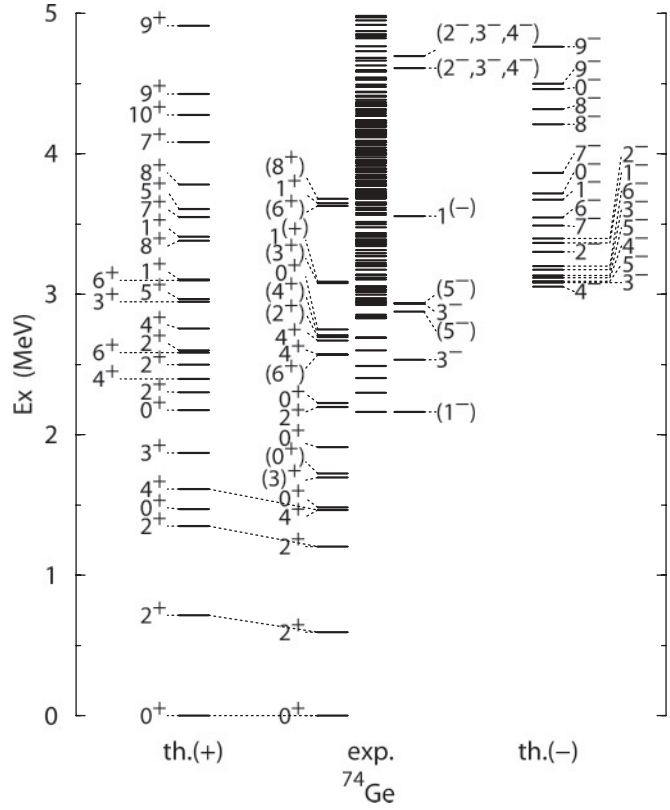

FIG. 22. Comparison of energy levels between the shell-model results and the experimental data for ^{74}Ge. Experimental data are taken from Ref. [34]. Conventions are the same as those in Fig. 17.

TABLE IX. Transition matrix elements for ^{73}Ge. Conventions are the same as those in Table V.

Initial $J^\pi(E_x)$	Final $J^\pi(E_x)$	Multipole	Exp. (W.u.)	Th. (W.u.)
$5/2^+(13)$	$9/2^+(0)$	$E2$	23.1(8)	27.1
$1/2^-(67)$	$5/2^+(13)$	$M2$	0.00084(3)	0.318
$7/2^+(69)$	$9/2^+(0)$	$M1$	0.0316(24)	0.0017
		$E2$	41(8)	34.8
$7/2^+(499)$	$5/2^+(13)$	$M1$	0.0009(3)	0.0520
		$E2$	72(21)	4.0
	$9/2^+(0)$	$M1$	0.0008(5)	0.0367
		$E2$	6.3(4)	3.7
$13/2^+(826)$	$9/2^+(0)$	$E2$	30(2)	29.8

TABLE X. Transition matrix elements for ^{74}Ge. Conventions are the same as those in Table V.

Initial $J^\pi(E_x)$	Final $J^\pi(E_x)$	Multipole	Exp. (W.u.)	Th. (W.u.)
$2^+(596)$	$0^+(0)$	$E2$	33.0(4)	29.1
$2^+(1204)$	$2^+(596)$	$M1$	0.00099(15)	0.0125
		$E2$	43(6)	39.4
	$0^+(0)$	$E2$	0.71(11)	1.2
$4^+(1464)$	$2^+(596)$	$E2$	41(3)	42.2
$0^+(1483)$	$2^+(596)$	$E2$	9^{+9}_{-6}	14.0

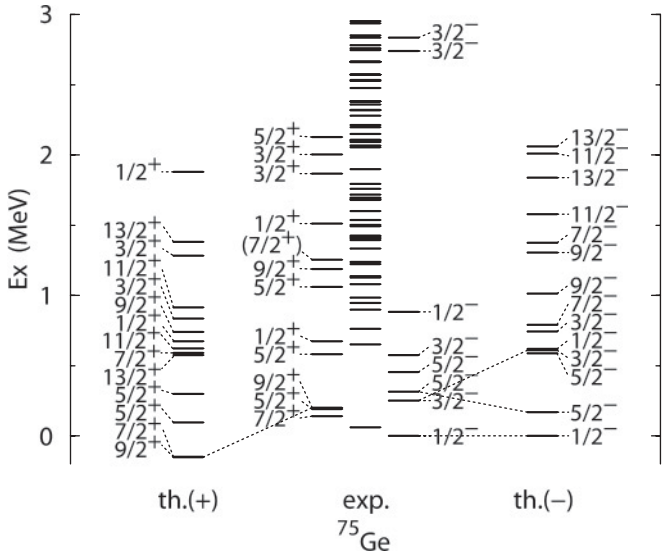

FIG. 23. Comparison of energy levels between the shell-model results and the experimental data for ^{75}Ge. Experimental data are taken from Ref. [34]. Conventions are the same as those in Fig. 17.

7. ^{75}Ge

The energy levels and the transition properties are shown in Fig. 23 and Table XI, respectively. The agreement between the shell-model results and the experimental data is not good for the energy levels of the low-lying states. The difficulties in the lowest $5/2^+$, $1/2^+$, and $3/2^-$ states are quite similar to those in the case of ^{73}Ge. We cannot discuss the high-spin states with $J \geqslant 11/2$ because experimental data are unavailable. Experimental data for transitions are also limited and with very large errors except for the $7/2^+ \to 1/2^-$ $E3$ transition. The shell-model prediction for this $E3$ transition is too small by three orders of magnitude, suggesting that the relevant single-particle orbits are missing in the present model space.

8. *Magicity of* $N = 40$

As demonstrated above, the present shell-model calculations describe properly energy levels and transition properties for isotopes around ^{72}Ge, although there are several problems that can naturally attributed to the small model space. By using the shell-model wave functions we can analyze the structure of the 0_2^+ states. The occupation number of the neutron $g_{9/2}$ orbit is shown in Fig. 24. The behavior of the occupation number looks very similar for the 0_1^+ and the 2_1^+ states, suggesting the same intrinsic structure, which varies smoothly as a function of N. If we assume a naive filling configuration,

TABLE XI. Transition matrix elements for ^{75}Ge. Conventions are the same as those in Table V.

Initial $J^\pi(E_x)$	Final $J^\pi(E_x)$	Multipole	Exp. (W.u.)	Th. (W.u.)
$7/2^+(140)$	$1/2^-(0)$	$E3$	0.0289(10)	0.0000284
$5/2^+(192)$	$7/2^+(140)$	$M1$	$8^{+7}_{-6} \times 10^{-5}$	0.0101
		$E2$	31^{+24}_{-28}	40.8

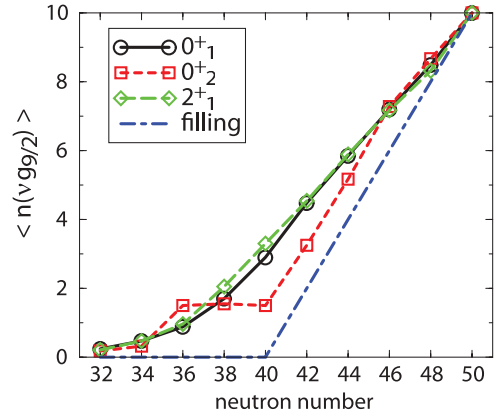

FIG. 24. (Color online) Occupation numbers of the neutron $g_{9/2}$ orbit in the shell-model wave functions. The filling configuration corresponds to the dot-dashed line.

i.e., $\nu(pf_{5/2})^{N-28}$ for $N \leqslant 40$ and $\nu(pf_{5/2})^{12}(g_{9/2})^{N-40}$ for $N > 40$, the $g_{9/2}$ occupation number is expected to be 0 for $N \leqslant 40$ and $N - 40$ for $N > 40$ as shown in the same figure. However, in the shell-model wave functions, it can be seen that additional neutrons are excited to the $g_{9/2}$ orbit, because of the deformation and the pairing effect. The expectation value of such additional neutrons increases toward the middle of the model space and reaches the largest value of about three at $N = 40$. There is no shell-model configuration that dominates the wave functions of these states. For example, in the case of the ^{72}Ge 0_1^+ state, the shell-model configuration $\pi(p_{3/2})^2(f_{5/2})^2\nu(p_{3/2})^4(f_{5/2})^4(p_{1/2})^2(g_{9/2})^2$ carries the largest probability of only 8% in the wave function, and many other configurations give non-negligible contributions. Thus, these states can be interpreted as collective states. Note that such an enhanced filling of the $g_{9/2}$ orbit due to the pairing correlations around $N = 40$ has been pointed out also for Zn and Ni isotopes [50].

On the other hand, the occupation number of the 0_2^+ state shows quite different N dependence for $36 \leqslant N \leqslant 44$. It is close to 2 for $N \leqslant 40$ and $N - 38$ for $N > 40$, which is consistent with the picture of two-neutron excitation from the pf shell to the $g_{9/2}$ orbit on top of the filling configuration. As for the ^{72}Ge, the wave function of the 0_2^+ state is dominated by the neutron closed pf-shell configuration $\pi(p_{3/2})^4\nu(p_{3/2})^4(f_{5/2})^6(p_{1/2})^2$ with the probability of 37%, which suggests a nearly spherical shape. Thus, our shell-model results support the picture of the spherical-deformed shape coexistence in ^{72}Ge. Similarly, in ^{74}Ge, 27% of the 0_2^+ wave function consists of the $\nu(g_{9/2})^2$ configuration on top of the neutron closed pf shell, As for ^{70}Ge, the dominating configuration in the 0_2^+ wave function is the $\nu(f_{5/2})^{-2}$ configuration with 17% probability.

We can understand the lowering of the excitation energy of the 0_2^+ state toward $N = 40$ as a result of the magicity of the $N = 40$ closed-shell configuration. The ESPE shell-gap at $N = 40$ is about 3 MeV in Ge isotopes, which is not large enough to stabilize the closed-shell configuration as a ground state. Because of strong collective correlations such as the pairing and the quadrupole-quadrupole force, this shell gap is

overcome and the closed-shell effect is almost washed out in the ground-state band. The structure of the ground state varies rather smoothly without showing any specific shell effects at $N = 40$. However, the magicity of the $N = 40$ subshell survives in the excited 0^+ state of Ge isotopes and rapidly disappears as adding or removing neutrons. Correspondingly, the excitation energy of the 0_2^+ state takes the minimum value at $N = 40$ and increases as number of neutrons departs from it.

H. $N = Z$ nuclei

The structure of $N = Z$ nuclei in the pfg-shell region has been attracting broad interests because of various reasons. Because protons and neutrons occupy the same valence shell, the strong proton-neutron interaction plays a crucial role and collective features become apparent. The nuclear shape changes rapidly along the $N = Z$ line, and sometimes different shapes coexist in the low-lying region of one particular nucleus. It should be noted that we have excluded experimental data of $N \approx Z$ nuclei with $A > 64$ (see Fig. 1) from the data to be fitted in the derivation of the effective interaction, because it is anticipated that the present model space is too small to describe collective features observed experimentally in this mass region. Therefore, it is interesting to investigate to what extent the applicability of the present interaction can be extended into this region and to clarify how it fails. In this subsection, the structure of $N = Z$ nuclei is studied in detail for ^{64}Ge, ^{66}As,^{68}Se, and ^{70}Br.

1. *Triaxiality of* ^{64}Ge

The structure of ^{64}Ge has been investigated from various viewpoints such as the ground-state shape and the octupole collectivity. In Fig. 25, one can find a reasonable correspondence between the shell-model results and experimental data, especially in the band structure. However, the calculated 3^+ state appears at much lower excitation energy than the experimental (3^+) state by about 0.9 MeV. This (3^+) state was proposed in Ref. [67] considering the dipole character of the transition to the (2^+) state, but it was reassigned as a (4^+) state in Ref. [68]. The experimental (4^+) state is lower in excitation energy than the (3^+) state, and its spin-parity was assigned [67] based on the quadrupole character of the transition to the (2^+) state. In the shell-model results, the $3^+ \rightarrow 2_2^+$ transition is almost completely $E2$ dominant. Thus, possible reassignments as 3^+-5^+-7^+ for the (4^+)-(6^+)-(8^+) states may improve the agreement between the shell-model results and the experimental data without any serious contradiction with observation.

The γ softness of ^{64}Ge has been proposed by various theoretical investigations based on the collective models and mean-field models [67,69]. It is interesting to see whether such a character can be described by the shell-model calculations using a modified realistic Hamiltonian. The calculated excitation-energy ratio $E_x(4^+)/E_x(2^+) = 2.50$ is in reasonable agreement with the experimental value 2.27, which corresponds to a γ-soft nucleus according to the Wilets-Jean model [70]. On the other hand, according to the rigid rotor model with triaxial deformation by Davydov and Filippov [71], the calculated ratio $B(E2; 2_2^+ \rightarrow 2_1^+)/B(E2; 2_2^+ \rightarrow 0_1^+) = 14$ corresponds to $\gamma \sim 23^\circ$. This value compares well with the value 27° in Ref. [67] obtained from experiment. Also, by adopting the value $\gamma = 23^\circ$, the Davydov model predicts the quadrupole moments of the two 2^+ states with an opposite sign, $Q(2_1^+) = -Q(2_2^+) = -0.216 Q_0$, where Q_0 stands for the intrinsic quadrupole moment. The shell-model results $Q(2_1^+) = -0.30\ e\,\mathrm{b}$ and $Q(2_2^+) = +0.29\ e\,\mathrm{b}$ are consistent with this prediction, using the intrinsic quadrupole moment $Q_0 = 1.3\ e\,\mathrm{b}$. The calculated $B(E2; 2_1^+ \rightarrow 0_1^+) = 24.9$ W.u. is in good agreement with the experimental value 27(4) W.u. [52] and corresponds to $Q_0 = 1.38\ e\,\mathrm{b}$. All the above properties are consistent with the Davydov model predictions with $\beta \sim 0.25$ and $\gamma \sim 23^\circ$. However, the calculated excitation-energy ratio $E_x(2_2^+)/E_x(2_1^+) = 1.47$ is much smaller than the corresponding value 2.8 and the experimental value 1.75.

In the calculated energy levels, one can find a sequence of the quasi-γ-band $J^\pi = 2_2^+, 3_1^+, 4_2^+, \ldots$. A discriminating quantity was introduced by Casten [72], $E_s(4) = [E_x(4_\gamma^+) - E_x(3_\gamma^+)] - [E_x(3_\gamma^+) - E_x(2_\gamma^+)]$, which takes a positive value for a rigid triaxial rotor [$E_s(4)/E_x(2_1^+) = 5/3$ for $\gamma = 30^\circ$] and a negative value for a γ-soft rotor [$E_s(4)/E_x(2_1^+) = -2$]. In the shell-model result, $E_s(4)/E_x(2_1^+) = 0.073$, which is in between these two cases.

It has been pointed out [73,74] that, for intuitive understanding, the total energy surface is useful for the shell-model effective Hamiltonian. Figure 26 shows the energy surface obtained by constrained Hartree-Fock calculations with the JUN45 interaction. It is seen that, in the case of ^{64}Ge, there is one energy minima at $\gamma \sim 23^\circ$, which is shallow in the γ

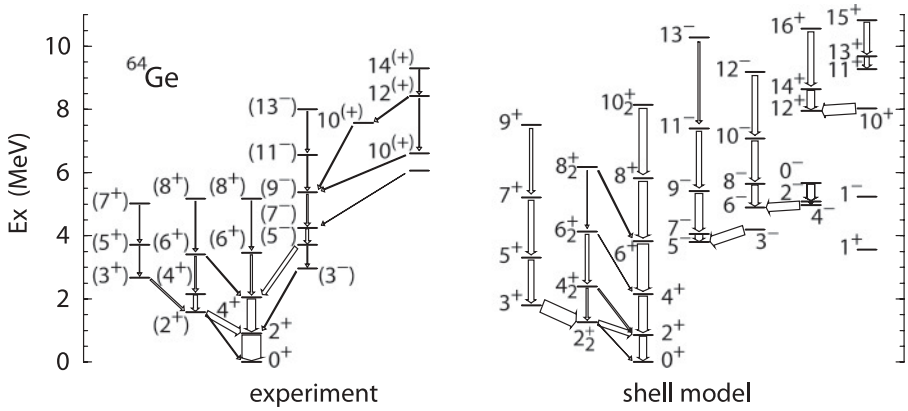

FIG. 25. Comparison of energy levels between the shell-model results and the experimental data for ^{64}Ge. Experimental data are taken from Refs. [67,68]. In Ref. [68], the (3^+) state is assigned to be (4^+). The width of the arrow drawn in the experimental part corresponds to the relative γ-ray intensity, while in the theoretical part, it stands for the relative $B(E2)$ value.

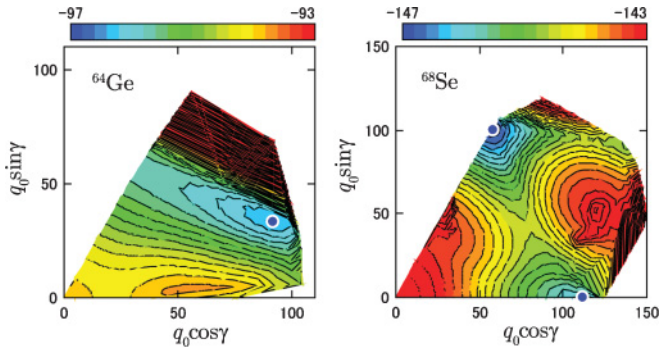

FIG. 26. (Color online) Total energy surfaces for ^{64}Ge and ^{68}Se obtained by Hartree-Fock calculations with constraints $\langle r^2 Y_{2,\pm1}\rangle = 0$, $\langle r^2 Y_{2,2}\rangle = \langle r^2 Y_{2,-2}\rangle$, $\langle 3z^2 - r^2\rangle = q_0 \cos\gamma$, $\sqrt{3}\langle x^2 - y^2\rangle = q_0 \sin\gamma$, and $\langle J_x\rangle = 0$. The contour lines are 200 keV apart. Closed circles indicate local energy minima.

direction, indicating an intermediate character of the γ-soft and the γ-rigid triaxial shape in the calculated energy spectra. This result is consistent with the above interpretation.

As for the negative-parity band, the excitation energies of the calculated 5^--7^--9^- members are in good agreement with experimental data, while the 11^- and 13^- are predicted to be too high in energy. The observed irregularity in the experimental energy spacing between the 11^- and the 9^- states suggests a possible band crossing. The calculated 3^-_1 states appears at 4.203 MeV, which is higher in energy than the 5^-_1 state. The large value $B(E2; 3^-_1 \to 5^-_1) = 31$ W.u. suggests that this 3^-_1 state is a member of the negative-parity two-quasiparticle band consisting of one hole in the pf orbit and one particle in the $g_{9/2}$ orbit. On the other hand, in the experimental data, the 3^-_1 state is lower than the 5^-_1 state, and the relatively wide energy splitting between the 3^- and the 5^- state as well as the weak transition intensity between them ($B(E2) = 1.0(5)$ W.u. in Ref. [68]) suggests a different structure of the 3^- state from the members of the negative-parity band. Thus, this 3^- state does not correspond to the calculated 3^-_1 state. One possible interpretation is that this 3^- state is a collective octupole vibrational state, which cannot be described in the present shell model due to the narrow model space.

In Ref. [68], a transition rate $B(M2; 5^-_1 \to 4^+_1) = 6.06^{+1.59}_{-1.13}$ W.u. is deduced from the measured multipole mixing ratio and the lifetime. Although this value is rather large compared with the recommended upper limit 1 W.u., $M2$ transitions with a similar order of magnitude have been observed in the neighboring nuclei ^{66}Ge [0.0040(19) W.u.] and ^{68}Ge [0.7(7) W.u.] [34]. On the other hand, the shell model predicts $B(M2) = 1.1 \times 10^{-5}$ W.u., 1.3×10^{-3} W.u., and 6.1×10^{-4} W.u. for ^{64}Ge, ^{66}Ge, and ^{68}Ge, respectively, which are significantly smaller than the above experimental values especially for ^{64}Ge. In the present model space, there is only one one-body $M2$ matrix element among the $f_{5/2}$ and the $g_{9/2}$ orbits. Because these two orbits are above the Fermi surface in the lowest filling configuration of ^{64}Ge, it is natural that the above $B(M2)$ becomes small. Thus the discrepancy between the experimental data and the shell-model results suggests the importance of orbits such as the $f_{7/2}$ and the $d_{5/2}$. These orbits are not included in the present model space.

2. *Isomeric states in* ^{66}As

In ^{66}As, two isomeric states have been reported [75,76] at the excitation energy 3024 keV with the lifetime $T_{1/2} = 8.2(5)$ μs and at 1357 keV with $T_{1/2} = 1.1(1)$ μs. The former one was tentatively assigned to be 9^+ and the latter 5^+. The shell-model results are compared with the experimental data in Fig. 27. One finds a reasonable agreement especially in the odd-spin sequences of states 1^+-3^+-5^+-7^+ and 9^+-11^+-13^+, although the experimental spin assignments are all tentative. As for the even-spin states, the calculated 0^+ and 2^+_2 states are $T = 1$, which correspond to the isobaric analog states of the ground state and the first excited state of ^{66}Ge, respectively. The correspondence between the experimental (12)-(14)-(16)-(18) states and the shell-model yrast 12^+-14^+-16^+-18^+ states is not very good. In the shell-model results, the level spacing is somewhat too large and the yrast 18^+ state decays predominantly to the 16^+_2 state.

The shell model predicts the yrast 5^+ state at lower excitation energies than the experimental candidates by 0.95 MeV. The structure of this state can be interpreted as an aligned proton-neutron pair in the $f_{5/2}$ orbit. In fact, in the calculated wave function, such a $[\pi f_{5/2} \nu f_{5/2}]_{J=5}$ configuration is found with 67% probability for the 5^+_1 state, while it is only 17% in the 5^+_2 state. Experimentally, the isomer (5^+) state is supposed to decay by $E2$ transitions to the (3^+) state, and the $B(E2)$ value is estimated to be 5.4(14) e^2 fm^4 [75]. Considering the revised lifetime in Ref. [76], the corresponding revised value should be about 9.3 e^2 fm^4. The shell-model prediction

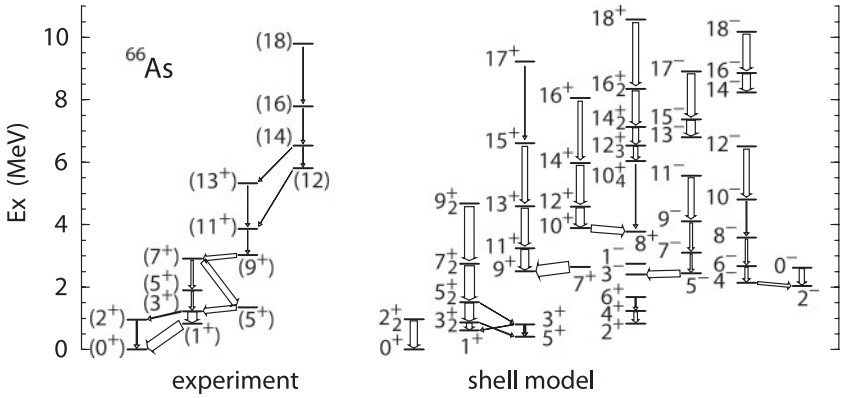

FIG. 27. Comparison of energy levels between the shell-model results and the experimental data for ^{66}As. Experimental data are taken from Refs. [75,76]. Conventions are the same as those of Fig. 25.

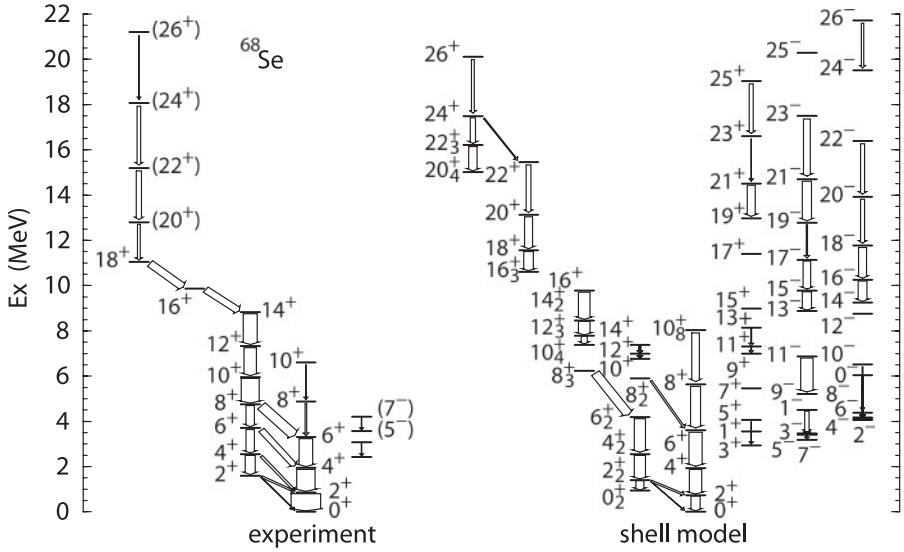

FIG. 28. Comparison of energy levels between the shell-model results and the experimental data for ^{68}Se. Experimental data are taken from Refs. [77,78]. Conventions are the same as those of Fig. 25.

$B(E2; 5_1^+ \to 3_2^+) = 16\ e^2\ \mathrm{fm}^4$ is not very far from this value. Therefore, the shell model reasonably describes the structure of the wave function but not the excitation energy. Further refinements of the TBME are necessary to improve the agreement with experiment.

Similarly, the shell model predicts the yrast 9^+ states to be 0.52 MeV below the possible experimental counterparts. The wave function of the calculated 9_1^+ state is dominated by configurations with a proton-neutron pair in the $g_{9/2}$ orbit coupled to $J = 9$ with 90% probability. The structure of the 7_1^+ state is quite similar, and the excitation energy is calculated to be higher than that of the 9_1^+ state, suggesting the decoupling between the ^{64}Ge core and the aligned proton-neutron pair. The yrast 7^+-9^+-11^+-13^+-15^+ states show a band structure connected by strong $E2$ transitions. One can find a similarity between this band and the negative-parity band in ^{64}Ge in the sense that both bands can be interpreted as two quasiparticle bands on top of the ^{64}Ge core. Because of this band structure, we interpret that the experimental (7^+) state to which the isomeric (9^+) state decays corresponds to the shell-model 7_2^+ state. The $B(E2)$ value is estimated to be $0.7(1)\ e^2\ \mathrm{fm}^4$ [75], which should revised to be $1.2\ e^2\ \mathrm{fm}^4$, taking into account the remeasured half-life [76]. The shell-model prediction is $B(E2; 9_1^+ \to 7_2^+) = 0.22\ e^2\ \mathrm{fm}^4$, which is too small, suggesting incorrect mixing with other 7^+ states.

3. *Shape coexistence in* ^{68}Se

The shape coexistence in ^{68}Se has been predicted based on the deformed potential model [79] due to the development of a large single-particle energy gap at $N = 34$ on both the prolate side and the oblate side. An experimental confirmation has been given recently [77], which is consistent with an interpretation that there exists a ground-state band with oblate deformation which is crossed by an excited band with prolate deformation at around $J \sim 8$. The experimental yrast sequence has been extended further [78] up to $J = 26$. Various theoretical approaches have been published [80–84] to explain this problem. However, there are hitherto no shell-model calculations based on realistic interactions.

Figure 28 shows the comparison of energy levels between experiment and our shell-model results. We see that the shell model successfully describes the qualitative features of the experimental band structure, such as the coexistence of two collective bands near the ground state and the higher-spin band above 10MeV excitation energy. The calculated $B(E2: 2^+ \to 0^+)$ values are 525 and 467 $e^2\ \mathrm{fm}^4$ for the ground-state band and the excited band, respectively, indicating a similar deformation for these two bands near the ground state. Assuming a quadrupole deformation, these values correspond to the $K = 0$ rotational band with the intrinsic quadrupole moment $|Q_0| \sim 1.6\ e$ b or the deformation parameter $|\beta| \sim 0.25$, which is close to the prediction $\beta = -0.26$ by the total Routhian surface (TRS) calculations using the Woods-Saxon cranking model [85]. The calculated spectroscopic quadrupole moments $Q(J)$ are shown in Fig. 29. The positive sign $Q(J) > 0$ in the ground-state band is consistent with the picture of collective oblate deformation, while $Q(J) < 0$ in the excited band due to the prolate deformation. Another estimate of Q_0 from the spectroscopic quadrupole moment is $Q_0 = -(7/2)Q(2_1^+) = -1.5\ e$ b, which is consistent with the estimate from the $B(E2)$

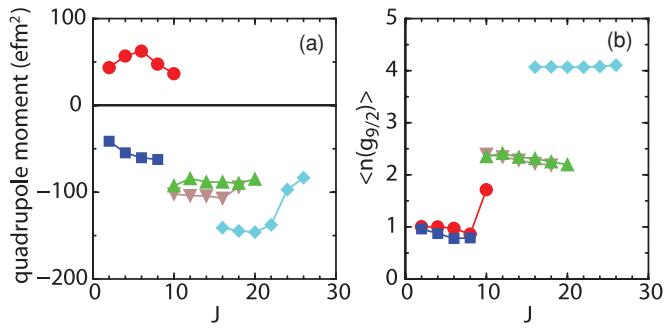

FIG. 29. (Color online) Calculated (a) quadrupole moments and (b) occupation numbers of the $g_{9/2}$ orbit for ^{68}Se. The band structure is assumed based on the $B(E2)$ values, and the members of each band are denoted by common symbols connected with lines: 0_1^+-2_1^+-4_1^+-6_1^+-8_1^+-10_8^+ (circles), 0_2^+-2_2^+-4_2^+-6_2^+-8_3^+ (squares), 10_1^+-12_2^+-14_3^+-16_4^+-18_3^+ (down-triangles), 10_4^+-12_3^+-14_2^+-16_1^+-18_2^+-20_3^+ (up-triangles), and 16_3^+-18_1^+-20_1^+-22_1^+-24_1^+-26_1^+ (diamonds).

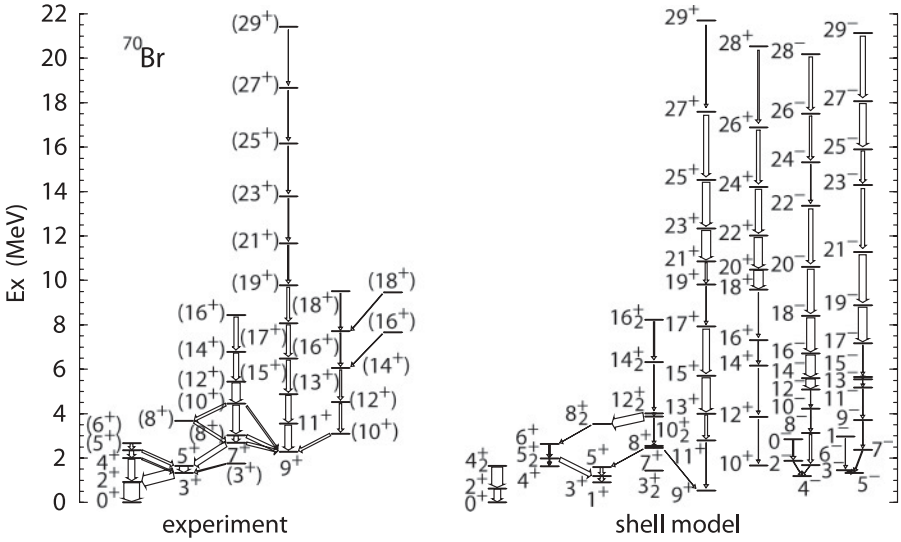

FIG. 30. Comparison of energy levels between our shell-model results and experimental data for ^{70}Br. Experimental data are taken from Ref. [34]. Conventions are the same as those of Fig. 25.

value, supporting the collective quadrupole deformation. Thus, the shape coexistence is realized in the shell-model results. Such a feature can also be seen in the total energy surface, which is shown in the right panel of Fig. 26. There exist two local energy minima with $\gamma = 0^\circ$ and 60°.

In Fig. 28, the theoretical band structure is shown by drawing energy levels that are connected to the yrast states with large $B(E2)$ values for stretched transitions. The band structure can also be seen in Fig. 29, where the calculated quadrupole moments vary smoothly as a function of the spin J within each band. According to the shell-model results, the $J = 10$ member of the ground-state band is found as the 10^+_8.

As shown in Fig. 29, the structure of these bands can be characterized by the occupation number of the $g_{9/2}$ orbit. In the ground-state oblate band and the low-spin prolate band, about one nucleon is excited to the $g_{9/2}$ orbit on average, while in the band with intermediate spin, the corresponding occupation number is about 2.3, and in the high-spin band, more than four nucleons are in the $g_{9/2}$ orbit. Thus, along the yrast line, higher-spin bands are constructed by successive excitations of nucleons into the $g_{9/2}$ orbit. These occupation numbers are almost constant within the bands, which suggest the stability of the corresponding intrinsic configurations. The calculated band-head energies of these bands are in good agreement with the experimental data. This can be interpreted, in terms of mean-field picture. The single-particle orbits in the deformed potential generated by the present effective interaction are reasonably described, at least for those states related to the $g_{9/2}$ orbit near the Fermi surface.

On the other hand, one can find clear deviations from experiment, in particular for the evolution of the band toward higher spin values. As for the low-spin bands, the calculated moment of inertia is smaller than the experimental one, especially for the excited prolate band. The experimental moment of inertia increases gradually toward higher spin. This feature can be seen in the shell-model results, but the increment is insufficient in comparison to the experimental data. As a result, the excited prolate band does not cross the ground-state oblate band. Because of the insufficient collectivity, the calculated moment of inertia becomes much smaller than the experimental one. Therefore, although the band-head energies agree well with experiment, with increasing spin values, the calculated level energies increase much faster than experimental values, giving rise to apparent deviations around intermediate spin values. We found such an insufficiency of collectivity, especially for the prolate of the Ge isotopes discussed in subsection III G.

4. ^{70}Br

In Fig. 30, one can find a reasonable correspondence between the experimental level scheme and the shell-model results for ^{70}Br. The 0^+ ground state and the first 2^+ state are predicted to have isospin $T = 1$, isobaric analog states of those in ^{70}Se. The theoretical counterparts of the yrast sequence of odd-spin levels (29^+)-(27^+)-$\cdots$-(9^+) can be found at reasonable excitation energies, although the level spacings are not necessarily well reproduced. It is also the case for the yrast even-spin states (18^+)-(16^+)-$\cdots$-(10^+). The irregularities in the level spacings of calculated yrast states again indicate the insufficient collectivity due to the narrow model space.

Experimentally, an isomer with a long half-life 2.2(2)s has been observed. This isomer was interpreted as the 9^+ state with the structure $[\pi[404]9/2^+\nu[404]9/2^+]9^+$ in terms of the Nilsson model [86]. The excitation energy of this isomer was suggested to be 1214 keV in Ref. [87], while 2293 keV was proposed in Ref. [88] on the basis of similar experiments but with improved statistics. Recently, the latter value was supported in Ref. [89] by the measurements of β-decay endpoint energies. Figure 30 was therefore drawn by adopting the data from Ref. [88]. In the shell-model results, the existence of an isomer 9^+ state is predicted in agreement with the experimental observation. However, the calculated excitation energy is 544 keV, much lower than the proposed experimental value. The calculated excitation energy of the 11^+ state is already lower than the experimental counterpart by 0.7 MeV, and the predicted energy difference between the 11^+ and the 9^+ state is much larger than the experimental one by 1 MeV. Such a large discrepancy can also be seen in the energy difference between the 12^+ and the 10^+ state.

In the calculated wave function of the 9^+_1 state, the configuration $(pf_{5/2})^{12}\otimes[\pi(g_{9/2})\nu(g_{9/2})]_{J=9}$ is found with

87% probability, which suggests a structure consisting of an aligned proton-neutron pair on top of the ^{68}Se core. It is interesting to note that the shell model predicts the 9_2^+ state at 2290 keV, which is very close to that of the experimental 9_1^+ state. This state shows a similar structure to the 9_1^+ state in the sense that it is also dominated (70%) by the $(pf_{5/2})^{12}\otimes[\pi(g_{9/2})\nu(g_{9/2})]_{J=9}$ configuration. Such a structure is expected if one recalls the shape coexistence of the ^{68}Se core. The too-low excitation energy of the calculated 9_1^+ state may originate from an incorrect mixing with this state and can be related to the drawback in the description of the prolate band in ^{68}Se.

The experimental 4_1^+ state is suggested to be $T = 1$ and decays to the 2_1^+ state, while the calculated 4_1^+ state is $T = 0$ and the $B(E2)$ to the 2_1^+ state is almost zero. The 4^+ state with $T = 1$ appears as the 4_2^+ state at 1646 keV in the shell-model results (21 keV above the 4_1^+ state), and it decays mainly to the 2_1^+ and the 3_1^+ states. which may corresponds to the experimental 4_1^+ state.

As in the case of ^{68}Se, the band structure can be characterized by the occupation number of the $g_{9/2}$ orbit. For example, in the calculated wave functions of positive-parity yrast states, this number is about 1.0 for $T = 0$, $J \leqslant 7$ states, and it increases to 2.4 for $8 \leqslant J \leqslant 17$, and it becomes about 4.2 for $18 \leqslant J \leqslant 27$, and 6.0 for $28 \leqslant J$. These numbers are almost constant for each J range. Note that the excitation energies of the lowest state for each J value are in good agreement with the experimental counterparts. Therefore, the irregular level spacings in the calculated results should be attributed to possible problems in the multipole part of the effective interaction or the insufficient model space.

In the experimental level scheme [88], no negative-parity states were proposed. The shell-model results predict that the negative-parity states become yrast for $J = 14 \sim 19$ (see Fig. 30). Further experimental studies are needed in order to clarify the possible existence of new negative party states or reassignments of negative parity to some of the observed states. This may improve the correspondence between the shell-model results and the experimental data.

I. Neutron-rich nuclei

Neutron-rich nuclei provide us with a good test of the effective Hamiltonian. Especially the proton-neutron part that connects the lower $(p_{3/2}, f_{5/2})$ proton orbits with the upper $(p_{1/2}, g_{9/2})$ neutron orbits can be studied directly from the energy spectra. Recently, a wealth of experimental data [90–93] for various neutron-rich nuclei toward ^{78}Ni has become available, some of which are within the scope of the present model space. As discussed in Sec. II, the present interaction successfully describe the behavior of low-lying states in neutron-rich Cu isotopes, suggesting reasonable properties of the $T = 0$ f5-g9 monopole part. Thus it is interesting to examine to what extent the present interaction can describe detailed spectroscopic properties of neighboring neutron-rich nuclei. We focus on the odd-odd nuclei with $N = 49$ and examine their structure by decreasing the number of protons from $Z = 39$ to 31. Note that these nuclei have been excluded from the data to be fitted in the derivation of the present interaction. As for the $T = 0$ part of the present interaction, the starting effective interaction has been modified mainly in the monopole part (see Table II). Thus, the appearance of $[j_\pi j_\nu]^J$ energy multiplets due to the coupling of the last proton and the last neutron are expected to inherit features of the original effective interaction. In that sense we can examine whether the modification in the $T = 0$ multipole part is required or not to describe the experimental data.

1. Systematics of j_π-j_ν multiplets

We first discuss the systematics in the appearance of the j_π-j_ν multiplets along the yrast line. Figure 31 shows the excitation energies of the calculated states for which the wave unctions are dominated by specific configurations classified in terms of the j_π-j_ν type. In the negative-parity states, the "p1g9" multiplets appear as the lowest states only in ^{88}Y, showing good correspondence with the experimental data. The behavior of the "p3g9" and "f5g9" multiplets is of our principal interest. On top of the lowest 0^+ configuration in the even-even core, these multiplets appear with $J = 3 \sim 6$ and $2 \sim 7$, respectively. In fact, if we focus on these spin ranges, several members of these multiplets are found along the yrast line, in reasonable agreement with the experimental data. As for the "p3g9" multiplet, $J = |j_\pi - j_\nu| = 3$ state becomes lowest in ^{88}Y, ^{86}Rb, and ^{84}Br, while $J = j_\pi + j_\nu - 1 = 5$ state is lowest in ^{82}As and ^{80}Ga, corresponding to the change from the hole-hole to particle-hole character of the multiplet. This is consistent with the experimental assignment of the low-lying (5^-) state in ^{82}As. Similarly, the "f5g9" multiplets appear in all nuclei, and among them, $J = |j_\pi - j_\nu| = 2$ state appears as the ground state in ^{86}Rb and ^{84}Br in reasonable agreement with experiment. On the other hand, $J = j_\pi + j_\nu - 1 = 6$ member comes down for less proton nuclei and becomes lowest in ^{80}Ga, which is almost degenerate with the 3^- and the 5^- states. It should be noted that the "f5g9" configuration appears also in higher spin states along the yrast line in ^{88}Y and ^{86}Rb on top of the excited configuration of the even-even core, showing reasonable correspondence with the experimental data.

As for the positive-parity states, the "g9g9" multiples can be seen in ^{88}Y, ^{86}Rb, and ^{84}Br, showing reasonable correspondence with the experimental yrast spectra. This configuration includes one proton excitation from the pf orbits to the $g_{9/2}$ orbit. As the proton number decreases, the excitation energies of these multiplets go up and the j_π-j_ν configuration gradually loses its purity. In fact, only three members of the multiplet with higher spin $(J = 7 \sim 9)$ can be seen in ^{80}Ga. The j_π-j_ν configurations within the pf shell, "p1p1," "p3p1," and "f5p1," consist of one neutron excitation from the $p_{1/2}$ to the $g_{9/2}$ orbit and appear in low-lying states with relatively low spin $(J = 0 \sim 3)$. The correspondence between the members of these multiplets and the experimental data can be assumed for several cases such as the 0^+ state in ^{88}Y and 1^+ state in ^{84}Br, but more data are needed for systematic understanding.

As demonstrated above, the overall description of the j_π-j_ν multiplets by the JUN45 interaction looks basically successful. This observation implies that the multipole part of the proton-neutron interaction that describes the j_π-j_ν multiplets is reasonably determined in JUN45 (and already in

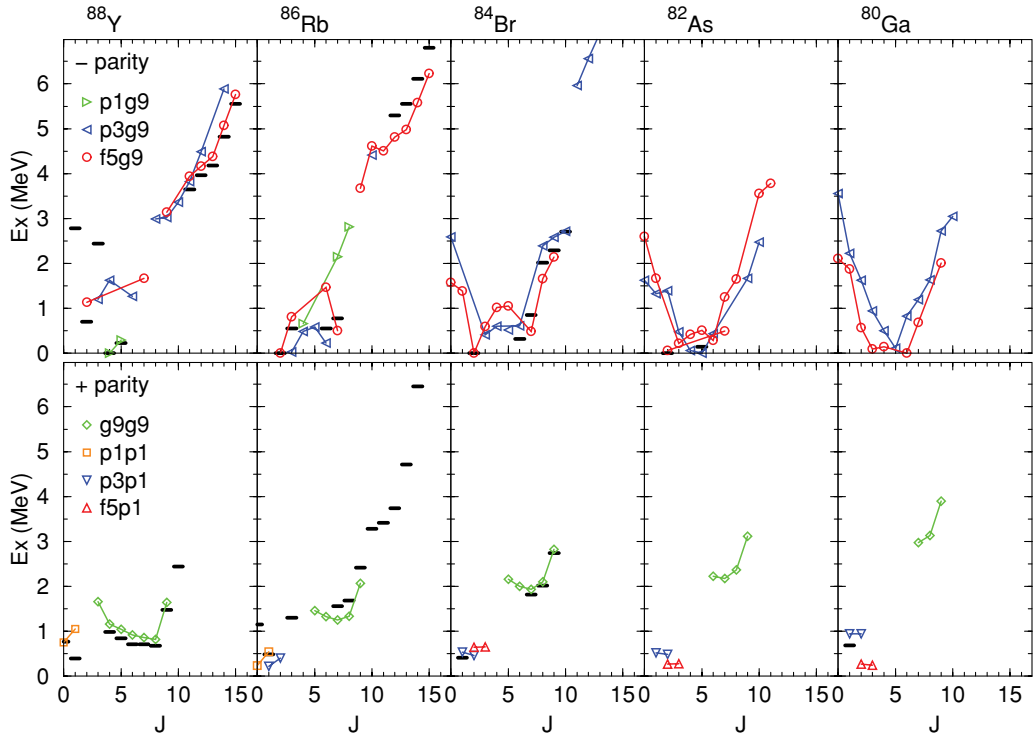

FIG. 31. (Color online) Excitation energies of the $[j_\pi\, j_\nu]^J$ multiplets as a function of the angular momentum J along the yrast line. Only the states for which the calculated wave functions are dominated (more than 30% probability) by a specific configuration with the unpaired proton in the orbit j_π and unpaired neutron in the orbit j_ν. The label "p1g9" stands for the configuration with $j_\pi = p_{1/2}$ and $j_\nu = g_{9/2}$, for instance. The symbols connected by solid lines correspond to the multiplets with common leading configurations. The same but disconnected symbols indicate that the corresponding states belong to different configurations of the paired nucleons (the core part). The upper (lower) panels show the negative- (positive-) parity states. The horizontal bars show the experimental data for (possible) yrast states taken from Ref. [34].

the original microscopic G-f5pg9 interaction). Similar results have been discussed in Ref. [94]. However, it is expected that the configuration mixing can cause displacements of some members of the multiplet. Such an effect should be apparent especially for states where the configurations outside the model space can largely contribute. In the following, we discuss each isotope in more detail. For some members of the multiplet, we find sizable deviation between the shell-model prediction and the experimental data.

2. $^{88}_{39}$Y

We start with ^{88}Y, which has been extensively studied by the shell model in the configuration space consisting of the $(p_{1/2}, g_{9/2})$ orbits only [17,19] and also in the f_5pg_9 shell [25]. Energy levels of ^{88}Y are shown in Fig. 32. It can be seen that the agreement between the experimental data and the shell-model results is rather good. However, there exist two remarkable differences. One is the 1^+_1 state, and the other is the 2^-_1 state, assuming that the experimental spin-parity assignment (2^-) is correct.

The first problem has already been pointed out from calculations within the $(p_{1/2}, g_{9/2})$ model space [17,19]. This state can naively be interpreted as a member of the doublet consisting of the $\pi(p_{1/2})\nu(p_{1/2})^{-1}$ configuration relative to the $^{88}_{38}$Sr$_{50}$ core. In Ref. [17], the effective interaction for the $(p_{1/2},g_{9/2})$ model space was derived based on this assumption. However, the resultant interaction failed to reproduce the strong $E3$ transition to the 4^- ground state. Considering that the 4^- ground state consists mainly of the $\pi(p_{1/2})\nu(g_{9/2})^{-1}$ configuration, a significant mixing of $\pi(p_{1/2})\nu(p_{3/2})^{-1}$ component in this 1^+ state was suggested. On the other hand, in Ref. [19], the authors derived the effective interaction by a fitting calculation but excluded this state (and all 1^+_1 states of neighboring odd-odd $N = 49$ nuclei) from the data to be fitted. The reason being that they found that the inclusion of these 1^+_1 states violates the constraint to keep an approximate charge independence of the effective interaction.

It is expected that the extended model space that can treat the neutron excitations from the $p_{3/2}$ orbit may improve the description of this 1^+ state. However, in the present calculation (and also in Ref. [25]), this 1^+ state cannot be successfully described, not only for the excitation energy but also for transition properties, as shown in Table XII. In the present shell-model results, the 1^+_1 state is dominated by the $\pi(p_{1/2})\nu(p_{1/2})^{-1}$ configuration (48%), while the $\pi(p_{1/2})\nu(p_{3/2})^{-1}$ component is only 1%. The latter configuration is found in the 1^+_2 state with 22% probability as a leading configuration. The $B(E3)$ value from this 1^+_2 state to the ground state is 11 W.u., which is of the same order as the experimental value, but this state appears at much higher excitation energy. Thus, within the present model space, it is unlikely that the mixing of such components should improve the description. One possible solution of this problem is to consider two-neutron excitation across the

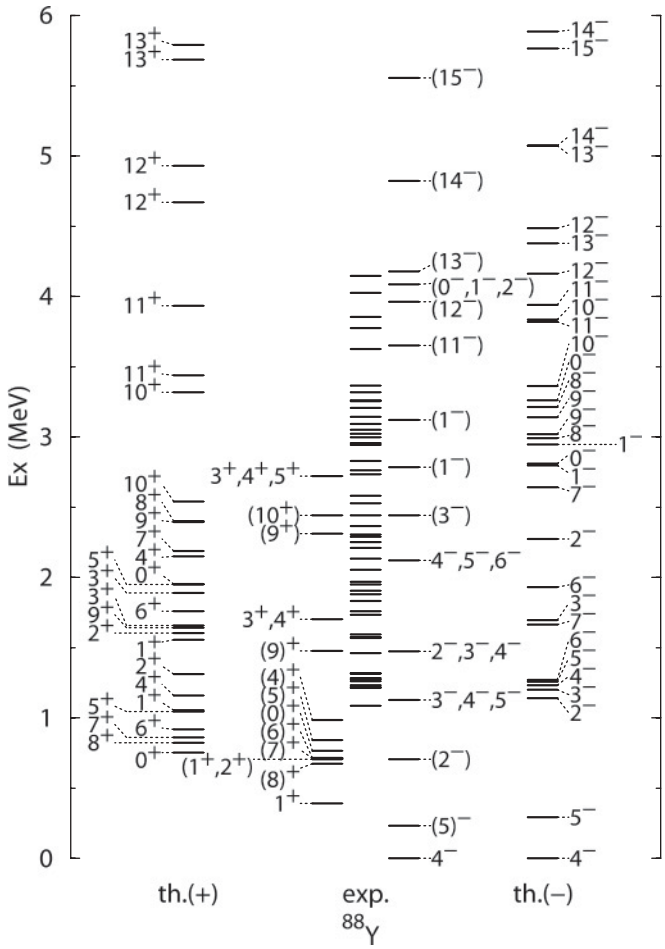

FIG. 32. Comparison of energy levels between the shell-model results and the experimental data for ^{88}Y. Conventions are the same as those in Fig. 17. Experimental data are taken from Ref. [34].

$N = 50$ shell-gap. Such an excitation cannot be described in the present model space but may give rise to an enhancement of the collectivity through the pairing correlations and lower the $\pi(p_{1/2})\nu(p_{1/2})^{-1}$ multiplets relative to the $\pi(g_{9/2})\nu(g_{9/2})^{-1}$ multiplets ($8^+_1, 7^+_1, \ldots$).

The second problem, concerning the 2^-_1 state, has not been recognized in the shell-model studies in the $(p_{1/2},g_{9/2})$ configuration space. This state can be interpreted as a member of the $[\pi(f_{5/2})^{-1}(p_{1/2})^2\nu(g_{9/2})^{-1}]^J$ multiplets, where $J = 2 \sim 7$. In the present shell-model result, this state is predicted to be too high by about 0.5 MeV. The calculated wave function contains a sizable amount of two-proton excitations into the $g_{9/2}$ orbit such as the $\pi(f_{5/2})^{-1}(g_{9/2})^2\nu(g_{9/2})^{-1}$ (25%) and the $\pi(f_{5/2})^{-1}(p_{3/2})^{-2}(p_{1/2})^2(g_{9/2})^2\nu(g_{9/2})^{-1}$ (13%) configurations. Such configurations with two-proton excitations are of less importance in the neighboring negative-parity states 3^-_1, 4^-_2, 5^-_2, 6^-_1, ... Thus, as in the case of the 1^+_1 state, an explicit introduction of the $d_{5/2}$ orbit in the model space may lower the 2^- state through the proton-neutron interaction among the $d_{5/2}$-$g_{9/2}$ orbits, improving the shell-model description.

TABLE XII. Transition matrix elements for ^{88}Y. Experimental data are taken from Ref. [34]. Conventions are the same as those in Table V.

Initial $J^\pi(E_x)$	Final $J^\pi(E_x)$	Multipole	Exp. (W.u.)	Th. (W.u.)
$5^-(232)$	$4^-(0)$	$M1$	0.0022(3)	0.0077
$1^+(393)$	$4^-(0)$	$E3$	5.91(6)	0.523
$8^+(675)$	$5^-(232)$	$E3$	0.0558(8)	0.262
$10^+(2444)$	$8^+(675)$	$E2$	0.6233(3)	7.0
$14^-(4824)$	$13^-(4178)$	$M1$	0.2723(4)	0.9530

The transition properties are shown in Table XII. The present shell-model results systematically overestimate the experimental values by a factor of 3–10 except for the $1^+ \to 4^-$ $E3$ transition mentioned above. This may indicate a problem in the effective operators especially in the neutron part, because there is only one valence neutron (hole) in this case. In addition, the number of valence protons is also essentially one in the lowest configurations for the $M1$ and the $E2$ transitions due to the parity selection rule.

3. $^{86}_{37}$Rb

In Fig. 33, the theoretical energy levels of ^{86}Rb are compared with the experimental ones. For most of the experimental excited states with spin-parity assignments (including a tentative one), we find reasonable shell-model counterparts. These states are, however, systematically lower in excitation energy compared with their experimental partners by roughly 0.5 MeV. In other words, if we shift down the calculated ground 2^- state by 0.5 MeV, the agreement between the data and the shell-model results becomes fairly good. This can be understood as the same problem as the observed for ^{88}Y in the above discussion. The structure of the calculated ground 2^- state is in fact very similar to that of ^{88}Y in the sense that it is dominated by the $\pi(f_{5/2})^{-1}\nu(g_{9/2})^{-1}$ configuration (58%) relative to the $^{88}_{38}$Sr$_{50}$ core.

Another member of the $[\pi(f_{5/2})^{-1}\nu(g_{9/2})^{-1}]^J$ multiplets ($J = 2 \sim 7$) appears as the 7^-_1 state. The energy difference between the experimental 2^- and (7^-) states is 780 keV, while the corresponding shell-model value is 502 keV. Thus the spreading of the multiplets is not precisely reproduced in the present shell-model calculation. The calculated 3^-_1, 6^-_1, 4^-_1, and 5^-_1 states are regarded as the members of the $[\pi(p_{3/2})^{-1}\nu(g_{9/2})^{-1}]^J$ multiplets, because such configurations carry more than 50% probability in the calculated wave functions. The 6^- state is predicted to be higher than the 3^- state by 204 keV. On the other hand, in the experimental data, the corresponding 6^- state appears as the lowest member of this multiplet, giving rise to the $T_{1/2} = 1.02$ min isomer. The (possible) second lowest member, $(3)^-$ state, is almost degenerate to the 6^- isomer. Again, the shell model fails in the description of detailed splitting of the multiplets. These results suggest a need for an explicit fine-tuning in the multipole part of the two-body matrix elements even in the $T = 0$ part.

Transition matrix elements are shown in Table XIII. The shell-model results reasonably agree with the experimental data, except for the $E1$ transition to the ground state.

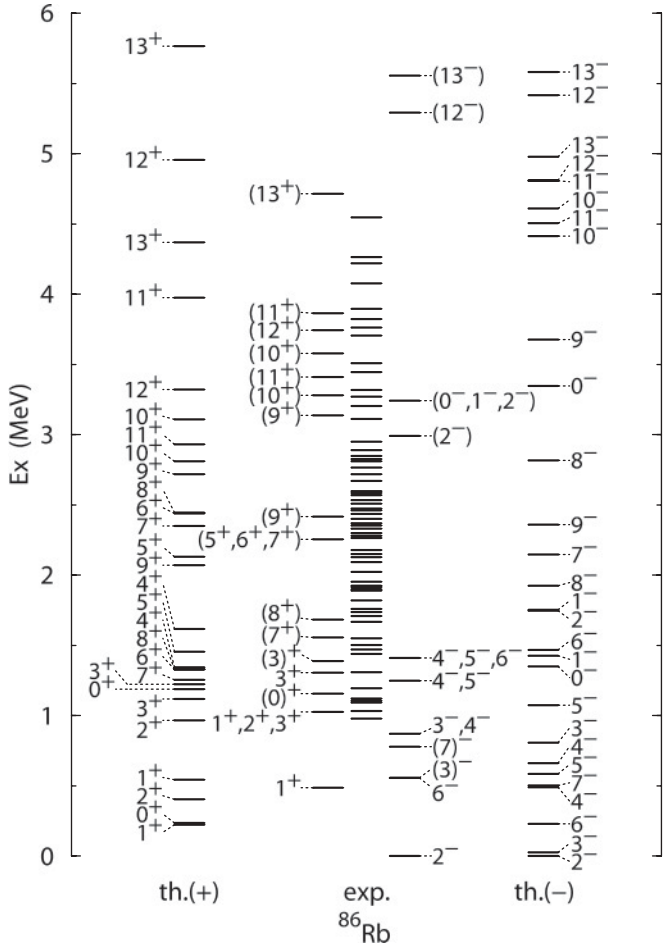

FIG. 33. Comparison of energy levels between the shell-model results and the experimental data for ^{86}Rb. Experimental data are taken from Ref. [34].

4. $^{84}_{35}$Br

Experimental energy levels of ^{84}Br above the 6^- isomer at 320(100) keV ($T_{1/2} = 6.0$ min) have been published recently [90]. Figure 34 shows the comparison of energy levels between these new data and the shell-model results. Here we assume that the excitation energy of the 6^- state is 320 keV and combine the data in Ref. [34] with those in Ref. [90]. The shell model successfully reproduces the ground 2^- state, and there is a reasonable agreement among the positive-parity states as well

TABLE XIII. Transition matrix elements for ^{86}Rb. Conventions are the same as those in Table V. Experimental data are taken from Ref. [34].

Initial $J^\pi(E_x)$	Final $J^\pi(E_x)$	Multipole	Exp. (W.u.)	Th. (W.u.)
$1^+(488)$	$2^-(0)$	$E1$	0.0012(2)	–
$6^-(556)$	$2^-(0)$	$E4$	1.455(6)	1.575
$10^+(3282)$	$9^+(3138)$	$M1$	0.73(19)	0.4794
	$8^+(1684)$	$E2$	1.7(5)	0.2
$11^+(3412)$	$10^+(3282)$	$M1$	1.7(5)	0.7597
$12^+(3743)$	$11^+(3412)$	$M1$	0.46(5)	0.6183

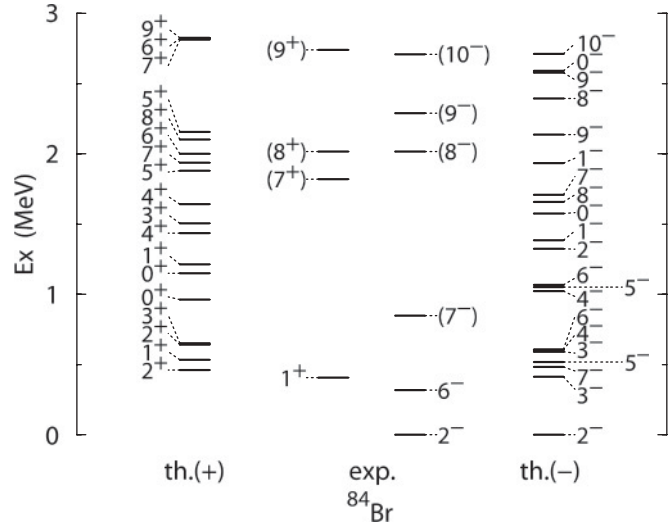

FIG. 34. Comparison of energy levels between the shell-model results and the experimental data for ^{84}Br. Experimental data are taken from Refs. [34,90].

as the $8^-, 9^-$, and 10^- states. However, the shell model predicts the 6^- state at higher excitation energy than the 3^- state, in disagreement with the experimental data. These 6^- and 3^- states are dominated by the $\pi(p_{3/2})^{-1}(f_{5/2})^{-2}\nu(g_{9/2})^{-1}$ configuration, with about 60% probability in the calculated wave functions. Therefore, the problem is the same as the we noted for ^{86}Rb. In addition, the experimental energy difference between the 7^- and 2^- states is 850(100) keV, while our calculation gives 484 keV. The leading configuration of these states is the $\pi(p_{3/2})^{-2}(f_{5/2})^{-1}\nu(g_{9/2})^{-1}$ configuration (about 60%). This difference is also very similar to the case reported for ^{86}Rb.

The 8^- and 9^- states are predicted to be at lower excitation energies than those of the experimental (8^-) and (9^-) states by about 0.4 MeV. These states consist mainly of the $\pi(p_{3/2})^{-2}(f_{5/2})^{-1}\nu(g_{9/2})^{-1}$ configuration (more than 50%), where two protons in the $p_{3/2}$ orbit should be coupled to $J = 2$. Thus the energy difference, 1.441 MeV, between the (7^-) and (9^-) states can be compared with the excitation energy of the 2^+ state of ^{86}Kr, which is 1.565 MeV experimentally and 1.255 MeV in the shell-model result.

As for the transition properties, relative γ-ray intensities are shown in Ref. [90] for several transitions, although absolute values of the matrix elements are unavailable. In Table XIV, we show shell-model values of the corresponding matrix elements. Assuming a pure $E4$ transition for the decay of the 6_1^- state with the γ-ray energy of 320 ± 100 keV, the shell model predicts the half-life $T_{1/2} = 9.4 \sim 3200$ min, which is somewhat longer than the experimental value (6.0 min) and strongly depends on the γ-ray energy. The predicted branching scheme of the higher-lying states is consistent with experiment, except for the decay of the (7^+) state to the (7^-) and (6^-) states. These are supposed to be of $E1$ character in Ref. [90] and are forbidden in the present shell-model calculation. In the present shell model, the decay of the 7^+ state to the lower-spin positive-parity states is predicted to be delayed because of large spin differences or small transition energies. In fact, the predicted partial half-lives are of the order of milliseconds

TABLE XIV. Transition matrix elements for ^{84}Br. Conventions are the same as those in Table V. Experimental data are taken from Ref. [34].

Initial $J^\pi(E_x)$	Final $J^\pi(E_x)$	Multipole	Exp. (W.u.)	Th. (W.u.)
$6^-(320)$	$2^-(0)$	$E4$		2.09
$(7^-)(850)$	$6^-(320)$	$M1$		1.14×10^{-5}
$(8^+)(2016)$	$(7^+)(1822)$	$M1$		1.32
		$E2$		22.2
$(8^-)(2016)$	$(7^-)(850)$	$M1$		0.153
		$E2$		8.80
$(9^-)(2291)$	$(8^-)(2016)$	$M1$		0.325
		$E2$		0.93
	$(7^-)(850)$	$E2$		1.32
$(10^-)(2710)$	$(9^-)(2291)$	$M1$		0.034
		$E2$		0.126
	$(8^-)(2016)$	$E2$		1.03
$(9^+)(2742)$	$(8^+)(2016)$	$M1$		0.90
		$E2$		21.5
	$(7^+)(1822)$	$E2$		1.42

or longer. This result supports the proposed decay scheme in Ref. [90].

5. $^{82}_{33}$As

We follow the spin-parity assignments in Ref. [92] instead of those in Ref. [34]. The ground state has quantum numbers (2^-), while the excited state at 146 ± 27 keV has received the assignment (5^-). In Fig. 35, energy levels are compared between the experimental data and the shell-model results. Here, it is assumed that the isomer state at uncertain excitation energy in Ref. [34] corresponds to the (5^-) state in Ref. [92]. As shown in this figure, the present shell model predicts the 5^- and the 2^- states as the lowest two states, which agrees nicely with the above spin-parity assignments, although the order is reversed. The dominating configuration of the calculated 2^- state is $\pi(f_{5/2})^5\nu(g_{9/2})^{-1}$ (48%) relative to the ^{78}Ni core, while it is $\pi(f_{5/2})^4(p_{3/2})^1\nu(g_{9/2})^{-1}$ (65%) for the 5^- state. The apparent agreement between data and the shell-model results suggests that the centroid energies of the $\pi(p_{3/2})\nu(g_{9/2})^{-1}$ and the $\pi(f_{5/2})\nu(g_{9/2})^{-1}$ multiplets are properly described by the present effective interaction even in this neutron-rich region.

Based on the analysis of the decay intensity, the lower limit of the partial half-life for the $M3$ transition from the (5^-) isomer to the (2^-) ground state is estimated to be 5×10^2 s [92]. The present shell model predicts 5×10^4s for this transition by using the experimental decay energy, which is much longer than the above lower limit.

6. $^{80}_{31}$Ga

Energy levels of ^{80}Ga are shown in Fig. 36. Experimental information of the spin-parity assignment for ^{80}Ga is limited to several 1^+ states that were obtained by the β-decay experiment [93]. A ground-state spin assignment of $J = 3$ is suggested in Ref. [34], but it is not established experimentally. In the shell-model results, the ground state is predicted to be 6^-, but there are also 3^- and 3^+ states at low excitation energies, 99 and 246 keV, respectively.

Experimentally, six possible 1^+ states have been observed [34], while the shell model predicts eight 1^+ states below 3 MeV. The excitation energies of these 1^+ states show reasonable correspondence with the experimental data. The calculated β^--decay half-life of ^{80}Zn using the experimental Q value is 0.22 s, which underestimates the experimental values 0.54(2) s by a factor of 3. This is mainly because of the difference between the predicted Gamow-Teller strength distribution and the experimental one. The calculated β^--decay intensity is almost concentrated to the lowest 1^+ state (~55%) at 716 keV. On the other hand, the experimental intensities to the lowest two 1^+ states are small (16% in total) but that to the state at 1428 keV is the largest (36%). In Ref. [95],

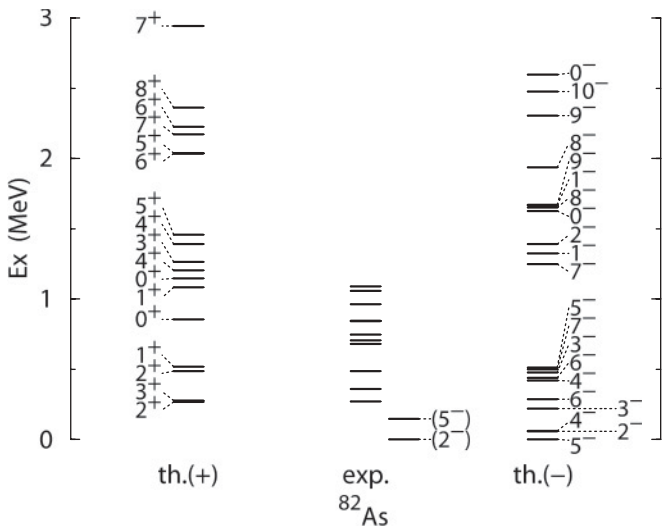

FIG. 35. Comparison of energy levels between the shell-model results and the experimental data for ^{82}As. Experimental data are taken from Refs. [34,92].

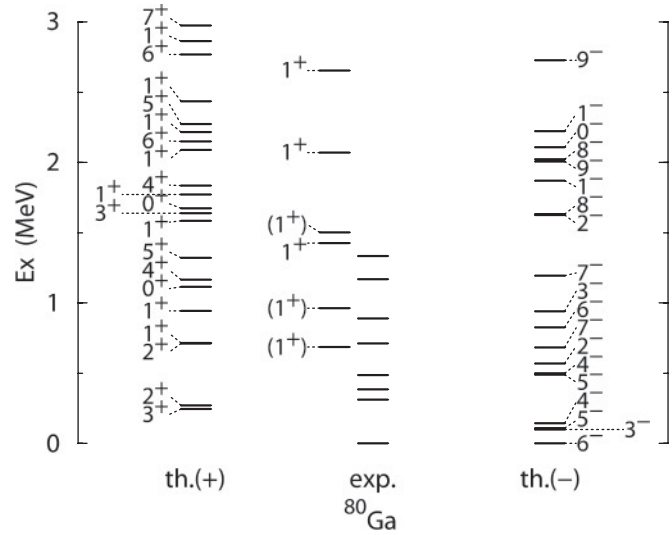

FIG. 36. Comparison of energy levels between the shell-model results and the experimental data for ^{80}Ga. Experimental data are taken from Ref. [34].

it is argued that the observed β^--decay properties can be explained by assuming a deformation of low-lying excited states above 0.6 MeV. This result suggests again a problem in the shell-model wave functions due to the narrow model space.

IV. SUMMARY

In summary, we have developed an effective interaction JUN45 for shell-model calculations in the f_5pg_9-shell space. As a starting Hamiltonian, we took an effective interaction derived from the realistic Bonn-C potential in a microscopic way. Modifications to it were made iteratively on 45-well-determined linear-combinations of the 135 TBME and four SPE by fitting to a body of 400 experimental binding and excitation energy data. The most significant changes were given in the monopole parts, as expected from similar studies in the sd-shell and pf-shell mass regions.

The resultant interaction has been tested in several ways. In the binding-energy systematics, reasonable agreement between the experimental data and the shell-model results were found along the $N \sim 50$ isotone chains, while there were large discrepancies along the Ni and Cu isotope chains. Such a result was expected from the pf-shell results [13] and understood in terms of a significant influence of the $f_{7/2}$ orbit. Similarly, possible effects of the missing $f_{7/2}$ orbit were found in the excitation energies, magnetic moments, and quadrupole moments of Ni isotopes.

The description of the magnetic moments was clearly improved by introducing a significant quenching in the spin g factors $g_s^{(\text{eff.})} = 0.7 g_s^{(\text{free})}$, in contrast to the cases in the sd shell and the pf shell, where the free g factors already gave very good results. This result can be attributed to the incompleteness of the f_5pg_9 space with respect to the spin-orbit partners. The quality of the overall description is satisfactory in spite of such an insufficient model space. In the pf-shell results, large discrepancies from experimental data were found in the 2_1^+ states of Zn isotopes, which was interpreted as an influence of the $g_{9/2}$ orbit. In fact, in the present results, the description has been remarkably improved.

The description of the quadrupole moment was found to be much less successful than that of the magnetic moment. One possible reason is that the quadrupole moment is directly related to the shape of the nucleus, and the present model space is insufficient to describe the development of the deformation in the prolate direction, mainly due to the missing $d_{5/2}$ orbit. This problem was typically seen in the even-even Zn and Ge isotope chain and also in various results in the present study such as in the prolate band of ^{68}Se and the excitation energies of the lowest $9/2^+$ states in Ga, As isotopes.

The calculated low-lying energy levels of odd mass nuclei were found to follow reasonably well the experimental data, except for the above mentioned $9/2^+$ states. This result suggests that the single-particle energies driven by the valence particles were successfully described by the monopole part of the present effective interaction.

Encouraged by the above observation, we studied the magicity of the $N = 40$ subshell closure in Ge isotopes. Through a detailed comparison between the available experimental information and the shell-model predictions, we concluded that the $N = 40$ closed subshell structure, which appeared to vanish in Ge isotopes in the ground states, has been found in the second 0^+ states. As a result, the irregular behavior in their excitation energy (sharp decrease at $N = 40$) has been explained.

In the derivation of the present effective interaction, we avoided taking data for the fitting from nuclei in the middle of the shell along the $N = Z$ line, because the present model space might be insufficient to describe the development of collectivity expected in these nuclei. In order to find out to what extent this interaction can describe such a collectivity produced by strong proton-neutron correlations, we studied the structure of the $N = Z$ nuclei ^{64}Ge, ^{66}As, ^{68}Se, and ^{70}Br. We found that the shell model describes very well the expected properties of these nuclei such as the triaxiality, isomer states, the oblate ground-state deformation and the shape coexistence. However, the agreement with the experimental data was not necessarily in good quantitative agreement, partly because of the insufficient quadrupole collectivity from the prolate side and partly because an insufficient tuning of the TBME which determine the detailed spreading of energy levels among the proton-neutron pair multiplets.

The latter problem was also found in the description of neutron-rich odd-odd nuclei. In many cases, data for the very neutron-rich nuclei are still not firmly established, a feature that makes it difficult to evaluate the theoretical predictions. Future experiments will provide guidance for further improvements in the interaction.

Because of various drawbacks discussed above, the present f_5pg_9 model space cannot be a good basis for the "unified model." Nevertheless, we believe that this interaction can provide an enlightening starting point for more advanced interactions with wider model spaces, which are desired for the study of more neutron-rich nuclei or more collective states becoming accessible presently in new experimental facilities.

ACKNOWLEDGMENTS

This work has been a part of the CNS-RIKEN joint research project on large-scale nuclear-structure calculations. This work was supported in part by a Grant-in-Aid for Scientific Research (A) (20244022) from the MEXT and also by the JSPS core-to-core program International Research Network for Exotic Femto Systems (EFES).

[1] J. Hakala *et al.*, Phys. Rev. Lett. **101**, 052502 (2008).
[2] H. Iwasaki *et al.*, Phys. Rev. C **78**, 021304(R) (2008).
[3] I. Stefanescu *et al.*, Phys. Rev. C **79**, 034319 (2009).
[4] I. Stefanescu *et al.*, Phys. Rev. Lett. **100**, 112502 (2008).
[5] J. Van de Walle *et al.*, Phys. Rev. C **79**, 014309 (2009).
[6] J. Ljungvall *et al.*, Phys. Rev. Lett. **100**, 102502 (2008).
[7] J. P. Schiffer *et al.*, Phys. Rev. Lett. **100**, 112501 (2008).
[8] S. Cohen and D. Kurath, Nucl. Phys. **73**, 1 (1965).
[9] B. A. Brown and B. H. Wildenthal, Annu. Rev. Nucl. Part. Sci. **38**, 29 (1988).
[10] B. A. Brown and W. A. Richter, Phys. Rev. C **74**, 034315 (2006).

[11] T. Suzuki, R. Fujimoto, and T. Otsuka, Phys. Rev. C **67**, 044302 (2003).
[12] M. Honma, T. Otsuka, B. A. Brown, and T. Mizusaki, Phys. Rev. C **65**, 061301(R) (2002).
[13] M. Honma, T. Otsuka, B. A. Brown, and T. Mizusaki, Phys. Rev. C **69**, 034335 (2004).
[14] E. Caurier, G. Martínez-Pinedo, F. Nowacki, A. Poves, and A. P. Zuker, Rev. Mod. Phys. **77**, 427 (2005).
[15] T. Otsuka, T. Suzuki, R. Fujimoto, H. Grawe, and Y. Akaishi, Phys. Rev. Lett. **95**, 232502 (2005).
[16] I. Talmi and I. Unna, Nucl. Phys. **19**, 225 (1960).
[17] F. J. D. Serduke, R. D. Lawson, and D. H. Gloeckner, Nucl. Phys. **A256**, 45 (1976).
[18] H. Herndl and B. A. Brown, Nucl. Phys. **A627**, 35 (1997).
[19] R. Gross and A. Frenkel, Nucl. Phys. **A267**, 85 (1976).
[20] I. P. Johnstone and L. D. Skouras, Eur. Phys. J. A **11**, 125 (2001).
[21] W. Chung, Ph.D. thesis, Michigan State University, 1976.
[22] Xiangdong Ji and B. H. Wildenthal, Phys. Rev. C **37**, 1256 (1988); **40**, 389 (1989).
[23] A. F. Lisetskiy, B. A. Brown, M. Horoi, and H. Grawe, Phys. Rev. C **70**, 044314 (2004).
[24] J. Sinatkas, L. D. Skouras, D. Strottman, and J. D. Vergados, J. Phys. G: Nucl. Part. Phys. **18**, 1377 (1992).
[25] J. Sinatkas, L. D. Skouras, D. Strottman, and J. D. Vergados, J. Phys. G: Nucl. Part. Phys. **18**, 1401 (1992).
[26] T. Mizusaki, RIKEN Accel. Prog. Rep. **33**, 14 (2000).
[27] M. Honma, B. A. Brown, T. Mizusaki, and T. Otsuka, Nucl. Phys. **A704**, 134c (2002).
[28] T. Otsuka, M. Honma, T. Mizusaki, N. Shimizu, and Y. Utsuno, Prog. Part. Nucl. Phys. **47**, 319 (2001).
[29] T. Otsuka, M. Honma, and T. Mizusaki, Phys. Rev. Lett. **81**, 1588 (1998).
[30] A. P. Zuker, J. Retamosa, A. Poves, and E. Caurier, Phys. Rev. C **52**, R1741 (1995).
[31] M. Hjorth-Jensen (unpublished).
[32] M. Hjorth-Jensen, T. T. S. Kuo, and E. Osnes, Phys. Rep. **261**, 125 (1995).
[33] A. Poves and A. P. Zuker, Phys. Rep. **70**, 235 (1981).
[34] Data extracted using the NNDC WorldWideWeb site from the ENSDF database.
[35] K. T. Flanagan *et al.*, Phys. Rev. Lett. **103**, 142501 (2009).
[36] M. Honma *et al.*, Eur. Phys. J. A **25**, 499 (2005).
[37] B. J. Cole, Phys. Rev. C **59**, 726 (1999).
[38] G. Audi and A. H. Wapstra, Nucl. Phys. **A595**, 409 (1995).
[39] T. Otsuka, R. Fujimoto, Y. Utsuno, B. A. Brown, M. Honma, and T. Mizusaki, Phys. Rev. Lett. **87**, 082502 (2001).
[40] N. J. Stone, At. Data Nucl. Data Tables **90**, 75 (2005).
[41] G. Georgiev *et al.*, Eur. Phys. J. A **30**, 351 (2006).
[42] T. E. Cocolios *et al.*, Phys. Rev. Lett. **103**, 102501 (2009).
[43] N. J. Stone *et al.*, Phys. Rev. C **77**, 014315 (2008).
[44] J. Leske *et al.*, Phys. Rev. C **71**, 044316 (2005).
[45] B. A. Brown, Prog. Part. Nucl. Phys. **47**, 517 (2001).
[46] I. S. Towner, Phys. Rep. **155**, 263 (1987).
[47] A. Bohr and B. R. Mottelson, *Nuclear Structure* (Benjamin, New York, 1975), Vol. 2, Chap. 6.
[48] R. du Rietz *et al.*, Phys. Rev. Lett. **93**, 222501 (2004).
[49] S. Leenhardt *et al.*, Eur. Phys. J. A **14**, 1 (2002).
[50] O. Perru *et al.*, Phys. Rev. Lett. **96**, 232501 (2006).
[51] J. Van de Walle *et al.*, Phys. Rev. Lett. **99**, 142501 (2007).
[52] K. Starosta *et al.*, Phys. Rev. Lett. **99**, 042503 (2007).
[53] D. Ward *et al.*, Phys. Rev. C **63**, 014301 (2000).
[54] A. Görgen *et al.*, Eur. Phys. J. A **26**, 153 (2005).
[55] R. A. Kaye *et al.*, Phys. Rev. C **57**, 2189 (1998).
[56] S. Franchoo *et al.*, Phys. Rev. C **64**, 054308 (2001).
[57] N. A. Smirnova, A. De Maesschalck, A. Van Dyck. and K. Heyde, Phys. Rev. C **69**, 044306 (2004).
[58] M. Behar, A. Filevich, G. García Bermúdez, and M. A. J. Mariscotti, Phys. Rev. C **17**, 516 (1978).
[59] W. Scholz and F. B. Malik, Phys. Rev. **176**, 1355 (1968).
[60] D. Ardouin *et al.*, Phys. Rev. C **12**, 1745 (1975).
[61] M. N. Vergnes *et al.*, Phys. Lett. **B72**, 447 (1978).
[62] H. T. Fortune and M. Carchidi, Phys. Rev. C **36**, 2584 (1987).
[63] B. Kotliński *et al.*, Nucl. Phys. **A519**, 646 (1990).
[64] K. J. Weeks, T. Tamura, T. Udagawa, and F. J. W. Hahne, Phys. Rev. C **24**, 703 (1981).
[65] P. D. Duval, D. Goutte, and M. Vergnes, Phys. Lett. **B124**, 297 (1983).
[66] A. Petrovici, K. W. Schmid, F. Grümmer, A. Faessler, and T. Horibata, Nucl. Phys. **A483**, 317 (1988).
[67] P. J. Ennis *et al.*, Nucl. Phys. **A535**, 392 (1991) [Erratum-*ibid.* **A560**, 1075 (1993)].
[68] E. Farnea *et al.*, Phys. Lett. **B551**, 56 (2003).
[69] K. Kaneko, M. Hasegawa, and T. Mizusaki, Phys. Rev. C **66**, 051306(R) (2002).
[70] L. Wilets and M. Jean, Phys. Rev. **102**, 788 (1956).
[71] A. S. Davydov and G. F. Filippov, Nucl. Phys. **8**, 237 (1958).
[72] R. F. Casten, *Nuclear Structure from a Simple Perspective* (Oxford Univeristy Press, Oxford, 1990).
[73] T. Mizusaki, T. Otsuka, Y. Utsuno, M. Honma, and T. Sebe, Phys. Rev. C **59**, R1846 (1999).
[74] T. Mizusaki, T. Otsuka, M. Honma, and B. A. Brown, Phys. Rev. C **63**, 044306 (2001).
[75] R. Grzywacz *et al.*, Phys. Lett. **B429**, 247 (1998).
[76] R. Grzywacz *et al.*, Nucl. Phys. **A682**, 41c (2001).
[77] S. M. Fischer, D. P. Balamuth, P. A. Hausladen, C. J. Lister, M. P. Carpenter, D. Seweryniak, and J. Schwartz, Phys. Rev. Lett. **84**, 4064 (2000).
[78] S. M. Fischer, C. J. Lister, and D. P. Balamuth, Phys. Rev. C **67**, 064318 (2003).
[79] W. Nazarewicz *et al.*, Nucl. Phys. **A435**, 397 (1985).
[80] M. Yamagami, K. Matsuyanagi, and M. Matsuo, Nucl. Phys. **A693**, 579 (2001).
[81] Y. Sun, Eur. Phys. J. A **20**, 133 (2004).
[82] A. Petrovici, K. W. Schmid, and A. Faessler, Nucl. Phys. **A710**, 246 (2002).
[83] K. Kaneko, M. Hasegawa, and T. Mizusaki, Phys. Rev. C **70**, 051301(R) (2004).
[84] F. H. Al Khudair, Y. S. Li, and G. L. Long, Phys. Rev. C **75**, 054316 (2007).
[85] S. Skoda *et al.*, Phys. Rev. C **58**, R5 (1998).
[86] A. Piechaczek *et al.*, Phys. Rev. C **62**, 054317 (2000).
[87] G. de Angelis *et al.*, Eur. Phys. J. A **12**, 51 (2001).
[88] D. G. Jenkins *et al.*, Phys. Rev. C **65**, 064307 (2002).
[89] M. Karny *et al.*, Phys. Rev. C **70**, 014310 (2004).
[90] A. Astier *et al.*, Eur. Phys. J. A **30**, 541 (2006).
[91] N. Fotiades *et al.*, Phys. Rev. C **74**, 034308 (2006).
[92] H. Gausemel, K. A. Mezilev, B. Fogelberg, P. Hoff, H. Mach, and E. Ramstrom, Phys. Rev. C **70**, 037301 (2004).
[93] J. A. Winger *et al.*, Phys. Rev. C **36**, 758 (1987).
[94] L. Coraggio, A. Covello, A. Gargano, and N. Itaco, Phys. Rev. C **80**, 021305(R) (2009).
[95] K.-L. Kratz, V. Harms, A. Wöhr, and P. Möller, Phys. Rev. C **38**, 278 (1988).